論文 / 著書情報
Article / Book Information

題目(和文)	
Title(English)	Improving bio-oil yield in the hydrothermal liquefaction of microalgae and application of hydrochar as a low-cost adsorbent
著者(和文)	モハメド サベル
Author(English)	Mohammad Saber
出典(和文)	学位:博士(学術), 学位授与機関:東京工業大学, 報告番号:甲第10899号, 授与年月日:2018年3月26日, 学位の種別:課程博士, 審査員:吉川 邦夫,竹下 健二,日野出 洋文,加茂 徹,高橋 史武,時松 宏治
Citation(English)	Degree:Doctor (Academic), Conferring organization: Tokyo Institute of Technology, Report number:甲第10899号, Conferred date:2018/3/26, Degree Type:Course doctor, Examiner:,,,,,
学位種別(和文)	博士論文
Type(English)	Doctoral Thesis

IMPROVING BIO-OIL YIELD IN THE HYDROTHERMAL LIQUEFACTION OF MICROALGAE AND APPLICATION OF HYDROCHAR AS A LOW-COST ADSORBENT

Mohammad Saber

Supervisor: Professor Kunio Yoshikawa

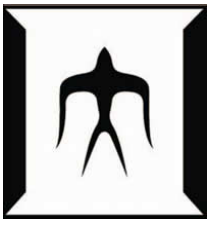

Doctoral Thesis

Department of Environmental Science and Technology

Interdisciplinary Graduate School of Science and Engineering

Tokyo Institute of Technology

Acknowledgement

This doctoral thesis is a requirement for graduation from the Department of Environmental Science and Technology, Tokyo Institute of Technology. Without the full support of numerous people, this thesis would not be completed. Therefore, the author would like to acknowledge and express his gratitude to:

- Prof. Kunio Yoshikawa, as the supervisor of this thesis, for giving me the precious opportunity to study in his laboratory and work on my topic of interest, as well as his encouragement, support and great attitude that trained me to be an independent researcher,
- Prof. Fumitake Takahashi, as the co-supervisor of this thesis, for his valuable guidance on this doctoral dissertation and one-by-one meeting which greatly improved the quality of my research,
- Prof. Koji Tokimatsu for his advice, guidance, and great support at all times in all aspects,
- Ministry of Education, Culture, Sports, Science, and Technology (MEXT), Japan for the four-year financial support during my study in Japan,
- Prof. Junko Nomura (Catalytic Chemistry Division, Chemical Resources Laboratory, Tokyo Institute of Technology), Prof. Serizawa (Department of Chemical Science and Engineering, Tokyo Institute of Technology), and Prof. Waki (Department of Chemical Science and Engineering, Tokyo Institute of Technology) for their support to use their laboratory facilities,
- Mrs. Eriko Ohno, laboratory secretary, for her sincere efforts in all administration works,
- Assistant Prof. Kiyoshi Tsuji for his support in the laboratory and providing safety instructions,

- All members of Yoshikawa-Takahashi-Tokimatsu Laboratory for their all kinds of support and close friendship, especially senior students who instructed me how to use the laboratory equipment.

Last but not least, I would like to express my sincere gratitude to my parents, older brother, and younger sister for their everlasting support and encouragement not only during my study in Japan but also for the entire life.

Mohammad Saber

February 2018

Abstract

This research aims to produce bio-oil from microalgae using the hydrothermal liquefaction technology (HTL). HTL technology can treat naturally-wet biomass such as microalgae. In this technology, pressure and temperature are high, and therefore expensive in the industrial scale. On the other hand, at a low pressure and temperature, bio-oil production yield is low. The purpose of this research is to increase the bio-oil production yield at low pressures and temperatures. For this purpose, catalysts and ultrasonic waves were applied to increase the conversion yield. The second objective of this study is to utilize hydrochar, which is a byproduct of the bio-oil production process, as a low-cost adsorbent. In this regard, microalgae hydrochar was used to remove heavy metals from wastewater. The utilization of the hydrochar in a new application would help to increase the profitability of the HTL process.

Table of Contents

List of Figures

List of Tables

Page

Chapter 1

1. Introduction

1.1. Background

Energy is one of the essential factors for human well-being in the world. Since energy demand is growing continuously, it is a challenge to meet energy demand to support economic and social growth. Figure 1.1 depicts the world energy consumption published by the U.S. Energy Information Administration (EIA), including history and projection until 2040 [1]. According to the Figure 1.1, two important points can be concluded about the future of the energy sector: (i) energy consumption increases annually for all energy carriers except for the coal, (ii) renewable energy sources have the fastest growth rate.

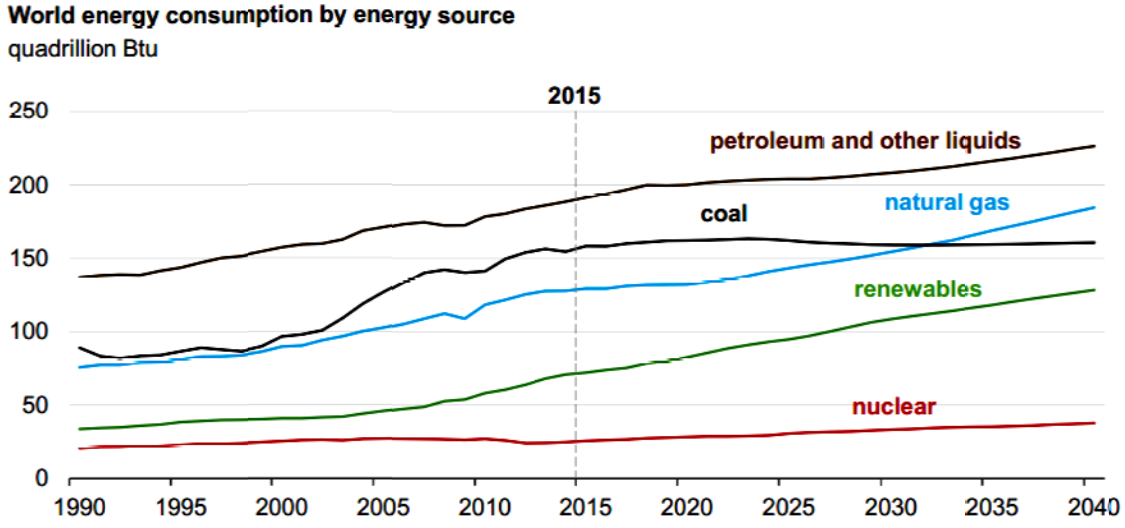

Figure 1.1. The world energy consumption by energy source (1990 - 2040) [1]

Even though the investment in the field of renewable energy has increased in the recent

past years, fossil fuels remain the major source of energy. On the other hand, there are several concerns regarding fossil fuel consumption: (i) fossil fuels are exhaustible energy sources, (ii) environmental pollution, especially carbon dioxide (CO_2) emission which is one of the main causes of global warming, (iii) energy security affected by the fluctuations of crude oil price. Therefore, more attention should be paid to developing renewable energy sources such as solar energy, wind energy, geothermal energy, hydropower, and biomass. In addition, new technologies are required to reduce the cost of renewable energy in order to (i) meet the growing energy demand in the world, (ii) reduce the environmental pollutions caused by the fossil fuels, and (iii) reduce dependency on imported fossil fuels.

Biomass is one of the alternatives to replace fossil fuels. Biomass is a renewable and sustainable source of energy developed from organic matter. Biomass can be used directly as a fuel to produce thermal energy, which is converted into electrical energy in the next step usually through a steam turbine power cycle. On the other hand, biomass can be converted into different solid, liquid, and gaseous fuels such as bioethanol, biodiesel, and biogas. According to the key world energy statistics report published by the International Energy Agency (IEA), biofuels and wastes had the 11.2% share of the world total energy consumption in 2015 (Figure 1.2) [2].

In order to convert biomass into different forms of energy and fuels, two pathways have been widely used: biochemical and thermochemical conversion processes [3]. The biochemical pathway is less mature, and there are several difficulties in the biochemical conversion of biomass including (i) high capital cost of the feedstock pre-treatment, (ii) low conversion efficiency, and (iii) high cost of enzymes. On the other hand, the thermochemical pathway has shown several advantages over biochemical pathway which are: (i) higher conversion efficiency, (ii) compatibility with the current technologies developed and utilized for fossil fuels, and (iii) ability to produce several types of fuels or products from a single process [4, 5].

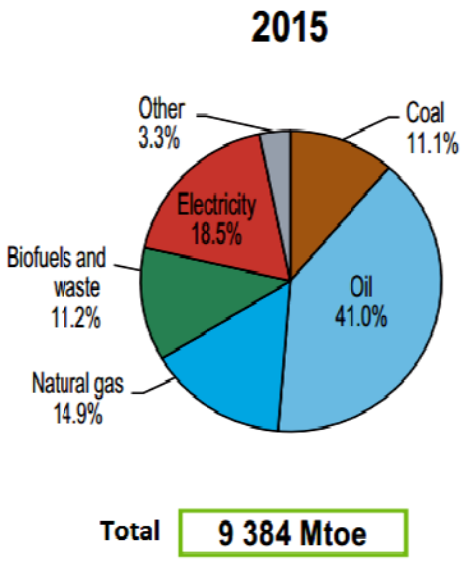

Figure 1.2. The world total energy consumption in 2015 (% of fuel shares) [2]

Various thermochemical conversion technologies have been developed so far including combustion [6], torrefaction (also called dry torrefaction or mild pyrolysis) [7], pyrolysis [8], gasification [9], hydrothermal carbonization (also called wet torrefaction) [10], hydrothermal liquefaction [11], and hydrothermal gasification (also called supercritical water gasification) [12].

Combustion is the burning of the biomass in the excess air for complete combustion. It is the most widely used process among thermochemical conversion processes due to its simplicity [13]. Torrefaction is a thermochemical conversion of biomass at mild conditions (200 - 300°C, atmospheric pressure) under the absence of oxygen. Under these conditions, biomass undergoes a partial decomposition. The main product of this process is a solid material (i.e. char) which can be used as a solid fuel [7]. Pyrolysis is typically defined as a thermochemical decomposition of biomass at medium to high temperatures (350–700 °C), low pressure, and under the absence of oxygen. Pyrolysis of biomass produces solid, liquid, and gaseous products which are of interest as alternative sources of energy [14]. The main operating parameters in pyrolysis are temperature, residence time, and heating rate. Based on these parameters, pyrolysis can be categorized into three subgroups: slow pyrolysis, fast

pyrolysis, and flash pyrolysis [14, 15]. Gasification is another thermochemical conversion process which transforms biomass into a gaseous mixture (i.e. syngas) and a solid product (i.e. char or biochar) under an oxygen-limited environment and high temperature (700 - 1400°C) [9].

Hydrothermal carbonization (HTC) of biomass is carried out in the hot compressed water (hydrothermal media) typically at a temperature range of 160-260°C, and pressures under 2MPa. The main product of this process is a solid material (i.e. char or hydrochar) which has several applications including solid fuel and adsorbent [10, 16]. Hydrothermal liquefaction (HTL) is another process conducted in hot compressed water at elevated temperature (200-370°C) and high pressure (2-22 MPa). HTL is also called solvolysis, hydrothermal upgrading, hydrothermal processing, and direct liquefaction [17]. The main product of HTL is an organic liquid phase (i.e. bio-oil or bio-crude oil), and the by-products are a gaseous phase, an aqueous phase, and the solid residue (i.e. hydrochar). Hydrothermal gasification (HTG) utilizes water under supercritical condition (above 374°C and 22.1 MPa) typically at a temperature range of 400-700°C and pressure 25-30 MPa. The main product of this process is the gas phase mainly containing CO_2, CO, CH_4, H_2. Short-chain hydrocarbons, C_2 - C_3, are also present in small quantity [12, 18].

In general, HTC, HTL, and HTG are suitable for treatment of feedstock with high moisture content since drying of feedstock is not required. On the other hand, torrefaction, pyrolysis, and gasification are suitable for treatment of feedstock with low moisture content. If these technologies are used for the treatment of biomass with high moisture content, the energy consumed for drying of feedstock reduces the conversion efficiency [4, 9]. Figure 1.3 summarizes the thermochemical conversion technologies for biofuel production from biomass, classified based on the moisture content of the feedstock and the primary product of the process [18].

		Moisture content		Temperature increase
		Low	High	
Primary product	Solid	Torrefaction	HTC	↓
	Liquid	Pyrolysis	HTL	
	Gas	Gasification	HTG	

Figure 1.3. Thermochemical conversion processes for biofuel production from biomass

1.2. Microalgae

Algae have been considered as one of the most promising alternative sources for biofuel production, known as the third generation biofuels. Algae are a group of eukaryotic organisms, ranging from unicellular to multicellular forms. In this thesis, algae refer to both microalgae and macroalgae. Microalgae are photosynthetic microorganisms which exist as individual cells or chains of cells. Contrary to macroalgae, they do not form various multicellular organisms [19]. Microalgae live in saline or freshwater environments and convert sunlight, carbon dioxide and water to algal biomass [20]. Compared with macroalgae, microalgae have faster growth rates, higher lipid contents, and less complex structures. Macroalgae are more difficult to grow in bioreactors, therefore they have not yet been researched as widely as microalgae [19].

Over the past few years, biofuel production from microalgae has been an area of considerable interest because of its advantages: (i) fast growth rate with some species having the doubling time of a few hours, (ii) ability to sequester CO_2 during growth through photosynthesis, (iii) ability to grow in non-arable lands and/or saline water and wastewater, (iv) high lipid content, (v) ability to produce different types of biofuels, (vi) having no overlap with food supply, and (v) lack of lignin, the firmest constituent of terrestrial biomass, which makes possible the thermochemical conversion of microalgae at milder conditions compared to terrestrial biomass [21, 22]. Currently, a rising number of companies are investing in developing algal biofuels. Not only for biofuel production, but also microalgae have been utilized for other applications including food supplement [23-25], food pigment [26], livestock food [27], cosmetics [28, 29], healthcare products [30], and medicine [31-33]

(Figure 1.4). Table 1.1 presents names of representative companies who are trying to commercialize algal biofuels and other industrial products.

Table 1.1. List of representative companies attempting to commercialize algal biofuels and other industrial products

Company (Country)	Website
Algae Link (Netherlands)	www.algaelink.com
Algae. Tec (Australia)	http://algaetec.com.au
AlgaFuel (Portugal)	www.a4f.pt
Algenol (USA)	www.algenol.com
AlgoSource (France)	http://algosource.com/en
ALG Western Oil (South Africa)	www.algbf.co.za
Aurora Algae Inc. (USA)	www.aurorainc.com
BP (England)	www.bp.com
BRTeam (Iran)	http://brteam.ir
Chevron (USA)	www.chevron.com
DENSO Corporation (Japan)	www.denso.co.jp
Diversified Energy (USA)	www.diversified-energy.com
Eni (Italy)	www.eni.com
Euglena (Japan)	www.euglena.jp/en
ExxonMobil (USA)	http://corporate.exxonmobil.com/en
Green Fuel Technologies (USA)	www.greenfuelonline.com
Idemitsu Kosan (Japan)	www.idemitsu.com
IHI Corporation (Japan)	www.ihi.co.jp
LiveFuels (USA)	www.livefuels.com
Neste Oil (Finland)	www.nesteoil.com
OilFox (Argentina)	www.oilfox.com.ar
Origin Oil (USA)	www.originoil.com
Pond Biofuels (Canada)	www.pondbiofuels.com
Sapphire Energy (USA)	www.sapphireenergy.com
Solix (USA)	www.solixbiofuels.com
Total (France)	www.total.com
Varicon Aqua Solutions (UK)	www.variconaqua.com

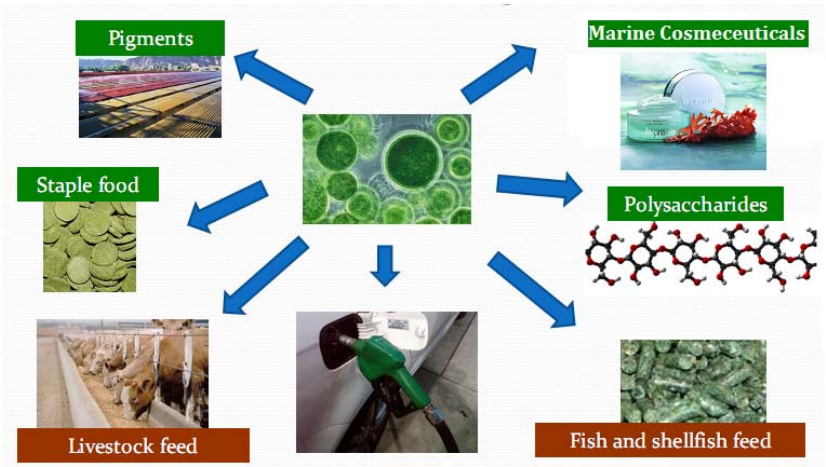

Figure 1.4. Commercial applications of microalgae

1.3. Microalgae as biofuel feedstock

As mentioned in Section 1.2, various types of biofuels can be produced from microalgae. Microalgae mainly consist of lipid, carbohydrate, and protein. Depending on the treatment process, different products can be produced from each constituent of microalgae or the whole algal cells. As an example, biodiesel can be produced from lipid fraction via solvent extraction and further catalytic chemical reaction [34]. Also, bioethanol can be produced from carbohydrate fraction through the fermentation process [35]. Another product is called bio-oil which is produced by the thermochemical conversion of all biomolecules constructing algal cells [17]. Figure 1.5 illustrates the thermochemical and biochemical conversion processes for algal biomass and their major products. Figure 1.5 includes physical cell disruption and solvent extraction methods which aim for lipid extraction and subsequent biodiesel production.

1.4. Bio-oil

Bio-oils are dark brown, free-flowing or viscous liquid having a distinctive odor [17, 36, 37]. Bio-oil is a complex mixture of several hundreds of organic compounds, chiefly containing acids, alcohols, aldehydes, esters, ketones, and phenols [17, 36]. Bio-oil is known as an alternative to crude oil to produce transportation fuels and valuable chemicals [17].

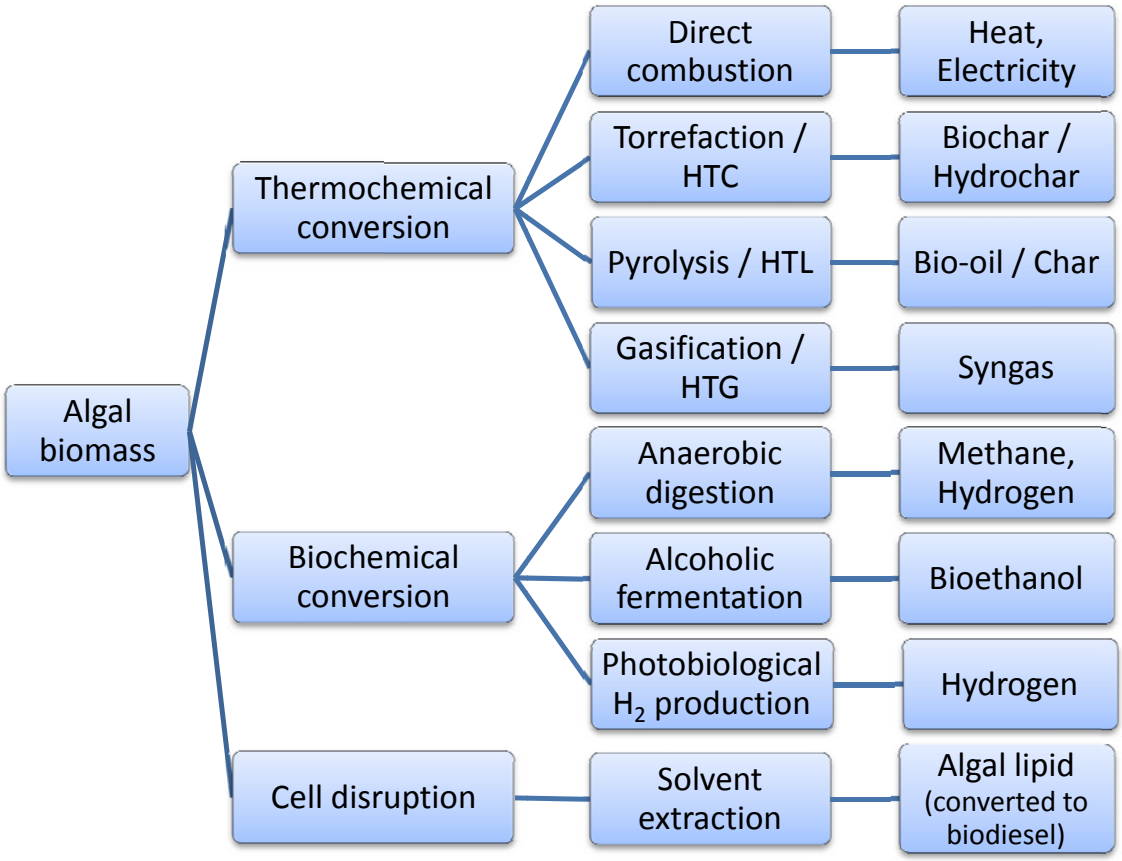

Figure 1.5. Energy conversion processes for algal biomass and major products

Bio-oils are CO_2/GHG neutral with negligible or zero SOx emissions since plant biomass contains insignificant amounts of sulfur. Therefore, bio-oils are cleaner than fossil fuels and cause less pollution [17]. Bio-oil can be used as a chemical feedstock for biorefinery to extract valuable chemicals or fuels. In fact, facilities similar to the current petroleum refineries can be used for this purpose. [17].

1.4.1. Bio-oil production

Currently, two main processes for bio-oil production are pyrolysis and hydrothermal liquefaction (HTL). One important point in the selection of the suitable production technique is the moisture content of the biomass feedstock. Since HTL does not necessitate drying of feedstock, it is suitable for processing of aquatic or naturally-wet biomass such as microalgae

or sludge. In general, if the moisture content of the biomass feedstock is higher than 30%, hydrothermal processing consumes less energy than drying and subsequent processing of the dried biomass [38]. On the other hand, HTL is conducted at high pressure which causes technical difficulties, safety concerns, and a high capital cost of the reactor in the industrial scale [36]. Also, bio-oils from pyrolysis and HTL exhibit different characteristics. As an example, pyrolysis-derived bio-oil, generally, has a higher oxygen content and consequently lower heating value than liquefaction-derived bio-oil [37, 39]. More details will be explained in the next section.

It is worthwhile to explain the difference between biodiesel and bio-oil production from microalgae. One approach to produce transportation fuels from microalgae is first lipid extraction and then conversion to biodiesel via esterification/transesterification reactions [40]. The other approach is bio-oil production through thermochemical conversion processes (e. g. pyrolysis and hydrothermal liquefaction) and upgrading the obtained bio-oil to transportation fuels [17]. Bio-oil production from microalgae is different from lipid or oil extraction. The latter aims to extract triacylglycerides (TAGs) and fatty acids from the algal cells to produce biodiesel via esterification/transesterification reactions. Several methods have been used for lipid extraction from microalgae including solvent extraction, Soxhlet extraction, electric field assisted extraction, supercritical fluid extraction, ultrasound-assisted extraction or sonication, bead-beating, and microwave-assisted extraction [41-44]. On the other hand, the bio-oil production aims to break all biomacromolecules (i.e. carbohydrate, protein, and lipid) into an organic liquid phase named bio-oil.

1.4.2. Bio-oil characterization

The chemical composition of the bio-oil depends on the feedstock type, the thermochemical process, and the operating conditions which results in different physical properties of bio-oils. Characterization of the bio-oil has been carried out extensively by many researchers.

Torri et. al. investigated the molecular characterization of HTL-derived bio-oil from microalgae Desmodesmus sp. [45]. They showed that lipids and some hydrophobic protein fragments were main compounds obtained at low temperatures. At higher temperature, proteins and cellulose started to break down, resulted in the production of carbohydrate derivatives (e.g., furans), amino acid side chains, and products from the cross-reaction of proteins and carbohydrates (e.g., pyrazines, pyrroles). Shuping et. al. characterized HTL-derived bio-oil from microalgae Dunaliella tertiolecta [46]. The results showed that the bio-oil was composed of fatty acids, fatty acid methyl esters, ketones, and aldehydes with an empirical formula of $CH_{1.44}O_{0.29}N_{0.05}$. Chemical properties of the HTL-derived bio-oil from different feedstock (i.e. Spirulina algae, swine manure, and digested anaerobic sludge) were compared by Vardon et. al. [47]. It was observed that feedstock type had an effect on the composition and functional group chemistry of the bio-oil. In their study, they found that the bio-oil from Spirulina had the lowest molecular weight as well as boiling temperature. Table 1.2 shows the physical properties of the pyrolysis-derived and liquefaction-derived bio-oil from microalgae as well as heavy petroleum fuel oil [46, 48-52].

In general, pyrolysis-derived bio-oil has a higher oxygen content and consequently lower heating value than liquefaction-derived bio-oil [37, 39]. Pyrolysis requires dried feedstock which necessitates a prior drying step which increases the energy consumption of the whole process. However, pyrolysis has a lower capital cost than liquefaction since it is usually conducted from 1 to 5 atm. Many pyrolysis technologies are being used commercially [36]. On the other hand, HTL-derived bio-oil is water-insoluble, and has a lower oxygen content and consequently higher energy content than pyrolysis bio-oil. However, the HTL bio-oils have a higher viscosity than pyrolysis bio-oils. Since HTL is conducted at high pressure, it causes technical difficulties, safety concerns, and a high capital cost of the reactor in the industrial scale [36]. HTL does not require a drying step and, therefore, it is ideal for processing of aquatic or naturally-wet biomass.

Table 1.2. Selected properties of liquefaction-derived and pyrolysis-derived bio-oil from microalgae

Properties		Liquefaction-derived bio-oil from Dunaliella tertiolecta cake [46]	Liquefaction-derived bio-oil from Spirulina [48]	Liquefaction-derived bio-oil from Dunaliella tertiolecta [49]
pH		3.5-4.2	-	3.8-4.0
Acid value (mgKOH/g)		-	1.8	-
Density (g/cm^3)		1180	1020 at 40°C	1150-1200 at 40°C
Viscosity (cP)		-	650 at 40°C	-
HHV(MJ/kg)		30.74	36.76	28.42
Elemental composition (wt%)				
	C	63.55	66.01	59.36
	H	7.66	11.56	7.58
	O	25.08	12.43	32.10
	N	3.71	9.54	0.96
	S	-	0.46	-
Water content (wt%)		8.73	-	13-20
Ash content (wt%)		0.2-0.5	-	0.4-0.7

1.5. Hydrothermal liquefaction

The hydrothermal liquefaction (HTL) is defined as the reaction of biomass in water at elevated temperature (200-370°C) and high pressure (2-22 MPa) with or without using a catalyst. Catalysts are usually used to increase the bio-oil yield. HTL is also called solvolysis, hydrothermal upgrading, hydrothermal processing, and direct liquefaction [17]. Water is the most common solvent as it is abundant and cheap. HTL of biomass results in four different products: (i) gaseous phase mainly containing CO_2, H_2, and CH_4 [53] (ii) aqueous phase which has been investigated as a nutrient for biomass and algae cultivation [54-56] and growth media for microorganisms [57], (iii) bio-oil as the main product, and (iv) solid residue or hydrochar which has several applications (more details will be explained in Chapter 4).

Table 1.2. Selected properties of liquefaction-derived and pyrolysis-derived bio-oil from microalgae (continued)

Properties		Pyrolysis-derived bio-oil from Spirulina [50]	Pyrolysis-derived bio-oil from Nannochloropsis sp. [51]	Heavy petroleum fuel oil [52]
pH		-	-	-
Acid value (mgKOH/g)		-	-	-
Density (g/cm^3)		-	-	940
Viscosity (cP)		-	-	180 at 40°C
HHV(MJ/kg)		21.68	37.2	40
Elemental composition (wt%)				
	C	46.05	80.2	85
	H	7.97	6.20	11
	O	36.28	5.81	1.0
	N	9.7	6.20	0.3
	S	-	1.59	-
Water content (wt%)		32.42	3.8	0.1
Ash content (wt%)		-	-	0.1

Water has three different roles in the HTL process: (i) reactant in hydrolysis reactions, (ii) solvent, and (iii) catalyst or catalyst precursor [53]. Liquid water at high temperature has different properties compared to liquid water at the ambient temperature. At high temperatures, the strength of hydrogen bonds in the bulk fluid decreases. Also, the dielectric constant of water decreases, and it becomes close to the dielectric constant of polar organic solvents at the ambient temperature [38]. For example, the dielectric constant of water is around 78.49 at the ambient temperature. However, it decreases to 34.79 at 200 °C, 20.39 at 300°C, and 14.07 at 350°C [58]. It means that solubility of organic compounds increases in water at high temperatures. In addition, the self-ionization constant of water (K_w) is another property that changes with the temperature. It increases from 10^{-14}

$(mol/L)^2$ at the ambient temperature to a maximum value at 250°C ($10^{-11.2}$ $(mol/L)^2$) [59]. This increase in K_w results in an increase in the concentration of H^+ and OH^- ions, which facilitate acid-catalyzed and alkali-catalyzed reactions or decomposition of biomass in the HTL process.

In the liquefaction, biomass is decomposed into small and unstable molecules which can be repolymerized into oily compounds [60]. Reactions such as solvolysis, depolymerization, decarboxylation, hydrogenolysis, and hydrogenation are involved during the liquefaction process [60]. As the solvent is heated along its vapor-liquid saturation curve, the value of pressure is determined by setting the temperature. Therefore, by increasing or decreasing the temperature, the pressure will increase or decrease accordingly. The main operating parameters in HTL are the temperature, the loading (mass of biomass per mass of solvent), and the holding time (which is usually in the range of 5 to 60 min). Compared to the pyrolysis, HTL is at a developmental stage, and more research is needed to understand the reaction mechanisms and kinetics [17].

The hydrothermal liquefaction of several algal species has been investigated including Botryococcus braunii [61, 62], Chlorella [63-67], Dunaliella [46, 68, 69], Enteromorpha [70, 71], Nannochloropsis [63, 65, 67, 72], Pavlova [73], Scenedesmus [65, 74], and Spirulina [47, 63, 64, 74, 75]. Table 1.3 summarizes literature data on HTL-derived bio-oil from microalgae.

1.6. Bio-oil yield

In the hydrothermal liquefaction of biomass, the bio-oil yield is defined as equation 1.1. It is typically in the range of 7–70%. The type of feedstock, temperature, pressure, holding time, type of solvents and catalysts are the main factors that affect the bio-oil yield [17].

$$\text{Bio} - \text{oil yield} = \frac{\text{Mass of bio} - \text{oil}}{\text{Mass of feedstock (Dry)}} * 100\% \quad (1.1)$$

Table 1.3. Review of literature on liquefaction-derived bio-oil from microalgae

Species	Temperature (°C)	Holding time (min)	Bio-oil yield (wt%)	HHV (MJ/kg)	Ref.
Spirulina	300	30	32.6	32-34.7	[47]
Botryucoccus brclunii	300	-	64	49	[62]
Nannochloropsis	350	60	34.6	34.5	[63]
Chlorella vulgaris	350	60	35.8	35.1	[67]
Dunaliella tertiolecta	250-340	5-60	30.9-43.8	33.3-37.8	[68]
Pavlova	250-350	60	40.5	32.2	[73]
Scenedesmus	300	30	24-45	35-37	[74]

For a specific type of feedstock, the temperature seems to be a critical factor affecting the bio-oil yield in the HTL process. Generally, the bio-oil yield increases to a maximum value with increasing the temperature. However, further increase in the temperature results in a decrease in the bio-oil yield, especially near the critical point of water. Particularly, in HTL of microalgae, the temperature range with the maximum bio-oil yield is reported to be from 280°C to 350°C in most previous researches [18]. In order to increase the bio-oil yield, several methods have been investigated so far including the use of organic solvent instead of water as well as applying a catalyst.

Organic solvents have been used in HTL process to increase the bio-oil yield including ethanol [48, 76, 77], acetone [76, 77], 2-propanol [78], methanol [48, 77, 79], 1,4-dioxane [48, 77], toluene [80], and glycerol [60]. The use of organic solvent instead of water has improved the bio-oil yield and its quality. Particularly, in HTL of microalgae, catalysts (both homogeneous and heterogeneous) have been used in order to increase the bio-oil yield or improve its quality including Na_2CO_3 [64, 81], KOH [64], CH_3COOH [64], HCOOH [64], NiO [81], $Ca_3(PO_4)_2$ [81], H_2SO_4 [49], and zeolite [53]. Both pathways, using organic solvents and catalysts, increase the process cost.

1.7. Objective and outline of the thesis

This research aims to produce bio-oil from microalgae using the hydrothermal liquefaction technology (HTL). HTL technology can treat naturally-wet biomass such as microalgae. In this technology, the pressure and the temperature are high, and therefore expensive in the industrial scale. On the other hand, at a low pressure and temperature, the bio-oil production yield is low. The purpose of this research is to increase the bio-oil production yield at a low pressure and temperature. For this purpose, catalysts and ultrasonic waves are applied to increase the conversion yield. The second objective of this study is to utilize the hydrochar, which is a byproduct of the bio-oil production process, as a low-cost adsorbent. In this regard, microalgae hydrochar is used to remove heavy metals from wastewater. The utilization of the hydrochar in a new application would help to increase the profitability of the HTL process. The content of this thesis is as follows.

Chapter 1. Introduction

In this chapter, the basic background of the hydrothermal liquefaction of microalgae is introduced. The advantages of biofuel production from microalgae as well as production technologies are reviewed, where the attention is paid to the HTL process. In addition, the characteristics of the bio-oil from microalgae are discussed. Finally, the objectives and the originality of this research are stated.

Chapter 2. Catalytic hydrothermal liquefaction of microalgae using heterogeneous catalysts

The objective of this chapter is to improve the bio-oil conversion yield by using heterogeneous catalysts. For this purpose, a nanocatalyst (nano-Ni/SiO_2), an acid catalyst (zeolite) and an alkali catalyst (Na_2CO_3) are used to increase the bio-oil yield at low temperatures (210°C, 230°C, 250°C). The yield, the elemental composition, and the heating value of the bio-oils from blank experiment, where no catalyst is used, and catalytic experiments are compared. Also, the effect of catalysts on the components of the bio-oil is

studied. Since application of catalyst results in an increase in the total process cost, the possibility of nanocatalyst recovery from solid residue (i.e. hydrochar) is also taken into account.

Chapter 3. Ultrasonic-assisted hydrothermal liquefaction; enhancing bio-oil conversion yield and heating value

In this chapter, a new method to increase the bio-oil yield at a low pressure and temperature is investigated. The microalgal cells are first pre-treated by ultrasonic waves for 30s, 60s, and 90s at 100W to make algal cells more fragile, and then bio-oil is produced using HTL at 210°C, 230°C and 250°C. After the experimental part, the effects of the ultrasonic pre-treatment on the yield, the elemental composition, the heating value, and the chemical composition of the bio-oils are analyzed. Since applying ultrasonic waves requires electrical energy, it increases the total energy consumption of the process. Therefore, the net energy is calculated to evaluate the effect of the sonication on the whole energy consumption.

Chapter 4. Characteristics and application of hydrochar as a low-cost adsorbent

This chapter aims to utilize the hydrochar, a by-product of the hydrothermal liquefaction of microalgae, in the adsorption of heavy metals from water or wastewater. In this study, hydrochar prepared from hydrothermal liquefaction of microalgae is characterized and investigated for copper removal from aqueous solution. Two hydrochars are prepared at 210°C (HD210) and 250°C (HD250). At first, the characteristics of both hydrochars are studied using the proximate and the elemental analysis, the surface area and the pore characteristic analysis, and FTIR. After then, the performance of the hydrochars in the copper removal from aqueous solution is evaluated. For this purpose, the effects of the initial solution pH, the initial Cu(II) concentration, the contact time, and the temperature on the adsorption capacity of hydrochars are investigated. In addition, the adsorption isotherm, kinetics, and thermodynamics are studied based on the experimental data.

Chapter 5. Conclusions and recommendations

This chapter summarizes the important concluding remarks of this thesis, along with some recommendations for future works.

1.7.1. Originality

The main difference between this research and most previous studies is the range of operating parameters (temperature and pressure) used in the HTL process. The most previous research focused on the high temperature and pressure ranges while this study concentrated on the HTL at low temperatures and pressures. Figure 1.6 illustrates the difference in the temperature and pressure range in this work and other researches. Also, nanocatalyst and ultrasonic pre-treatment are applied in the HTL of microalgae for the first time. Moreover, microalgae hydrochar is employed as a low-cost adsorbent in the removal of heavy metals from aqueous solution. The originality of each chapter is as follows:

- Chapter 2: Utilization of a nanocatalyst in HTL of microalgae
- Chapter 3: Utilization of the ultrasonic pre-treatment in HTL of microalgae
- Chapter 4: Using hydrochar from microalgae as a low-cost adsorbent for removing heavy metals from aqueous solution

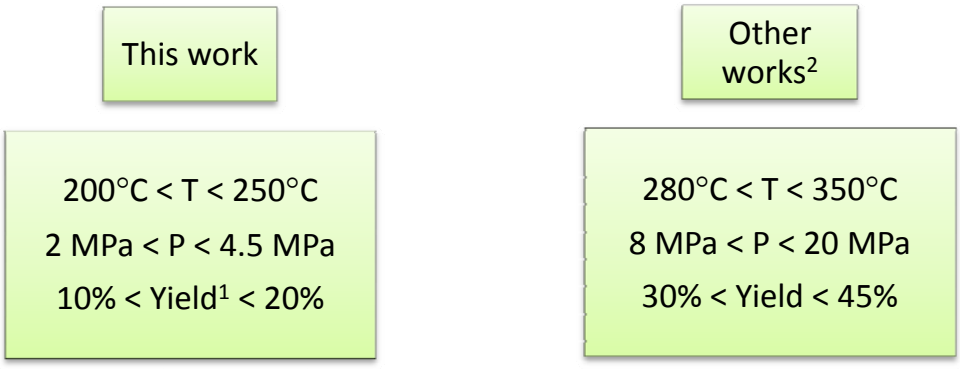

Figure 1.6. Main difference in the parameters in this work and other researches

1: Bio-oil yield for blank experiment without applying catalyst or ultrasonic pre-treatment

2: Average values of the parameters

1.8. References

[1] (EIA) USEIA. International Energy Outlook 2017. 2017.

[2] (IEA) IEA. Key world energy statistics. 2017.

[3] Yilmaz S, Selim H. A review on the methods for biomass to energy conversion systems design. Renew Sust Energ Rev. 2013;25:420-30.

[4] Raheem A AW, Yap T, Danquah M, Harun R. . Thermochemical conversion of microalgal biomass for biofuel production Renewable and Sustainable Energy Reviews. 2015;49:990-9.

[5] Sims REH, Mabee W, Saddler JN, Taylor M. An overview of second generation biofuel technologies. Bioresource Technol. 2010;101:1570-80.

[6] Abuelnuor AAA, Wahid MA, Hosseini SE, Saat A, Saqr KM, Sait HH, et al. Characteristics of biomass in flameless combustion: A review. Renew Sust Energ Rev. 2014;33:363-70.

[7] Chen WH, Peng JH, Bi XTT. A state-of-the-art review of biomass torrefaction, densification and applications. Renew Sust Energ Rev. 2015;44:847-66.

[8] Sharma A, Pareek V, Zhang DK. Biomass pyrolysis-A review of modelling, process parameters and catalytic studies. Renew Sust Energ Rev. 2015;50:1081-96.

[9] Ruiz JA, Juarez MC, Morales MP, Munoz P, Mendivil MA. Biomass gasification for electricity generation: Review of current technology barriers. Renew Sust Energ Rev. 2013;18:174-83.

[10] Bach QV, Skreiberg O. Upgrading biomass fuels via wet torrefaction: A review and comparison with dry torrefaction. Renew Sust Energ Rev. 2016;54:665-77.

[11] A.R.K. Gollakota NK, Sai Gu. A review on hydrothermal liquefaction of biomass. Renewable and Sustainable Energy Reviews. 2018;81:1378–92.

[12] Reddy SN, Nanda S, Dalai AK, Kozinski JA. Supercritical water gasification of biomass for hydrogen production. Int J Hydrogen Energ. 2014;39:6912-26.

[13] Zhang LH, Xu CB, Champagne P. Overview of recent advances in thermo-chemical

conversion of biomass. Energ Convers Manage. 2010;51:969-82.

[14] Marcilla A, Catala L, Garcia-Quesada JC, Valdes FJ, Hernandez MR. A review of thermochemical conversion of microalgae. Renew Sust Energ Rev. 2013;27:11-9.

[15] Brennan L, Owende P. Biofuels from microalgae-A review of technologies for production, processing, and extractions of biofuels and co-products. Renew Sust Energ Rev. 2010;14:557-77.

[16] Qian KZ, Kumar A, Zhang HL, Bellmer D, Huhnke R. Recent advances in utilization of biochar. Renew Sust Energ Rev. 2015;42:1055-64.

[17] Xiu SN, Shahbazi A. Bio-oil production and upgrading research: A review. Renew Sust Energ Rev. 2012;16:4406-14.

[18] Barreiro DL, Prins W, Ronsse F, Brilman W. Hydrothermal liquefaction (HTL) of microalgae for biofuel production: State of the art review and future prospects. Biomass Bioenerg. 2013;53:113-27.

[19] Bahadar A, Khan MB. Progress in energy from microalgae: A review. Renew Sust Energ Rev. 2013;27:128-48.

[20] Demirbas A. Use of algae as biofuel sources. Energ Convers Manage. 2010;51:2738-49.

[21] Scott SA, Davey MP, Dennis JS, Horst I, Howe CJ, Lea-Smith DJ, et al. Biodiesel from algae: challenges and prospects. Curr Opin Biotech. 2010;21:277-86.

[22] Campbell PK, Beer T, Batten D. Life cycle assessment of biodiesel production from microalgae in ponds. Bioresour Technol. 2011;102:50-6.

[23] Becker EW. Micro-algae as a source of protein. Biotechnology advances. 2007;25:207-10.

[24] Kay RA. Microalgae as Food and Supplement. Crit Rev Food Sci. 1991;30:555-73.

[25] Vaz BD, Moreira JB, de Morais MG, Costa JAV. Microalgae as a new source of bioactive compounds in food supplements. Curr Opin Food Sci. 2016;7:73-7.

[26] Dufosse L, Galaup P, Yaron A, Arad SM. Microorganisms and microalgae as sources of pigments for food use: a scientific oddity or an industrial reality? Trends Food Sci Tech. 2005;16:389-406.

[27] Yaakob Z, Ali E, Zainal A, Mohamad M, Takriff MS. An overview: biomolecules from microalgae for animal feed and aquaculture. J Biol Res-Thessalon. 2014;21.

[28] Wang HMD, Chen CC, Huynh P, Chang JS. Exploring the potential of using algae in cosmetics. Bioresource Technol. 2015;184:355-62.

[29] Gellenbeck KW. Utilization of algal materials for nutraceutical and cosmeceutical applications-what do manufacturers need to know? J Appl Phycol. 2012;24:309-13.

[30] Thomas NV, Kim SK. Beneficial Effects of Marine Algal Compounds in Cosmeceuticals. Mar Drugs. 2013;11:146-64.

[31] Mimouni V, Ulmann L, Haimeur A, Gueno F, Meskini N, Tremblin G. Marine microalgae used as food supplements and their implication in preventing cardiovascular diseases. Ocl Oils Fat Crop Li. 2015;22.

[32] Hoseini SM, Khosravi-Darani K, Mozafari MR. Nutritional and Medical Applications of Spirulina Microalgae. Mini-Rev Med Chem. 2013;13:1231-7.

[33] Borowitzka MA. Microalgae as Sources of Pharmaceuticals and Other Biologically-Active Compounds. J Appl Phycol. 1995;7:3-15.

[34] Mata TM, Martins AA, Caetano NS. Microalgae for biodiesel production and other applications: A review. Renew Sust Energ Rev. 2010;14:217-32.

[35] John RP, Anisha GS, Nampoothiri KM, Pandey A. Micro and macroalgal biomass: A renewable source for bioethanol. Bioresource Technol. 2011;102:186-93.

[36] Huber GW, Iborra S, Corma A. Synthesis of transportation fuels from biomass: chemistry, catalysts, and engineering. Chemical reviews. 2006;106:4044-98.

[37] Duan PG, Savage PE. Upgrading of crude algal bio-oil in supercritical water. Bioresource Technol. 2011;102:1899-906.

[38] Changi SM, Faeth JL, Mo N, Savage PE. Hydrothermal Reactions of Biomolecules Relevant for Microalgae Liquefaction. Ind Eng Chem Res. 2015;54:11733-58.

[39] Peterson AA, Vogel F, Lachance RP, Froling M, Antal MJ, Tester JW. Thermochemical biofuel production in hydrothermal media: A review of sub- and supercritical water technologies. Energ Environ Sci. 2008;1:32-65.

[40] Ahmad AL, Yasin NHM, Derek CJC, Lim JK. Microalgae as a sustainable energy source for biodiesel production: A review. Renew Sust Energ Rev. 2011;15:584-93.

[41] Halim R, Danquah MK, Webley PA. Extraction of oil from microalgae for biodiesel production: A review. Biotechnology advances. 2012;30:709-32.

[42] Mercer P, Armenta RE. Developments in oil extraction from microalgae. Eur J Lipid Sci Tech. 2011;113:539-47.

[43] Lee JY, Yoo C, Jun SY, Ahn CY, Oh HM. Comparison of several methods for effective lipid extraction from microalgae. Bioresource Technol. 2010;101:S75-S7.

[44] Cravotto G, Boffa L, Mantegna S, Perego P, Avogadro M, Cintas P. Improved extraction of vegetable oils under high-intensity ultrasound and/or microwaves. Ultrasonics sonochemistry. 2008;15:898-902.

[45] Torri C, Alba LG, Samori C, Fabbri D, Brilman DWF. Hydrothermal Treatment (HTT) of Microalgae: Detailed Molecular Characterization of HTT Oil in View of HTT Mechanism Elucidation. Energ Fuel. 2012;26:658-71.

[46] Zou SP, Wu YL, Yang MD, Kaleem I, Chun L, Tong JM. Production and characterization of bio-oil from hydrothermal liquefaction of microalgae Dunaliella tertiolecta cake. Energy. 2010;35:5406-11.

[47] Vardon DR, Sharma BK, Scott J, Yu G, Wang ZC, Schideman L, et al. Chemical properties of biocrude oil from the hydrothermal liquefaction of Spirulina algae, swine manure, and digested anaerobic sludge. Bioresource Technol. 2011;102:8295-303.

[48] Yuan XZ, Wang JY, Zeng GM, Huang HJ, Pei XK, Liu ZF, et al. Comparative studies of thermochemical liquefaction characteristics of microalgae using different organic solvents.

Energy. 2011;36:6406-12.

[49] Zou SP, Wu YL, Yang MD, Li C, Tong JM. Thermochemical Catalytic Liquefaction of the Marine Microalgae Dunaliella tertiolecta and Characterization of Bio-oils. Energ Fuel. 2009;23:3753-8.

[50] Chaiwong K, Kiatsiriroat T, Vorayos N, Thararax C. Study of bio-oil and bio-char production from algae by slow pyrolysis. Biomass Bioenerg. 2013;56:600-6.

[51] Guo QJ, Wu M, Wang K, Zhang L, Xu XF. Catalytic Hydrodeoxygenation of Algae Bio-oil over Bimetallic Ni-Cu/ZrO2 Catalysts. Ind Eng Chem Res. 2015;54:890-9.

[52] Oasmaa A, Czernik S. Fuel oil quality of biomass pyrolysis oils - State of the art for the end user. Energ Fuel. 1999;13:914-21.

[53] Duan PG, Savage PE. Hydrothermal Liquefaction of a Microalga with Heterogeneous Catalysts. Ind Eng Chem Res. 2011;50:52-61.

[54] Biller P, Ross AB, Skill SC, Lea-Langton A, Balasundaram B, Hall C, et al. Nutrient recycling of aqueous phase for microalgae cultivation from the hydrothermal liquefaction process. Algal Res. 2012;1:70-6.

[55] Jena U, Vaidyanathan N, Chinnasamy S, Das KC. Evaluation of microalgae cultivation using recovered aqueous co-product from thermochemical liquefaction of algal biomass. Bioresource Technol. 2011;102:3380-7.

[56] Du ZY, Hu B, Shi AM, Ma XC, Cheng YL, Chen P, et al. Cultivation of a microalga Chlorella vulgaris using recycled aqueous phase nutrients from hydrothermal carbonization process. Bioresource Technol. 2012;126:354-7.

[57] Nelson M, Zhu L, Thiel A, Wu Y, Guan M, Minty J, et al. Microbial utilization of aqueous co-products from hydrothermal liquefaction of microalgae Nannochloropsis oculata. Bioresource Technol. 2013;136:522-8.

[58] Uematsu M, Franck EU. Static Dielectric-Constant of Water and Steam. J Phys Chem Ref Data. 1980;9:1291-306.

[59] Bandura AV, Lvov SN. The ionization constant of water over wide ranges of temperature and density. J Phys Chem Ref Data. 2006;35:15-30.

[60] Demirbas A. Liquefaction of biomass using glycerol. Energ Source Part A. 2008;30:1120-6.

[61] Dote Y, Sawayama S, Inoue S, Minowa T, Yokoyama S. Recovery of Liquid Fuel from Hydrocarbon-Rich Microalgae by Thermochemical Liquefaction. Fuel. 1994;73:1855-7.

[62] Sawayama S, Inoue S, Dote Y, Yokoyama SY. Co2 Fixation and Oil Production through Microalga. Energ Convers Manage. 1995;36:729-31.

[63] Biller P, Ross AB. Potential yields and properties of oil from the hydrothermal liquefaction of microalgae with different biochemical content. Bioresource Technol. 2011;102:215-25.

[64] Ross AB, Biller P, Kubacki ML, Li H, Lea-Langton A, Jones JM. Hydrothermal processing of microalgae using alkali and organic acids. Fuel. 2010;89:2234-43.

[65] Valdez PJ, Tocco VJ, Savage PE. A general kinetic model for the hydrothermal liquefaction of microalgae. Bioresource Technol. 2014;163:123-7.

[66] Yu G, Zhang Y, Schideman L, Funk TL, Wang Z. Hydrothermal Liquefaction of Low Lipid Content Microalgae into Bio-Crude Oil. T Asabe. 2011;54:239-46.

[67] Biller P, Riley R, Ross AB. Catalytic hydrothermal processing of microalgae: Decomposition and upgrading of lipids. Bioresource Technol. 2011;102:4841-8.

[68] Minowa T, Yokoyama S, Kishimoto M, Okakura T. Oil Production from Algal Cells of Dunaliella-Tertiolecta by Direct Thermochemical Liquefaction. Fuel. 1995;74:1735-8.

[69] Yang C, Jia L, Chen C, Liu G, Fang W. Bio-oil from hydro-liquefaction of Dunaliella salina over Ni/REHY catalyst. Bioresour Technol. 2011;102:4580-4.

[70] Zhou D, Zhang LA, Zhang SC, Fu HB, Chen JM. Hydrothermal Liquefaction of Macroalgae Enteromorpha prolifera to Bio-oil. Energ Fuel. 2010;24:4054-61.

[71] Yang WC, Li XG, Liu SS, Feng LJ. Direct hydrothermal liquefaction of undried macroalgae

Enteromorpha prolifera using acid catalysts. Energ Convers Manage. 2014;87:938-45.

[72] Brown TM, Duan PG, Savage PE. Hydrothermal Liquefaction and Gasification of Nannochloropsis sp. Energ Fuel. 2010;24:3639-46.

[73] Shakya R, Whelen J, Adhikari S, Mahadevan R, Neupane S. Effect of temperature and Na2CO3 catalyst on hydrothermal liquefaction of algae. Algal Res. 2015;12:80-90.

[74] Vardon DR, Sharma BK, Blazina GV, Rajagopalan K, Strathmann TJ. Thermochemical conversion of raw and defatted algal biomass via hydrothermal liquefaction and slow pyrolysis. Bioresource Technol. 2012;109:178-87.

[75] Jena U, Das KC, Kastner JR. Effect of operating conditions of thermochemical liquefaction on biocrude production from Spirulina platensis. Bioresource Technol. 2011;102:6221-9.

[76] Liu ZA, Zhang FS. Effects of various solvents on the liquefaction of biomass to produce fuels and chemical feedstocks. Energ Convers Manage. 2008;49:3498-504.

[77] Mazaheri H, Lee KT, Bhatia S, Mohamed AR. Sub/supercritical liquefaction of oil palm fruit press fiber for the production of bio-oil: Effect of solvents. Bioresource Technol. 2010;101:7641-7.

[78] Ogi T, Minowa T, Dote Y, Yokoyama SY. Characterization of Oil Produced by the Direct Liquefaction of Japanese Oak in an Aqueous 2-Propanol Solvent System. Biomass Bioenerg. 1994;7:193-9.

[79] Yang Y, Gilbert A, Xu C. Production of Bio-Crude from Forestry Waste by Hydro-Liquefaction in Sub-/Super-Critical Methanol. Aiche J. 2009;55:807-19.

[80] Matsui TO, Nishihara A, Ueda C, Ohtsuki M, Ikenaga NO, Suzuki T. Liquefaction of micro-algae with iron catalyst. Fuel. 1997;76:1043-8.

[81] Jena U, Das KC, Kastner JR. Comparison of the effects of Na2CO3, Ca-3(PO4)(2), and NiO catalysts on the thermochemical liquefaction of microalga Spirulina platensis. Appl Energ. 2012;98:368-75.

Chapter 2

2. Catalytic hydrothermal liquefaction of microalgae using heterogeneous catalysts

Abstract

Due to exhaustibility of fossil fuels and their adverse effects on the environment, bio-oil has been considered as an alternative energy source for fuel applications. Currently, there are two main processes for bio-oil production: pyrolysis and hydrothermal liquefaction (HTL). In this chapter, HTL of microalgae is investigated at low temperatures and pressures. The hydrothermal liquefaction is defined as a biomass-to-liquid conversion route carried out in the hot compressed water with or without using a catalyst. The major concern in HTL is the high pressure of the process which results in a high capital cost of equipment in the industrial scale. Thus, the process pressure and temperature should be reduced. However, at low pressures and temperatures, the bio-oil yield is not high enough to make HTL an economical process for sustainable fuel production. This research investigates the applicability of a nanocatalyst (nano-Ni/SiO_2), an acid catalyst (synthesized zeolite), and an alkali catalyst (Na_2CO_3) to increase the bio-oil yield at low temperatures (210°C, 230°C, 250°C). The major result of this work was higher bio-oil yields with the order of nano-Ni/SiO_2 > zeolite > Na_2CO_3 in the hydrothermal liquefaction of microalgae Nannochloprosis sp.. The highest bio-oil yield (30.0 wt%) was obtained at 250°C by using Nano-Ni/SiO_2. Moreover, applying catalyst resulted in a decrease in the oxygen and the nitrogen contents of the bio-oil and consequently an increase in its heating value. The results of this research also suggest the possibility of nanocatalyst recovery for 2-3 times.

2.1. Background

As outlined in Chapter 1, the major concern in HTL is the high pressure of the process

which results in a high capital cost of equipment in the industrial scale. Also more expensive and elaborated safety systems are required. In this process, water is heated along its vapor–liquid saturation curve. Therefore, the pressure is determined by setting the temperature. In order to reduce the process pressure, the process temperature should be reduced, but at a lower temperature, the bio-oil yield is not high enough to make HTL economical for sustainable fuel production.

Catalysts can be used to increase the bio-oil yield in the hydrothermal liquefaction of microalgae [1-9]. Duan et. al. [1] investigated the catalytic hydrothermal liquefaction of Nannochloropsis sp. in the presence of six different catalysts (Pd/C, Pt/C, Ru/C, Ni/SiO_2-Al_2O_3, $CoMo/\gamma$-Al_2O_3, and zeolite). Experiments were conducted at 350°C. The major result was higher yields of the bio-oil. As an example, Ni/SiO_2-Al_2O_3 and zeolite increased the bio-oil yield from 35% up to 50% and 45%, respectively. Therefore, Ni/SiO_2-Al_2O_3 had better performance to increase the bio-oil yield compared to that of zeolite. Ross et. al. [2] has studied the hydrothermal liquefaction of Chlorella vulgaris and Spirulina for bio-oil production. Experiments were performed at 300°C and 350°C. Catalysts were employed, including the alkali (KOH and Na_2CO_3) and the organic acids (CH_3COOH and HCOOH). The major result was higher yields of crude bio-oil with the order of CH_3COOH > HCOOH > KOH > Na_2CO_3. Their work showed that acid catalysts had better performance to increase the bio-oil yield, however, a part of acid catalysts were consumed during the reaction.

Table 2.1 summarizes representative literature data on the catalytic hydrothermal liquefaction of microalgae. Although the bio-oil yield has increased, the mechanism of the catalytic liquefaction is still unknown. As it can be seen, most previous studies on the catalytic HTL were conducted at temperatures higher than 250°C, and more specifically higher than 300°C. Meanwhile, no research work has been performed on the application of nanocatalysts in the HTL process.

Table 2.1. Representative literature data on the catalytic hydrothermal liquefaction of microalgae

Catalyst	Species	Condition	Effects	Ref.
Pd/C, Pt/C, Ru/C, Ni/SiO_2-Al_2O_3, $CoMo/\gamma$-Al_2O_3, Zeolite	Nannochloropsis sp.	350°C, 60 min	Increased bio-oil yield from 35% to maximum 56% for Pd/C, Increased heating value	[1]
CH_3COOH, HCOOH, KOH, Na_2CO_3	Chlorella vulgaris, Spirulina	300-350°C, 60 min	Yield ranges from 6.4 % to 19.5%, Increased heating value, Decreased boiling point	[2]
Na_2CO_3	Dunaliella tertiolecta	280-380°C, 10-90 min	Increased bio-oil yield (highest bio-oil yield of 25.8 wt % at 360^{oC} with 5wt % Na_2CO_3)	[3]
Na_2CO_3	Spirulina platensis	300-350°C, 30-60 min	Increased bio-oil yield from 39.9% to 51.6% at 350°C and 60 min	[4]
NaOH	Chlorella pyrenoidosa	240-280°C, 30 min	Increased bio-oil yield by 10%	[5]
Ce/HZSM-5	Chlorella pyrenoidosa	300°C, 20 min	Increased bio-oil yield from 33% to 50%, Increased C and H content Decreased N content	[6]
Na_2CO_3	Microcystis viridis	300-340°C, 30-60 min	Increased bio-oil yield to 33%, Decreased O content	[7]
Na_2CO_3	Nannochloropsis, Pavlova, Isochrysis	250-350°C, 30-60 min	Increased bio-oil yield	[8]
H_2SO_4, CH_3COOH	Enteromorpha prolifera	230-290°C, 20 min	Highest bio-oil yield of 28.4 wt% at 290°C	[9]

Nanocatalysts have recently been used in different industries including fuel production from biomass. Nanocatalytic conversion of biomass to biofuel has been reported to improve the conversion yield [10]. In biomass gasification, the nanocatalysts have been used for tar removal and increasing the conversion yield under relatively mild conditions including nano-sized NiO [11] and Fe [12]. Nanocatalysts were also applied in biodiesel production

including Cs/Al/Fe_3O_4 nanocatalyst [13], nanocrystalline MgO [14], and nanocrystalline CaO [15]. Due to the background of using nanocatalyst in bioenergy production, we utilized a nanocatalyst (nano-Ni/SiO_2) in the hydrothermal liquefaction of microalgae to investigate its effects on the yield and the composition of the bio-oil. Two other types of catalysts (synthesized zeolite, and Na_2CO_3) were also applied. Since most previous studies on the catalytic HTL have been performed in temperatures higher than 250°C, we conducted experiment at temperatures lower than 250°C, and investigated the effects of the catalysts on the yield, the elemental composition, and the heating value. Meanwhile, recovery of the nanocatalyst was also investigated.

2.2. Experimental section

2.2.1. Materials

Microalgae

Nannochloprosis sp. in dried powder form was purchased from Xi'an Lyphar Biotech Co., Ltd and was used as received. Nannochloprosis sp. was selected in this research because of its high lipid content, high growth rate, and the ability to grow in saline water. The lipid content, the protein content, the proximate and ultimate analysis, and the higher heating value (HHV) of the microalgae are listed in Table 2.2. The data of the lipid content (21.9 %) and the protein content (40.5 %) were provided by the supplier. The proximate analysis was carried out by the thermal gravimetric analysis (TGA) (TGA-50, Shimadzu) from the ambient temperature to 900°C under 150 $ml.min^{-1}$ nitrogen flow. The temperature was raised from the ambient temperature to 105°C at 25°C.min^{-1} and was kept constant for 30 minutes. Then, it was raised again until 900°C at 50°C.min^{-1} and was kept constant for 20 minutes. Seven minutes after the temperature reached 900°C, the oxygen valve was opened to start combustion using 150 $ml.min^{-1}$ oxygen flow. The ultimate analysis was performed by the elemental analyzer (CHN: JM10, J-Science; O: Vario Micro Cube, Elementar Inc.; S: HSU-20, Yanaco). HHV was calculated by using Dulong's formula (equation 2.1) [16].

$$HHV\ \left(\frac{MJ}{kg}\right) = 0.338C + 1.428\left(H - \frac{O}{8}\right) + 0.095S \quad (2.1)$$

where C, H, O, and S are the weight percentages of carbon, hydrogen, oxygen, and sulfur, respectively.

Table 2.2. Characteristics of microalgae Nannochloropsis sp.

Lipid Content (wt%)	21.9
Protein content (wt%)	40.5
Proximate analysis (wt%)	
Moisture	2.6
Volatile material	81.6
Fixed carbon	11.3
Ash	4.4
Ultimate analysis (wt%)	
C	49.93
H	7.91
N	6.33
O	28.71
S	0.64
Cl	2.08
HHV (MJ/kg)	23.11

Catalysts

Nano-Ni/SiO_2 was employed as a nanocatalyst in this research. Two other types of catalyst (synthesize zeolite, Na_2CO_3) were also applied. Nano-Ni/SiO_2 (Surface area: 141.8 $m^2.g^{-1}$, % loading Ni: 20%) and zeolite (Type: Analcime, Surface area: 540 $m^2.g^{-1}$, Si/Al ratio: 2) were synthesized at University of Tehran (Tehan, Iran). Details about the catalyst synthesis methods and characterization have been explained elsewhere [17, 18]. Na_2CO_3 was purchased from Wako Chemicals (Tokyo, Japan). Ni was selected as it was reported to

increase the bio-oil yield in HTL of Nannochloprosis sp. at 350°C from 35% to 50% [1]. Zeolite, as an acidic catalyst, has been also applied for the hydrothermal liquefaction of microalgae and resulted in higher yields of the bio-oil [1]. Na_2CO_3, as an alkali catalyst, is one of the most common catalysts used in HTL. Na_2CO_3 can increase the bio-oil yield and reported to have deoxygenation effect [7].

In order to determine the nanocatalyst activity (in terms of the total acidity) temperature-programmed desorption of ammonia (NH_3-TPD) was conducted. Before the adsorption of ammonia, nanocatalyst was treated under helium at 500°C. Temperature was raised from 25°C to 500°C in 50 minutes and was kept constant for 60 minutes. The sample was then cooled to 100°C under He flow, then treated with an ammonia flow for 30 minutes at 100°C. The desorption of ammonia was run between 100°C and 600°C to allow the total evacuation of NH_3 molecules followed by an on-line gas chromatograph provided with a thermal conductivity detector. The value of the total acidity was calculated as 0.142 $mmol.g^{-1}$. The thermal stability of the nanocatalyst was investigated by the thermal gravimetric analysis (TGA) (TGA-50, Shimadzu) from the ambient temperature to 900°C under 150 $ml.min^{-1}$ nitrogen flow. The temperature was raised from the ambient temperature to 900°C at 10°C.min^{-1} and was kept constant for 30 minutes. Mass of nanocatalyst decreased during TGA which can be explained by desorption of moisture and other components adsorbed by silicate. Figure 2.1 shows the NH3-TPD and weight loss of the nanocatalyst calculated from TGA data.

Reactor

The hydrothermal liquefaction was carried out in a 500 ml batch reactor (model MMJ500) purchased from OM Labtech (Japan). The 316 stainless steel reactor is equipped with an automated stirrer, an electric heater, a temperature controller, and a quartz-made sample tube (Figure 2.2) which can be used up to 300°C and 20 MPa.

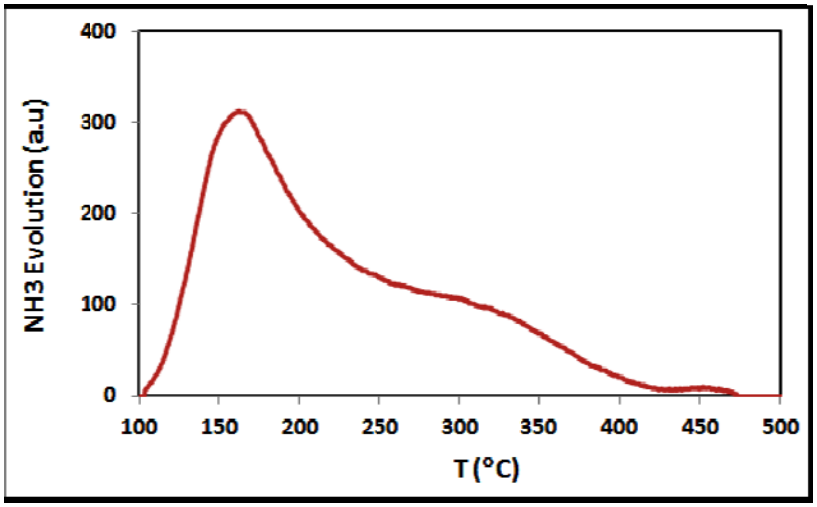

(a): NH_3-TPD

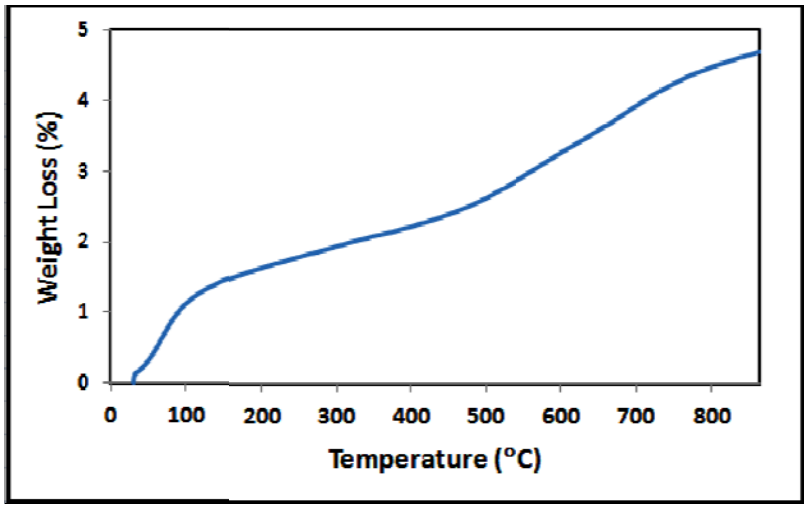

(b): Weight loss calculated from TGA data

Figure 2.1. Nanocatalyst characterization

2.2.2. Experimental procedure

In each experimental run, 10 g of dried microalgae was introduced into the sample tube of the reactor followed by adding 150 ml deionized water. Deionized water was produced in-house. In experimental runs including catalyst, 0.5 g catalyst (5 wt%) was also loaded into the sample tube. The air inside the reactor was purged by argon gas to avoid combustion inside the reactor. The reactor was then heated from the ambient temperature to the desired temperatures (210°C, 230°C, and 250°C) at an average heating rate of 6°C/min. The

automated stirrer was used at a constant stirring rate of 200 rpm to keep the temperature uniform inside the sample tube. After reaching the set point temperature, the sample was kept inside the reactor for 60 minutes holding time. Once the holding time was completed, the temperature was set to the ambient temperature to cool down the reactor.

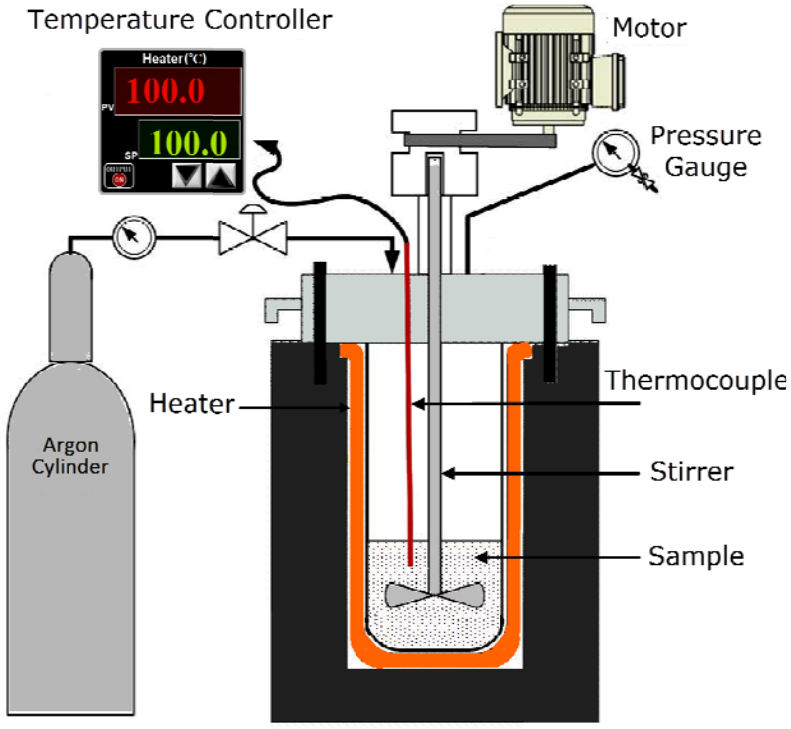

Figure 2.2. Schematic diagram of the HTL reactor

After cooling down, the reactor was depressurized before opening. The product was collected and mixed with 150 ml dichloromethane (DCM) (Sigma-Aldrich, 99% purity). The aim of adding DCM is the extraction of organic components from both liquid and solid products. Therefore, bio-oil is also defined as the DCM-soluble fraction [19]. The mixture was then filtered by a glass filter connected to a vacuum pump. The filter paper, used in the glass filter, was a 2.7 µm pore size microfiber filter paper (GF/D, Whatman). The filter cake is called solid residue and two immiscible liquid phases (DCM soluble, water soluble) were separated by a separation funnel. The DCM was evaporated by using a rotary evaporator

under a vacuum of about 1 kPa at 35°C for 20 minutes. The bio-oil was obtained after the evaporation of DCM and had a dark color and high viscosity. During the evaporation of DCM, some light components of the bio-oil were lost which is reported to be less than 3% of the total mass of the bio-oil [20]. Figure 2.3 represents the overall experimental procedure for the separation of the products.

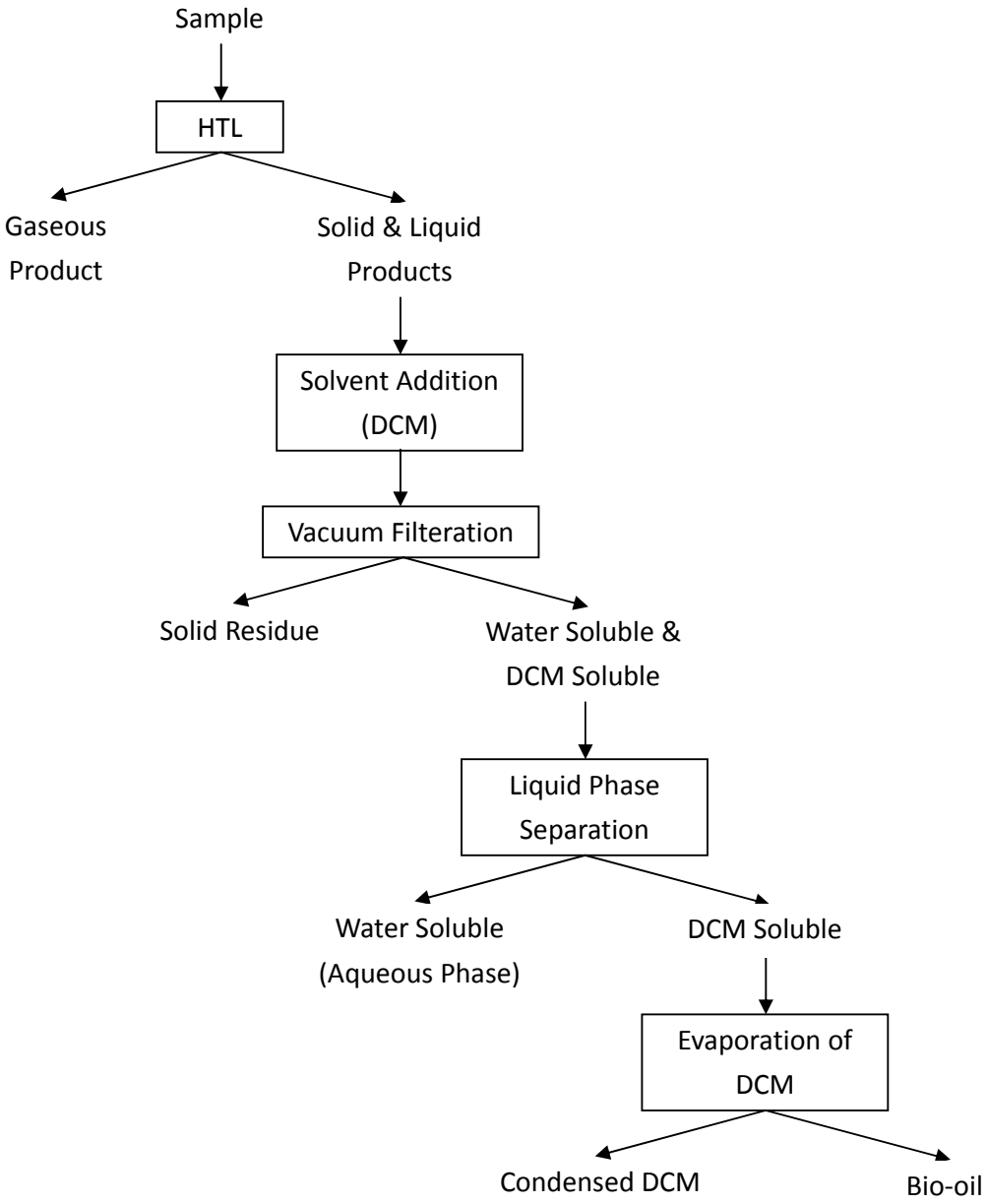

Figure 2.3. Product recovery and separation procedure

2.2.3. Catalyst recovery

After HTL experiment, it is important to recover the catalyst especially if the catalyst is expensive. In this work, recovery of the nanocatalyst from the solid residue was conducted following two different approaches.

Solid residue is one of the products in HTL of the microalgae. If the solid residue is used as a by-product, it can improve the economic feasibility of the whole process. Since HTL experiment is conducted at low temperatures, there is a possibility that the solid residue still contains hydrocarbons, and consequently it can be used as a potential solid fuel. The idea of burning the solid residue as a solid fuel will be also helpful in the process of catalyst recovery. After burning the solid residue, which contains solid catalysts, catalyst particles can be separated and recovered from the ash.

Therefore, in order to recover nano-Ni/SiO_2, the solid residue from the catalytic HTL experiment (conducted at 210°C) was burnt in a furnace at 550°C for 2 h. The elemental composition and the heating value of the solid residue are shown in Table 2.3. After then, nano-Ni/SiO_2 was separated from the ash by using a sieve since the particle sizes were different. However, not the whole nanocatalyst particles were recovered. The recovered nano-Ni/SiO_2 was employed in the HTL of Nannochloprosis sp. to investigate its activity for the bio-oil production. No new nanocatalyst was employed.

In the second approach, the mixture of the ash and catalyst particles was returned to the reactor after burning the solid residue. No separation of the ash and catalyst was conducted because part of the catalyst was lost during separation from the ash. The results of the catalyst recovery will be presented in section 2.3.4.

Table 2.3. Elemental composition and heating value of the solid residue from the HTL of Nannochloprosis sp. (Catalyst: nano-Ni/SiO_2, Temperature: 210°C)

Ultimate analysis (wt%)	
C	54.89
H	6.42
N	5.98
O	21.79
S	0.50
Ash	10.40
HHV (MJ/kg)*	23.88

*: Calculated by the equation (2.1).

2.2.4. Analysis

The proximate and ultimate analysis results of the microalgae were presented in Table 2.2, and the equipment and the procedure used, were explained in the section 2.2.2. After the DCM evaporation, the bio-oil was weighted to calculate the bio-oil yield by equation (2.2). Energy Recovery (ER) was calculated by the equation (2.3).

$$\text{Bio} - \text{oil Yield } (\%) = \frac{\text{Mass of Bio} - \text{oil (g)}}{\text{Mass of Dried Microalgae (g)}} * 100\% \quad (2.2)$$

$$\text{Energy Recovery } (\%) = \frac{(\text{Mass} * \text{HHV})_{\text{Bio-oil}}}{(\text{Mass} * \text{HHV})_{\text{Microalgae}}} * 100\% \quad (2.3)$$

However, there are other definitions for the bio-oil yield in the literature [21] but in the present article, equation (2.2) was used to calculate the bio-oil yield.

The ultimate analysis of the bio-oil was performed by the elemental analyzer. HHV was calculated by using Dulong's formula (equation 2.1). Bio-oil was also analyzed by GC/MS (GCMS-QP2010 SE, Shimadzu Inc.). The separation was achieved by using a Rtx-5MS capillary

column, 30 m long, 0.25 mm ID, and 0.25 µm film thickness. The initial oven temperature was set at 40°C for 10 minutes, ramped to 60°C at 2°C/min, followed by ramping to 300°C at 4°C/min and was held constant for 10 minutes. The sample injection volume was 1 µL and the column head pressure was set to 63.9 kPa. It is worthwhile to mention that not all of the components in the bio-oil can be identified by GC/MS. Lighter components were lost during DCM evaporation, and very heavy components were not probably eluted from the GC column [16].

2.3. Results and discussion

This section provides the results of the hydrothermal liquefaction of Nannochloprosis sp. at the temperatures of 210°C, 230°C, and 250°C by applying three different types of catalysts (Nano-Ni/SiO_2, zeolite, Na_2CO_3) regarding to the bio-oil yield, the elemental composition, the heating value, and the GC/MS results.

2.3.1. Bio-oil yield

The bio-oil yield is defined as the mass of the bio-oil divided by the mass of the dried algae (equation 2.2). Figure 2.4 shows the bio-oil yields at 210°C, 230°C, and 250°C for all types of catalysts as well as the blank experiment where no catalyst was applied. For the blank experiment, the bio-oil yields at 210°C, 230°C, and 250°C were 11.8%, 17.0%, and 20.2% which shows an increasing trend by increasing the reaction temperature. This trend can be seen in the catalytic experiment where the bio-oil yield increased by an increase in the reaction temperature. The maximum yield was 30.0% obtained by the Nano-Ni/SiO_2 catalyst at 250°C. Except at 250°C, the bio-oil yield in the experiments using the acid catalyst (zeolite) was higher than that of the alkali catalyst (Na_2CO_3). The yields of the bio-oil followed the general trend of nano-Ni/SiO_2 > zeolite > Na_2CO_3 > blank.

Previous works on HTL of microalgae have shown that catalysts can generally increase the

bio-oil yield as summarized in Table 2.1. However, there are contradictions among the results. Na_2CO_3 is the most commonly used catalyst and there are enough data to evaluate its performance. Dote et. al. [22] reported that Na_2CO_3 could increase the bio-oil yield in HTL of Botryococcus braunii at 300°C compared to the non-catalytic condition. However, the bio-oil yield in the catalytic experiment was lower than that of the non-catalytic experiment at 340°C. In contrast, Yang et. al. [7] showed that Na_2CO_3 could increase the bio-oil yield in HTL of Microcystis viridis at both 300°C and 340°C compared to the non-catalytic condition. These inconsistent results may be due to the differences in microalgae species. Different microalgae species have different biochemical compositions which respond differently to the presence of a catalyst as investigated by [19]. Not only the temperature range, but also the holding time has been reported to affect the catalytic performance of Na_2CO_3. Minowa et. al. [23] employed Na_2CO_3 in HTL of Dunaliella tertiolecta. At 250°C, applying Na_2CO_3 resulted in an increae in the bio-oil yield after 5 minutes holding time, but a decrease in the bio-oil yield was observed after 60 minutes holding time. At 300°C, using Na_2CO_3 resulted in a decrease after 5 minutes holding time, but an increase after 60 minutes holding time.

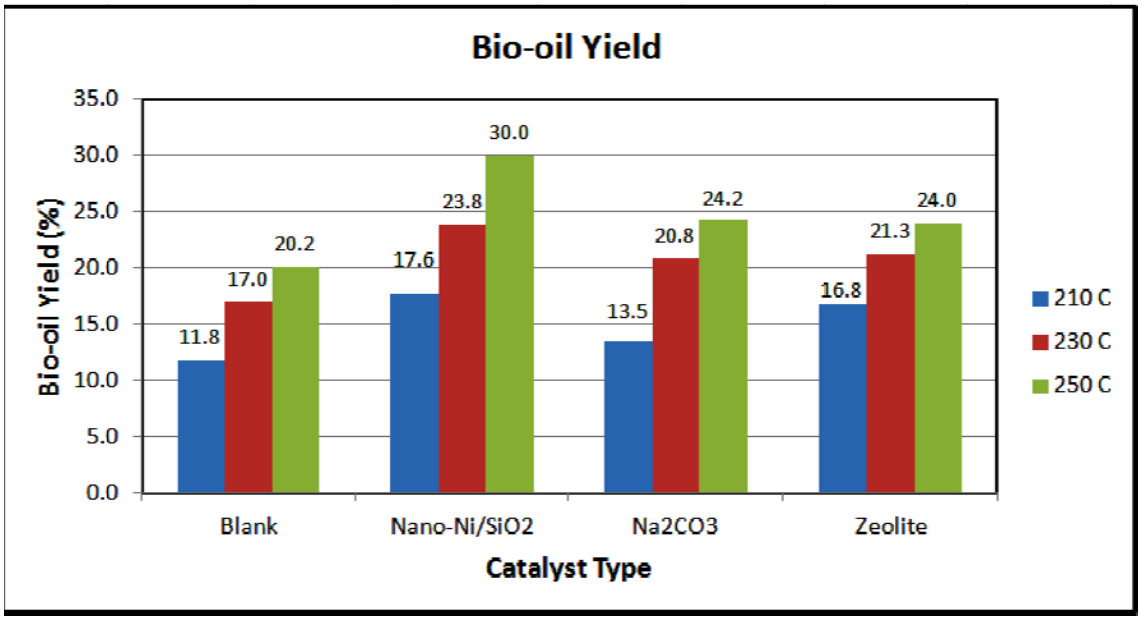

Figure 2.4. Bio-oil yields (average value)

Other than the bio-oil yield, it is worthwhile to investigate the effect of catalysts on the conversion yield of other products (i.e. solid, aqueous, and gaseous co-products) of the HTL process. Figure 2.5 presents the yields of the bio-oil, solid, aqueous, and gaseous products from non-catalytic and catalytic experiments at 210°C. Two major differences can be distinguished in the yields of products from non-catalytic and catalytic experiments. (i) The yield of the solid phase from the Na_2CO_3 experiment is higher than that of other experiments. A possible explanation could be the soap formation. In fact, fatty acids react with alkali to form soap in the solid phase. More explanations are provided in section 2.3.3. (ii) The yield of the gaseous phase from the Nano-Ni/SiO_2 experiment has the highest value among non-catalytic and catalytic experiments. This result is consistent with previous research that Ni catalyst increased the production of hydrogen gas and promoted gasification in HTL of microalgae [1, 4].

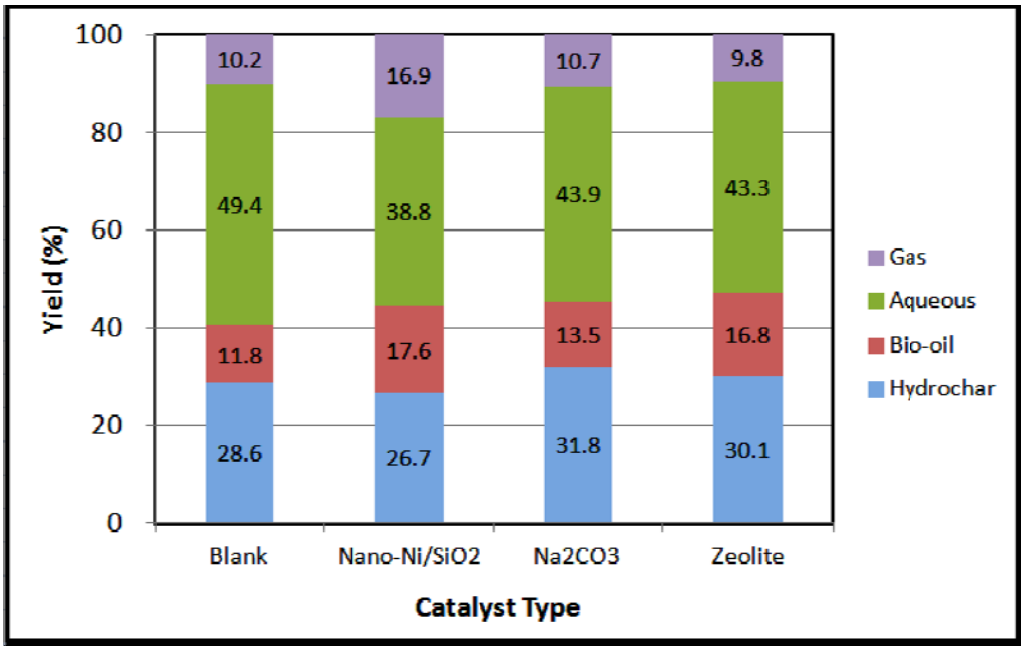

Figure 2.5. Yields of the bio-oil and co-products (Temperature: 210°C)

Even though, the catalyst can generally increase the bio-oil yield, it also adds cost to the process. Since the solid catalyst remains in the solid residue, separation and recycling of the

catalyst from the solid residue is a challenge. In this work, catalyst recovery experiment was also conducted and the results will be explained in section 2.3.4.

2.3.2. Elemental composition, heating value, energy recovery

The ultimate analysis, atomic ratios, HHV, and Energy Recovery (ER) of the bio-oil produced at 210°C, 230°C, and 250°C without using catalyst are listed in Table 2.4. The elemental composition and HHV of the microalgae and the crude oil are also presented to compare with those of the bio-oil.

The C and H contents of the bio-oil were higher than 70% and 10%, respectively, and also higher than those of the microalgae at all temperature levels. However, the C content of the bio-oil was less than the C content of the crude oil which is typically in the range of 83-87%. The O, N, and S contents of the bio-oil were lower than those of the microalgae, which shows that HTL had deoxygenation, denitrogenation, and desulfurization effects. However, the O, N, and S contents of the bio-oil were still higher than that of the crude oil which necessitates upgrading of the bio-oil to remove heteroatoms. The heating value of the bio-oil was in the range of 36.16 - 37.20 $MJ.kg^{-1}$ which was higher than that of the microalgae (23.08 $MJ.kg^{-1}$).

Changing of the temperature had different effects on the elemental composition of the bio-oil. By increasing the temperature, the C and H contents showed a gradual increase. The N content increased by increasing the temperature from 3.77% to 5.13%. Since nitrogen comes from protein, it provides evidence that decomposition of protein was accelerated by increasing the temperature from 210°C to 250°C. The oxygen content of the bio-oil decreased from 13.80% to 10.88% by increasing the temperature. This reduction in the oxygen content can be explained by the decarboxylation mechanism which will be discussed later in section 2.3.3. The heating value increased from 36.16 $MJ.kg^{-1}$ to 37.20 $MJ.kg^{-1}$ by increasing the temperature as a result of the reduction in the oxygen content, however, it

was still lower than that of the crude oil (42.7 $MJ.kg^{-1}$). The S content of the bio-oil was very low since the S content of the microalgae itself is very low, and it did not show any specific trend with the temperature change. The atomic ratio of H/C did not show any specific trend with temperature change, but the O/C decreased from 0.14 to 0.11 as a result of the decrease in the oxygen content and the increase in the carbon content. The atomic ratio of N/C increased by increasing the temperature from 0.045 to 0.061 as the nitrogen content increased faster than the carbon content. ER increased with the temperature increase from 18.48% to 32.49% as both the bio-oil yield and HHV increased along with the temperature increase.

Table 2.4. Elemental composition, atomic ratios, heating value, and energy recovery of the bio-oil (Catalyst: None, Temperatures: 210°C, 230°C, 250°C)

	C	H	N	O	S	H/C	O/C	N/C	HHV (MJ/kg)	ER (%)
Microalgae	49.93	7.91	6.33	28.71	0.64	1.90	0.43	0.109	23.11	
Bio-oil										
210°C	71.81	10.02	3.77	13.80	0.42	1.67	0.14	0.045	36.16	18.48
230°C	72.47	10.02	4.70	11.71	0.40	1.66	0.12	0.056	36.75	27.05
250°C	72.65	10.19	5.13	10.88	0.42	1.68	0.11	0.061	37.20	32.49
Crude Oil	83-87	10-14	0.1-2	0.1-1.5	0.5-6				42.7	

The ultimate analysis, the atomic ratios, HHV, and Energy Recovery (ER) of the bio-oil produced at 210°C by using different types of catalysts (Nano-Ni/SiO_2, Zeolite, Na_2CO_3) are listed in Table 2.5.

The C and H contents of the bio-oil from the catalytic HTL were higher than 73% and 10%, respectively, and also higher than those of the blank experiment, however, still less than that of the crude oil. The O, N, and S contents of the bio-oil from the catalytic HTL were lower than those of the blank experiment. Even though the difference in the O, N, and S contents of the bio-oil was not considerable, one could come to the conclusion that catalysts could

contribute to reduce the number of heteroatoms in the bio-oil. However, the O, N, and S contents of the bio-oil were still higher than that of the crude oil. The heating value of the bio-oil was in the range of 37.93 - 38.31 $MJ.kg^{-1}$ which was higher than that of the blank experiment (36.16 $MJ.kg^{-1}$) as a result of a lower O content. The ER was in the range of 22.45% to 28.94%, which was higher than that of the blank experiment at 210°C (18.48%).

The C content of the bio-oil obtained from the catalytic HTL was in the range of 73 - 74 %. The use of the zeolite resulted in the highest C content (73.37%), however, the difference in the C content was not considerable. Meanwhile, the zeolite resulted in the highest H content (11.01%) and the lowest S content (0.31%) in the bio-oil compared to other catalysts, while, the difference was still negligible. The using of the alkali catalyst resulted in the highest N content (3.67%) in the catalytic HTL which was very close to the N content of the blank experiment (3.77%). On the other hand, Na_2CO_3 resulted in the lowest oxygen content (12.07%) which is consistent with the previous work [24].

The atomic ratios of O/C and N/C for the bio-oil obtained from Nano-Ni/SiO_2 were similar with the zeolite catalyst. The use of Na_2CO_3 resulted in the lowest O/C ratio (0.12) and the highest N/C ratio (0.044) compared to the other catalysts because of a lower O content and a higher N content. The heating value of the bio-oil obtained from Na_2CO_3 had the highest value (38.31 $MJ.kg^{-1}$) as a result of a lower oxygen content. ER of the bio-oil obtained at 210°C by using Nano-Ni/SiO_2 showed the highest value of 28.94% because of the highest bio-oil yield.

Similar to the bio-oil yield, there is an inconsistency among the results for N content of the bio-oil using Na_2CO_3 as a catalyst. In Minowa et. al. [23] work, the N content of the bio-oil increased in most experimental conditions applying Na_2CO_3 compared to non-catalytic experiment. However, Yang et. al. [7] reported a decrease in the bio-oil nitrogen content after 60 minutes holding time using Na_2CO_3.

Table 2.5. Elemental composition, atomic ratios, heating value, and energy recovery of the bio-oil (Temperature: 210°C, Catalyst: None, Nano-Ni/SiO_2, Zeolite, Na_2CO_3)

	C	H	N	O	S	H/C	O/C	N/C	HHV (MJ/kg)	ER (%)
Microalgae	49.93	7.91	6.33	28.71	0.64	1.90	0.43	0.109	23.11	
Catalyst										
None	71.81	10.02	3.77	13.80	0.42	1.67	0.14	0.045	36.16	18.48
Nano-Ni/SiO_2	73.14	10.84	2.97	12.87	0.32	1.78	0.13	0.035	37.93	28.94
Na_2CO_3	73.32	10.96	3.76	12.07	0.33	1.79	0.12	0.044	38.31	22.45
Zeolite	73.37	11.01	2.99	12.62	0.31	1.80	0.13	0.035	38.30	27.88
Crude Oil	83-87	10-14	0.1-2	0.1-1.5	0.5-6				42.70	

2.3.3. Component analysis

The bio-oil is a complex mixture of several hundreds of organic compounds which are products of the decomposition of biomolecules constructing microalgae including lipid, protein, and carbohydrate. As an example, lipids can be hydrolyzed to fatty acids in subcritical water. Microalgae also contains cholesterol, which results in the presence of the cholesterol and its derivative in the bio-oil. As the HTL process temperature increases, fatty acid can be decomposed into alkane and carbon dioxide which is called the decarboxylation reaction (equation 2.4). As oxygen is removed in the form of CO_2, the decarboxylaion has the deoxygenation effect. Therefore, a higher temperature results in a lower oxygen content of the bio-oil and consequently a higher heating value.

$$\mathrm{R-COOH} \rightarrow \mathrm{R-H} + \mathrm{CO_2} \qquad (2.4)$$

The hydrolysis of protein produces N-containing components such as amide, amine, pyrrole, and pyrazine. The hydrolysis of carbohydrate can produce a wide range of O-containing components such as aromatic like phenol and its derivatives. As the reaction progresses, protein derivatives and carbohydrate derivatives can react to form heterocyclic components like pyrazine and pyrrole derivatives [25]. The decomposition of chlorophyll

produces chlorophyll derivatives like phytol and phytane as well as nitrogen-containing heterocyclic compounds like indole [26].

In this research, the bio-oil was analyzed by GC/MS to identify its components. The parameters used in GC-MS analysis were described in section 2.2.4. Figure 2.6 shows chromatograms for the blank and catalytic experiment at 210°C. Several major components are presented on the chromatogram. Tables 2.6 - 2.9 present the name and area % of the 30 major components at 210°C.

For the blank experiment (Figure 2.6.(a); Table 2.6), the highest peak is related to n-hexadecanoic acid (palmitic acid, C16:0). Other fatty acids with different carbon numbers (C16:1, C14:0; C18:1; C20:5) are amongst the major components. The bio-oil also contains cholesterol, phytol, N-containing components (e.g. pyrazine derivative, pyrrole derivative, amide), alkene, alkane, and cycloalkane. Long chain fatty acids and alkane in the bio-oil can lead to the bio-oil with high viscosity.

For Nano-Ni/SiO_2 experiment (Figure 2.6.(b); Table 2.7), the highest peak is still related to n-hexadecanoic acid (palmitic acid, C16:0) followed by palmitoleic acid (C16:1). Similar to the blank experiment, different components are present in the bio-oil including N-containing components, alkane, alkyne and ester. Based on the qualitative analysis, major components in the bio-oil from blank experiment and Nano-Ni experiment are very similar, but with different area%. As an example, the area% for palmitic acid is 32.31% for the nanocatalyst experiment, but it equals 23.45% for the blank experiment. The total peak area for fatty acids in the blank experiment (57.22%) is lower than that of the nanocatalyst experiment (64.92%). Also, some minor components are different. For example, ester is among 30 major components in the bio-oil using nano-Ni/SiO_2, but it is not present in the major components of the bio-oil from blank experiment. It should be noted that qualitative analysis only gives an estimate of component mass fractions, and quantitative analysis is necessary to obtain

the precise amount of those quantities which is not in the scope of this thesis.

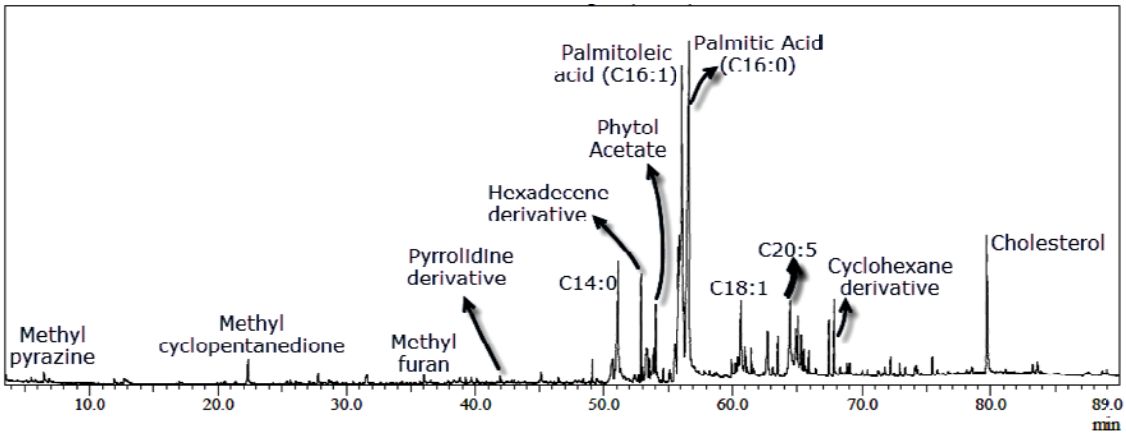

(a)

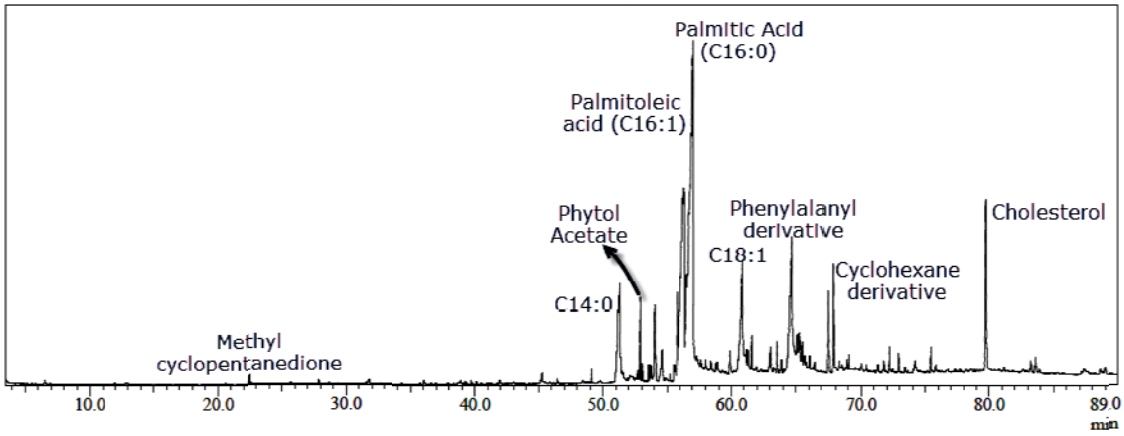

(b)

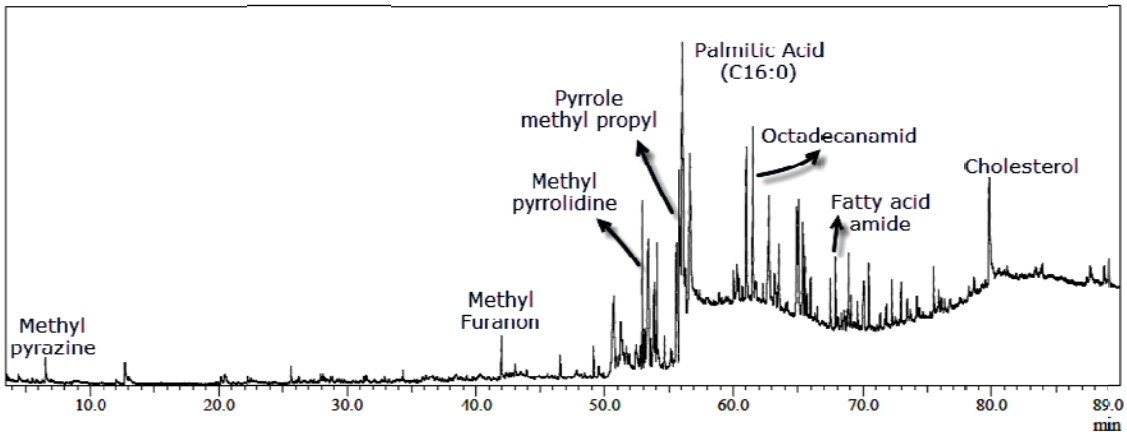

(c)

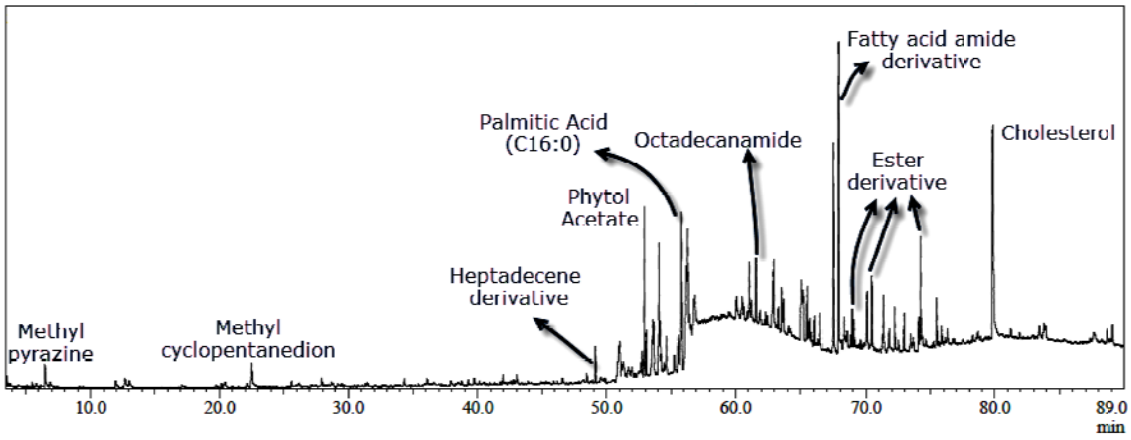

(d)

Figure 2.6. GC/MS of the bio-oil at 210°C for (a) Catalyst: Blank; (b) Catalyst: Nano-Ni/SiO_2; (c) Catalyst: Na_2CO_3; (d) Catalyst: Zeolite

Table 2.6. Major components of the bio-oil at 210°C for blank experiment

Peak#	Name	Area %	Peak#	Name	Area %
1	n-Hexadecanoic acid (C16:0)	23.45	16	Phenylalanyl derivative	1.34
2	cis-9-Hexadecenoic acid (C16:1)	19.49	17	Methylpiperazine derivative	1.27
3	Tetradecanoic acid (C14:0)	5.68	18	Piperazinedione derivative	0.99
4	Oleic acid (C18:1)	4.51	19	Butane derivative	0.97
5	Eicosapentaenoic acid (C20:5)	4.09	20	Phenylalanyl derivative	0.93
6	Cholesterol	4.09	21	1,2-Cyclopentanedione	0.71
7	Phytol acetate	3.15	22	Pyrrole derivative	0.69
8	Piperazinedione derivative	1.97	23	Hexadecanamide	0.55
9	Pyrazine derivative	1.87	24	Piperazinedione derivative-	0.54
10	Phenylalanyl derivative	1.85	25	Pyrrole derivative	0.46
11	2-Hexadecene derivative	1.83	26	Piperazinedione derivative	0.44
12	1-(3-Methylbutyryl) pyrrolidine	1.74	27	Phytol	0.43
13	Piperazinedione derivative	1.58	28	Hexadecen derivative	0.42
14	1,3,5-Trisilacyclohexane	1.37	29	Fucosterol	0.39
15	Pyrrole derivative	1.34	30	Pyrrole derivative	0.38

Table 2.7. Major components of the bio-oil at 210°C for the catalytic experiment (Nano-Ni/SiO_2)

Peak#	Name	Area %	Peak#	Name	Area %
1	n-Hexadecanoic acid (C16:0)	32.31	16	Piperazine derivative	0.98
2	cis-9-Hexadecenoic acid (C16:1)	14.61	17	Phytol acetate	0.95
3	Docosahexaenoic acid	8.50	18	Methyl piperazinedione derivative	0.90
4	Oleic Acid (C18:1)	5.72	19	Hexadecanamide	0.87
5	Cholesterol	3.79	20	Acetate derivative	0.65
6	Tetradecanoic acid (C14:0)	3.38	21	Piperazinedione derivative	0.57
7	Phenylalanyl derivative	2.45	22	Tridecanoic acid ethyl ester	0.52
8	Phenylalanyl derivative	1.80	23	Methyldodecanamide	0.51
9	1,3,5-Trisilacyclohexane	1.73	24	Pyrazine derivative	0.48
10	Acetic acid derivative	1.64	25	Phytol	0.46
11	Piperazinedione derivative	1.43	26	2,5-Piperazinedione derivative	0.44
12	Isophytol	1.29	27	Pyrrole derivative	0.43
13	Butane derivative	1.25	28	Eicosapentaenoic acid, methyl ester	0.43
14	3-Eicosyne (Alkyne)	1.21	29	Pyrrole derivative	0.42
15	Octadecenamide	1.04	30	Octadecanoic acid (C18:0)	0.40

For Na_2CO_3 experiment (Figure 2.6.(c); Table 2.8), the area% for fatty acids is less than that of the blank and Nano-Ni/SiO_2 experiments. Possible explanation could be (i) neutralization of fatty acids by alkali catalyst or (ii) soap formation. In fact, fatty acids react with alkali to form soap in the solid phase. In contrast, the area% of N-containing components (e.g. pyrrole derivative, pyrrolidine derivative, piperazinedione derivative, and octadecanamide derivative) is higher than that of the nanocatalyst and zeolite experiment. From Table 2.8, it can be seen that the highest area% belongs to N-containing component (pyrrole derivative). Having more N-containing components is consistent with CHNOS results where the bio-oil from Na_2CO_3 experiment has the highest nitrogen content in the catalytic experiment.

Table 2.8. Major components of the bio-oil at 210°C for the catalytic experiment (Na_2CO_3)

Peak#	Name	Area %	Peak#	Name	Area %
1	Pyrrole derivative	11.64	16	Phenylalanyl derivative	1.79
2	n-Hexadecanoic acid (C16:0)	8.70	17	Hexadecen derivative	1.70
3	Pyrrolidine derivative	5.00	18	Piperazinedione derivative	1.63
4	Pyrrole derivative	3.45	19	Acetic acid ester derivative	1.23
5	Piperazinedione derivative	3.31	20	Eicosapentaenoic acid, methyl ester-	1.23
6	Tocopheryl acetate	3.25	21	Piperazinedione derivative	1.11
7	Piperazinedione derivative	3.08	22	Imidazolidinedione derivative	1.03
8	Octadecanamide derivative	2.79	23	Fatty acid amide derivative	1.01
9	Octadecenamide derivative	2.73	24	Acetic acid derivative	0.90
10	Isophytol	2.72	25	Piperazinedione derivative	0.88
11	Phenylalanyl derivative	2.61	26	Octadecenamide derivative	0.86
12	Heptadecandione derivative	2.42	27	Phytol, acetate	0.82
13	Pyrrole derivative	2.21	28	Piperazine derivative	0.81
14	Heptadecandione derivative	2.05	29	Pyrrole derivative	0.73
15	Hexadecen derivative	2.01	30	1-Heptacosanol	0.72

Figure 2.6.(d) shows the chromatogram for the bio-oil from zeolite experiment. Table 2.9 represents the name and area% of the 30 major components. Contrary to the blank experiment, the highest area% does not belong to palmitic acid. In fact, the area% of fatty acid in the zeolite experiment is lower than that of the blank experiment. One possible explanation could be the esterification of fatty acid to the ester in the presence of the acid catalyst, i.e. zeolite. The presence of the hexanoic acid ester among 30 major components could be an evidence of the esterification of the hexanoic acid catalyzed by the acid catalyst.

Another distinguished difference in the GC-MS chromatograms is the presence of fatty acid amide derivatives in the Na_2CO_3 and zeolite experiments. Fatty acid amides are produced by a reaction between free fatty acids (from algal lipid) and amine (from algal protein). Amines are the products of the amino acid decomposition in HTL process. Li and

Brill [27] have shown that the decomposition of several types of amino acids was accelerated under acidic and alkali conditions, which leads to an increase in the amine production. The amine can react with other components including fatty acid to form fatty acid amide derivatives. Figure 2.7 presents a summary of the components formed by HTL of Nannochloprosis sp..

Table 2.9. Major components of the bio-oil at 210°C for the catalytic experiment (Zeolite)

Peak#	Name	Area %	Peak#	Name	Area %
1	Cholesterol	9.32	16	Acetic acid ester derivative	1.46
2	Pyrrole derivative	8.40	17	Phenylalanyl derivative	1.42
3	Fatty acid amide derivative	6.59	18	Tetradecanamide	1.41
4	Dimethybutane derivative	4.43	19	Pyrrole derivative	1.41
5	Isophytol	3.93	20	9-Octadecenamide	1.30
6	Phytol, acetate	2.85	21	n-Hexadecanoic acid (C16:0)	1.27
7	3-Eicosyne (alkyne)	2.68	22	Methylpiperazine derivative	1.25
8	Docosahexaenoic acid, methyl ester	2.53	23	5,8-Tridecadione	1.25
9	Piperazinedione derivative	2.49	24	Hexanoic acid ester	1.17
10	Phenylalanyl derivative	2.38	25	Piperazinedione derivative	1.04
11	Octadecanamide	1.81	26	Pyrazine derivative	1.02
12	Hexadecen-1-ol derivative	1.63	27	(Z)-14-Tricosenyl formate	0.95
13	Dimethyl butane derivative	1.58	28	Tridecanoic acid, 2-ethyl-2-methyl-, ethyl ester	0.93
14	Acetate derivative	1.48	29	Piperazinedione derivative	0.91
15	7-Ethyl-4,6-heptadecandione	1.47	30	1-Heptacosanol	0.91

2.3.4. Catalyst recovery and re-use

In this research, it was shown that the use of solid catalysts, including nano-Ni/SiO_2 catalyst can increase the bio-oil yield and decrease its oxygen and nitrogen contents. On the other hand, using catalyst will increase the process cost. Thus, it is important to recover and re-use the solid catalyst, especially if the catalyst is expensive. In this work, recovery of the nanocatalyst from the solid residue was conducted following two different approaches

which were explained in section 2.2.3.

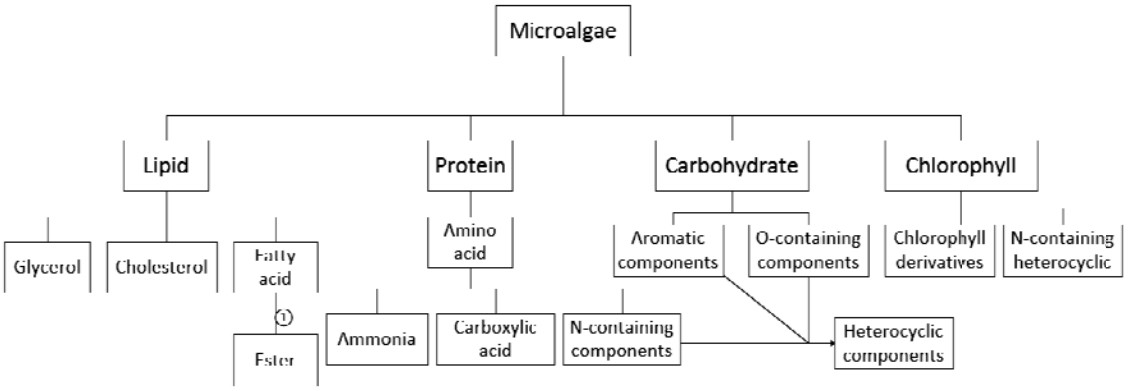

[1]: promoted by the zeolite catalyst

Figure 2.7. Components produced by HTL of Nannochloprosis sp.

Table 2.10 presents the percentage of the nanocatalyst recovered after each recycling step using the first approach. As can be seen from Table 2.10, 62% and 18% of the original nano-Ni/SiO_2 was recovered in the first and the second recycling efforts. Meanwhile, in the third recycling effort, no nano-Ni/SiO_2 was recovered. It seems that during the HTL process, nano-Ni/SiO_2 particles were crushed. Consequently, it couldn't be separated from the ash by using the sieve because of the reduction in the particle size.

Table 2.10. Percentage/amount of the recovered nano-Ni/SiO_2 catalyst in the recovery process

Experiment	Catalyst Recovered	
	Mass	%
Original	0.5 g (500 mg)	100%
1st Recycle	0.31 g (310 mg)	62%
2nd Recycle	0.09 g (90 mg)	18%
3rd Recycle	0	0%

The recovered catalyst was then used in the HTL of Nannochloprosis sp. at 210°C. The bio-oil yields for the experiment using recovered catalyst are shown in Figure 2.8. The bio-oil yield for the recovered catalyst was lower than that of the original experiment but higher than that of the non-catalytic experiment. This reduction of the bio-oil yield can be due to either the reduction of the mass or deactivation of the recovered nanocatalyst or both.

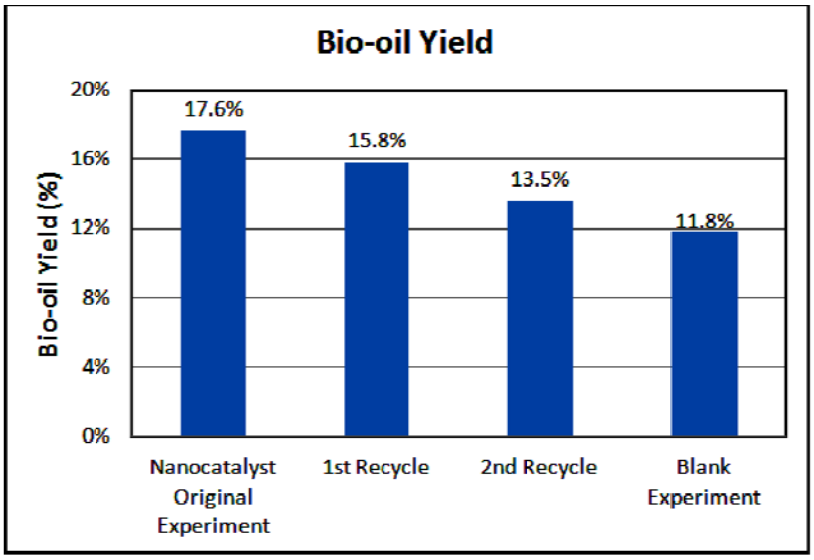

Figure 2.8. Bio-oil yields (nanocatalyst recovery experiment at 210°C, separation of the catalyst particles from the ash)

Since there was a dramatic reduction in the bio-oil yield compared to the original nano-Ni/SiO_2 experiment, another approach was employed in the catalyst recovery step. In the second approach, the mixture of the ash and catalyst particles was returned to the reactor after burning the solid residue. No separation of the ash and catalyst was conducted because part of the catalyst was lost during separation from the ash. Figure 2.9 presents the bio-oil yields for the experiment using recovered catalyst in the second approach. Although, there was a reduction in the bio-oil yield due to the nanocatalyst deactivation, the results were more promising in comparison with the first approach. The second approach of the nanocatalyst recovery may suggest the recycling of the nanocatalsyt for 2 or 3 times; and could reduce the burden of the nanocalyst price for the whole process.

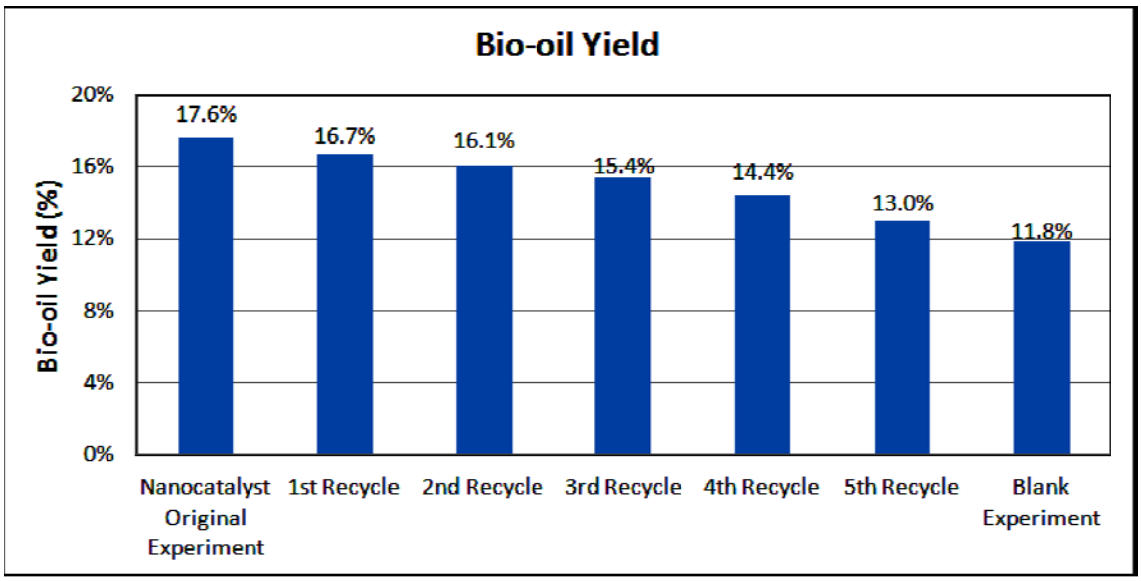

Figure 2.9. Bio-oil yields (nanocatalyst recovery experiment at 210°C, mixture of the ash and nanocatlyst particles was used without separation)

2.4. Conclusions

In this chapter, the catalytic hydrothermal liquefaction of Nannochloprosis sp. was carried out at low temperatures (210°C, 230°C, 250°C). Nanocatalyst (Nano-Ni/SiO_2) was applied to investigate its effects on the bio-oil yield and its composition as well as an acid catalyst (zeolite) and an alkali catalyst (Na_2CO_3). The major result of this work was higher bio-oil yields with the order of nano-Ni/SiO_2 > zeolite > Na_2CO_3 in the hydrothermal liquefaction of Nannochloprosis sp.. The highest bio-oil yield (30.0 wt%) was obtained at 250°C by using nano-Ni/SiO_2. It should be noted that these results do not necessarily come to the conclusion that all acid catalysts have better performance compared to alkali catalysts since different catalysts have different effects on the bio-oil yield and the elemental composition. As discussed in section 2.3, the biochemical composition of microalgae, the temperature range and the holding time could affect the catalyst performance.

For the blank experiment, the elemental composition results showed that the oxygen content of the bio-oil decreased by increasing the temperature, and consequently its heating value increased by the increase of the temperature. On the other hand, the nitrogen content

in the bio-oil increased with increasing the temperature. For the catalytic experiment, the oxygen and the nitrogen contents of the bio-oil for all types of catalyst were less than that of the blank experiment, and the heating value was higher for the bio-oil produced by the catalytic HTL. The energy recovery of the bio-oil at 210°C by using Nano-Ni/SiO_2 had the highest value of 30.46% because of the highest bio-oil yield. GC/MS results showed that the major components of the bio-oil by using nano-Ni/SiO_2 were very similar to that of the blank experiment. However, the use of alkali and acid catalysts resulted in the different characterization of the bio-oil. The bio-oil produced by using Na_2CO_3 had more nitrogen-containing components compared to other catalysts. In addition, the catalyst recovery experiment suggested the possibility of nanocatalyst recovery for 2-3 times.

The results of this paper depict that using solid catalysts including a nanocatalyst can increase the bio-oil yield at low temperatures and decrease its oxygen and nitrogen contents which opens the horizon for commercialization of HTL at a low temperature and pressure.

2.5. References

[1] Duan PG, Savage PE. Hydrothermal Liquefaction of a Microalga with Heterogeneous Catalysts. Ind Eng Chem Res. 2011;50:52-61.

[2] Ross AB, Biller P, Kubacki ML, Li H, Lea-Langton A, Jones JM. Hydrothermal processing of microalgae using alkali and organic acids. Fuel. 2010;89:2234-43.

[3] Zou SP, Wu YL, Yang MD, Kaleem I, Chun L, Tong JM. Production and characterization of bio-oil from hydrothermal liquefaction of microalgae Dunaliella tertiolecta cake. Energy. 2010;35:5406-11.

[4] Jena U, Das KC, Kastner JR. Comparison of the effects of Na2CO3, Ca-3(PO4)(2), and NiO catalysts on the thermochemical liquefaction of microalga Spirulina platensis. Appl Energ. 2012;98:368-75.

[5] Yu G, Zhang YH, Guo B, Funk T, Schideman L. Nutrient Flows and Quality of Bio-crude Oil

Produced via Catalytic Hydrothermal Liquefaction of Low-Lipid Microalgae. Bioenerg Res. 2014;7:1317-28.

[6] Xu YF, Zheng XJ, Yu HQ, Hu XG. Hydrothermal liquefaction of Chlorella pyrenoidosa for bio-oil production over Ce/HZSM-5. Bioresource Technol. 2014;156:1-5.

[7] Yang YF, Feng CP, Inamori Y, Maekawa T. Analysis of energy conversion characteristics in liquefaction of algae. Resour Conserv Recy. 2004;43:21-33.

[8] Shakya R, Whelen J, Adhikari S, Mahadevan R, Neupane S. Effect of temperature and Na2CO3 catalyst on hydrothermal liquefaction of algae. Algal Res. 2015;12:80-90.

[9] Yang WC, Li XG, Liu SS, Feng LJ. Direct hydrothermal liquefaction of undried macroalgae Enteromorpha prolifera using acid catalysts. Energ Convers Manage. 2014;87:938-45.

[10] Akia M YF, Motaee E, Han D, Arandiyan H. A review on conversion of biomass to biofuel by nanocatalysts. Biofuel Research Journal. 2014;1:16-25.

[11] Li J, Yan R, Xiao B, Liang D, Du L. Development of nano-NiO/Al2O3 catalyst to be used for tar removal in biomass gasification. Proceedings of the 6th International Symposium on Coal Combustion. 2007:86-92.

[12] Yu J, Tian FJ, Mckenzie LJ, Li CZ. Char-supported nano iron catalyst for water-gas-shift reaction - Hydrogen production from coal/biomass gasification. Process Saf Environ. 2006;84:125-30.

[13] Feyzi M, Hassankhani A, Rafiee HR. Preparation and characterization of Cs/Al/Fe3O4 nanocatalysts for biodiesel production. Energ Convers Manage. 2013;71:62-8.

[14] Verziu M, Cojocaru B, Hu JC, Richards R, Ciuculescu C, Filip P, et al. Sunflower and rapeseed oil transesterification to biodiesel over different nanocrystalline MgO catalysts. Green Chem. 2008;10:373-81.

[15] Reddy C, Reddy V, Oshel R, Verkade JG. Room-temperature conversion of soybean oil and poultry fat to biodiesel catalyzed by nanocrystalline calcium oxides. Energ Fuel. 2006;20:1310-4.

[16] Brown TM, Duan PG, Savage PE. Hydrothermal Liquefaction and Gasification of Nannochloropsis sp. Energ Fuel. 2010;24:3639-46.

[17] Hosseinpour M, Charkhi A, Ahmadi SJ. Nanocrystalline zeolites in supercritical water. Part A: Opportunities and challenges for synthesis using organic templates. J Supercrit Fluid. 2015;102:40-9.

[18] Outokesh M, Saket A, Ahmadi SJ, Hosseinpour M, Khanchi AR. Comparative Study on Adsorption of Iodine Vapor by Silica-Supported Cu Nanoparticles and Micronized Copper. Ind Eng Chem Res. 2012;51:15315-23.

[19] Biller P, Ross AB. Potential yields and properties of oil from the hydrothermal liquefaction of microalgae with different biochemical content. Bioresource Technol. 2011;102:215-25.

[20] Valdez PJ, Nelson MC, Wang HY, Lin XXNN, Savage PE. Hydrothermal liquefaction of Nannochloropsis sp.: Systematic study of process variables and analysis of the product fractions. Biomass Bioenerg. 2012;46:317-31.

[21] Barreiro DL, Prins W, Ronsse F, Brilman W. Hydrothermal liquefaction (HTL) of microalgae for biofuel production: State of the art review and future prospects. Biomass Bioenerg. 2013;53:113-27.

[22] Dote Y, Sawayama S, Inoue S, Minowa T, Yokoyama S. Recovery of Liquid Fuel from Hydrocarbon-Rich Microalgae by Thermochemical Liquefaction. Fuel. 1994;73:1855-7.

[23] Minowa T, Yokoyama S, Kishimoto M, Okakura T. Oil Production from Algal Cells of Dunaliella-Tertiolecta by Direct Thermochemical Liquefaction. Fuel. 1995;74:1735-8.

[24] Yeh TM, Dickinson JG, Franck A, Linic S, Thompson LT, Savage PE. Hydrothermal catalytic production of fuels and chemicals from aquatic biomass. J Chem Technol Biot. 2013;88:13-24.

[25] Torri C, Alba LG, Samori C, Fabbri D, Brilman DWF. Hydrothermal Treatment (HTT) of Microalgae: Detailed Molecular Characterization of HTT Oil in View of HTT Mechanism Elucidation. Energ Fuel. 2012;26:658-71.

[26] Guo Y, Yeh T, Song WH, Xu DH, Wang SZ. A review of bio-oil production from hydrothermal liquefaction of algae. Renew Sust Energ Rev. 2015;48:776-90.

[27] Li J, Brill TB. Spectroscopy of hydrothermal reactions 25: Kinetics of the decarboxylation of protein amino acids and the effect of side chains on hydrothermal stability. J Phys Chem A. 2003;107:5987-92

Chapter 3

3. Ultrasonic-assisted hydrothermal liquefaction; enhancing bio-oil conversion yield and heating value

Abstract

In this chapter, a new method to increase the bio-oil yield at low pressures and temperatures is investigated. The microalgae (Nannochloropsis sp.) are first pre-treated by ultrasonic waves for 30s, 60s, and 90s at 100W to make the algal cell more fragile, and then bio-oil is produced using HTL at 210°C, 230°C and 250°C. The results depicted that using the ultrasonic-assisted hydrothermal liquefaction (UHTL) could increase the bio-oil yield up to the maximum of 28.9% (90s sonication time at 250°C). Moreover, applying ultrasonic pre-treatment resulted in a decrease in the oxygen content of the bio-oil and consequently an increase in its heating value. However, the average nitrogen content did not change dramatically by using UHTL. In this study, it was shown that UHTL could increase the bio-oil yield at a low temperature and pressure. Moreover, the heating value of the bio-oil from UHTL was higher than that of HTL. It means that more thermal energy was produced using UHTL compared with HTL as a result of the higher bio-oil yield and heating value. However, using ultrasonic waves results in an increase in the total energy consumption of the process since it requires electrical energy. Therefore, the net energy was calculated to evaluate the effect of the sonication on the whole energy consumption. According to the results, the net energy was positive at all experimental conditions showing that UHTL increased the bio-oil production yield without a negative effect on the energy efficiency of the process.

3.1. Background

The hydrothermal liquefaction (HTL) has been applied for bio-oil production from microalgae as drying of feedstock is not necessary. On the contrary, the high pressure of the

process results in a high capital cost of equipment in the industrial scale. Also, more expensive and elaborated safety systems are required. Therefore, the process pressure and temperature should be reduced. But, at a low temperature and pressure, the bio-oil yield decreases dramatically.

Different methods have been applied to increase the bio-oil yield and its quality in previous works including catalyst [1-5]. In Chapter 1, we investigated the effect of three different catalysts on the bio-oil yield and its quality. Other than catalysts, several ideas have been proposed by researchers including the co-liquefaction [6-10], the microwave pre-treatment [11-13], the co-solvent [14, 15], and the two-stage hydrothermal liquefaction [16]. Catalysts have been widely employed in HTL of microalgae and generally reported to have a positive effect on the conversion yield [17]. Gai et. al. [7] observed a synergistic interaction in the co-liquefaction of microalgae and rice husk. The maximum conversion yield was reported for a mixture of 50% microalgae and 50% rice husk. Zhuang et. al. [12] investigated the effect of the microwave pre-treatment in the direct liquefaction of microalgae (Ulva prolifera) and reported a dramatic increase in the bio-oil yield. In another study, using ethanol–water co-solvent resulted in an increase in the bio-oil yield in the hydrothermal liquefaction of Chlorella pyrenoidosa, with a maximum value of 57.3% achieved at an ethanol/water mass ratio of five [14]. In addition, application of the two-stage hydrothermal liquefaction was investigated and resulted in a lower nitrogen content in the liquefaction of a high-protein microalga (Chlorella) [16].

In this chapter, another approach (i. e. ultrasonic pre-treatment) has been taken into consideration to increase the bio-oil yield at a low temperature and pressure. Ultrasonic waves have been used for cell disruption of microalgae and also combined with solvent extraction to extract lipids from microalgae, typically within 5-10 minutes at a power of 100-200 W [18-21]. Ma et. al. [18] investigated the effects of the ultrasonic pre-treatments on the lipid extraction of microalgae. The lipid extraction yield increased by increasing the sonication time; and after 10 minutes, it reached the highest value. Park et. al. [21] studied

the sonication-assisted homogenization method for the lipid extraction from Chlorella vulgaris. They reported an increase in the lipid extraction yield by this method compared with that by using either homogenization or sonication.

The purpose of this chapter is to study on the feasibility of using the ultrasonic pre-treatment to increase the bio-oil yield at low temperatures and pressures in HTL of microalgae. Since the sonication process consumes electrical energy, the sonication time was limited to the maximum of 90s in this research. It is worthwhile to mention that ultrasonic waves were used not for cell disruption, but for weakening microalgae cells. Therefore the sonication pre-treatment was used in a shorter period of time compared to the previous works on cell disruption and lipid extraction to avoid high electricity consumption. Afterwards, the pre-treated microalgae was fed to the HTL reactor for bio-oil production at low temperatures and pressures to investigate the effect of the ultrasonic pre-treatment. Moreover, the net energy calculation will be provided to show whether the ultrasonic-assisted hydrothermal liquefaction (UHTL) could be economically feasible in an industrial scale.

3.2. Experimental section

3.2.1. Materials

Microalgae

Similar to Chapter 2, Nannochloprosis sp. was used in this chapter. The lipid content, the protein content, the proximate and ultimate analysis, and the higher heating value (HHV) of the microalgae are presented in Chapter 2.

Reactor

The hydrothermal liquefaction was carried out in a 500 ml batch reactor (model MMJ500)

purchased from OM Labtech (Japan). Please refer to Chapter 2 for more details about the reactor.

3.2.2. Experimental procedure

10 grams of dried microalgae were mixed with 50 ml of deionized water and stirred for 5 minutes using a magnetic stirrer. The mixture was placed in the sonication device (Branson Sonifier 250, USA) for the ultrasonic pre-treatment at a power of 100 W for 30s, 60s, and 90s. After then, the mixture was introduced into the sample tube of the reactor followed by adding 100 ml deionized water. Deionized water was produced in-house. The air inside the reactor was purged by argon gas. The reactor temperature was then raised from the ambient temperature to the desired temperature (210°C, 230°C, and 250°C) at an average heating rate of 6°C/min. In order to keep the temperature uniform inside the sample tube, the automated stirrer was used at a constant stirring rate of 200 rpm. After temperature reached the set point value, the sample was kept inside the reactor for 60 minutes as the holding time. Once the holding time was completed, the reactor was cooled down to the ambient temperature.

After cooling down, the reactor was depressurized before opening. The products were collected and separated by the filtration and the solvent extraction. Details about the experimental procedure and product separation have been described in Chapter 2.

3.2.3. Analysis

The results of the proximate and ultimate analysis of the microalgae are presented in Chapter 2. The obtained bio-oil was weighted to calculate the bio-oil yield using the equation (3.1). Since the mass of dried microalgae is required for calculating the bio-oil yield, microalgae sample was dried in an oven at 105°C prior to the experiment. All of the experiments were repeated in triplicate, and the average values were reported. Energy

Recovery (ER) was calculated by the equation (3.2) which shows the percentage of the thermal energy of the raw microalgae recovered in the bio-oil fraction. It should be noted that HTL of microalgae results in four different products (gaseous product, aqueous product, bio-oil, and solid residue) and the mass of the bio-oil is lower than that of the microalgae.

$$Bio-oil\ Yield\ (\%) = \frac{Mass\ of\ Bio-oil\ (g)}{Mass\ of\ Dried\ Microalgae\ (g)} * 100\% \quad (3.1)$$

$$Energy\ Recovery\ (\%) = \frac{(Mass * HHV)_{Bio-oil}}{(Mass * HHV)_{Microalgae}} * 100\% \quad (3.2)$$

The ultimate analysis of the bio-oil was performed by the elemental analyzer (CHN: JM10, J-Science; O: Vario Micro Cube, Elementar Inc.; S: HSU-20, Yanaco). HHV was calculated by using Dulong's formula. Bio-oil was also analyzed by GC-MS (GCMS-QP2010 SE, Shimadzu Inc.). More detail about the GC-MS analysis can be found in Chapter 2.

3.3. Results and discussion

This section provides the results of the hydrothermal liquefaction of Nannochloropsis sp. at temperatures 210°C, 230°C, and 250°C by applying the ultrasonic pre-treatment containing the bio-oil yield, the elemental composition, the heating value, the GC/MS results, and the net energy results.

3.3.1. Bio-oil yield

The bio-oil yield is defined as the mass of the bio-oil divided by the mass of the dried algae (equation 3.1). Figure 3.1 shows the bio-oil yields at 210°C, 230°C, and 250°C with different sonication times as well as those of the experiment where the ultrasonic pre-treatment was not applied. The average values are shown on the graph. For the HTL experiment, the average bio-oil yields at 210°C, 230°C, and 250°C were 11.8%, 17.0%, and

20.2%, respectively, which shows an increasing trend by increasing the temperature. This trend can also be seen in the ultrasonic-assisted experiment where the bio-oil yields increased by an increase in the temperature. Meanwhile, at a given temperature, the bio-oil yield increased by increasing the sonication time. Therefore, both the temperature and the sonication time had a positive effect on the bio-oil yield. The maximum yield was 28.9% at 250°C and 90s sonication time.

Even though, UHTL can increase the bio-oil yield, it also increases the total energy consumption of the whole process since the sonicator requires electrical energy. In order to evaluate the effect of the electrical energy consumption of the sonication on the process economy, the net energy calculations were performed and will be described in Section 3.3.4.

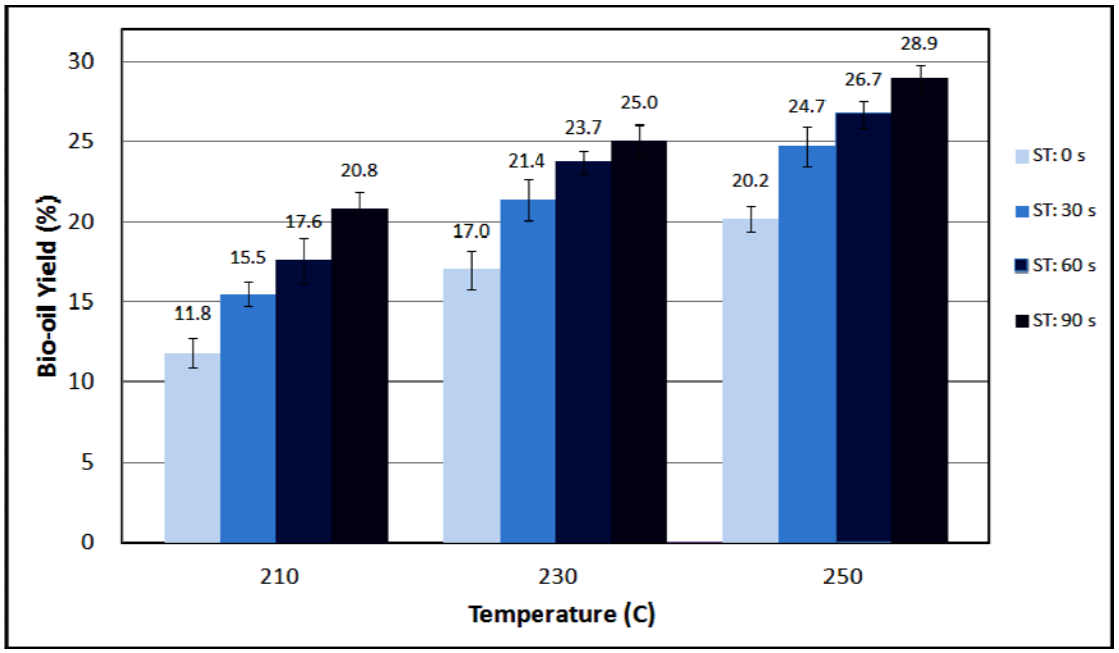

Figure 3.1. Bio-oil yields

ST = Sonication time (s)

3.3.2. Elemental composition, heating value, energy recovery

The ultimate analysis, the atomic ratios, HHV, and Energy Recovery (ER) of the bio-oil

produced at different conditions are listed in Table 3.1. The elemental composition and HHV of microalgae and crude oil are also presented to compare with those of the bio-oil.

Table 3.1. Elemental composition, atomic ratios, heating value, energy recovery of the bio-oil

Temperature		C	H	N	O	S	H/C	O/C	N/C	HHV (MJ/kg)	ER (%)
Microalgae		49.93	7.91	6.33	28.71	0.64	1.90	0.43	0.109	23.11	
Temperature = 210°C											
ST	0s	71.81	10.02	3.77	13.80	0.42	1.67	0.14	0.045	36.16	18.48
	30s	73.24	10.11	3.30	12.43	0.29	1.66	0.13	0.039	37.00	24.79
	60s	73.48	10.57	3.52	11.94	0.39	1.73	0.12	0.041	37.84	28.80
	90s	73.11	10.56	3.55	11.95	0.38	1.73	0.12	0.042	37.69	33.91
Temperature = 230°C											
ST	0s	72.47	10.02	4.70	11.71	0.40	1.66	0.12	0.056	36.75	27.05
	30s	74.23	10.31	4.31	10.87	0.48	1.67	0.11	0.050	37.92	35.10
	60s	73.26	10.24	5.02	10.96	0.37	1.68	0.11	0.059	37.46	38.42
	90s	74.06	10.51	4.43	10.57	0.31	1.70	0.11	0.051	38.18	41.36
Temperature = 250°C											
ST	0s	72.65	10.19	5.13	10.88	0.42	1.68	0.11	0.061	37.20	32.49
	30s	72.96	9.8	5.75	10.84	0.48	1.61	0.11	0.068	36.72	39.35
	60s	74.61	10.5	4.78	10.10	0.46	1.69	0.10	0.055	38.45	44.46
	90s	72.89	9.84	5.89	10.70	0.57	1.62	0.11	0.069	36.83	46.11

ST = Sonication Time (s)

In the experiments without using ultrasonic waves, the temperature change has different effects on the elemental composition of the bio-oil. The N content increased by increasing the temperature while the oxygen content of the bio-oil decreased from 13.80% to 10.88% by increasing the temperature. ER increased with the temperature increase from 18.48% to 32.49% as both the bio-oil yield and HHV increased along with the temperature increase.

General comparison of the bio-oil produced by UHTL and HTL shows that the carbon

content in the UHTL-derived bio-oil is higher than that of the HTL-derived bio-oil, however there is no specific trend in terms of the H and N contents. Meanwhile, the oxygen content of the UHTL-derived bio-oil was lower than that of the HTL-derived bio-oil resulted in a lower O/C ration and a higher heating value. ER of UHTL is in the range of 24.79% to 46.11%, which is higher than that of HTL at the same temperature because of a higher bio-oil yield as well as a higher heating value.

3.3.3. Component analysis

Bio-oil is a complex mixture of several hundreds of organic compounds which are products by the decomposition of biomolecules constructing microalgae. In this research, the bio-oil was analyzed by GC/MS to identify its components. Figure 3.2 shows the chromatograms for the HTL and UHTL experiments at 210°C. Several major components are presented in the chromatogram. Tables 3.2 - 3.5 present the name and area% of the 14 major components at 210°C.

For HTL experiment (Figure 3.2.(a); Table 3.2), the highest peak is related to n-hexadecanoic acid (palmitic acid, C16:0). Other fatty acids with different carbon numbers are amongst the major components. The bio-oil also contains cholesterol, phytol, N-containing components (e.g. pyrazine or pyrrole derivative), alkene, and cycloalkane.

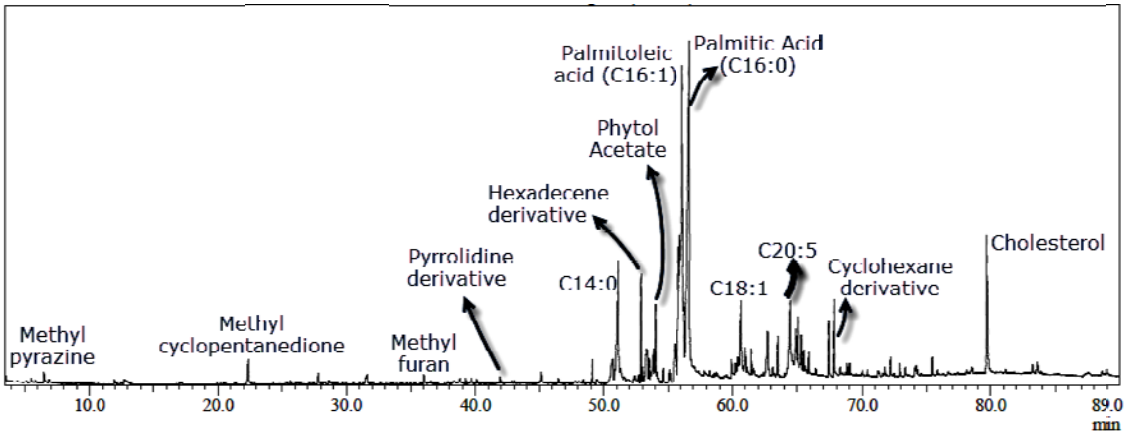

(a)

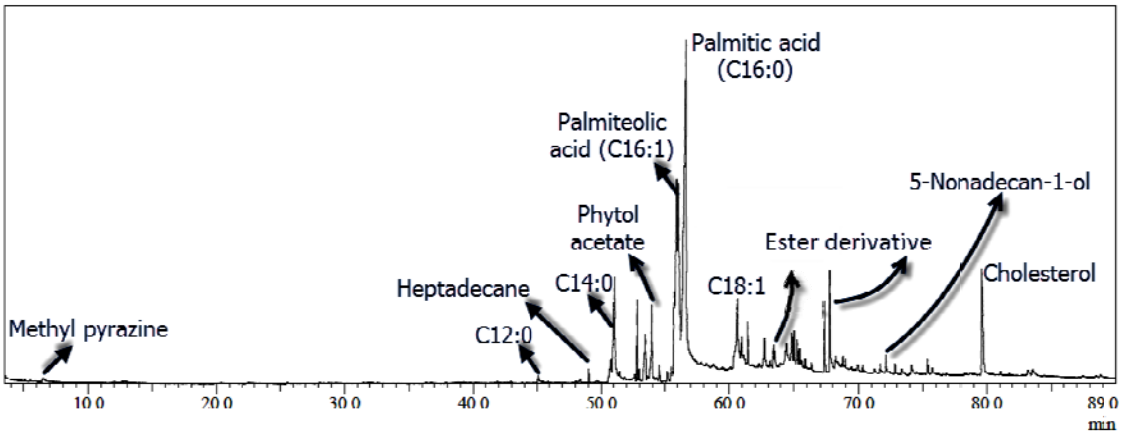

(b)

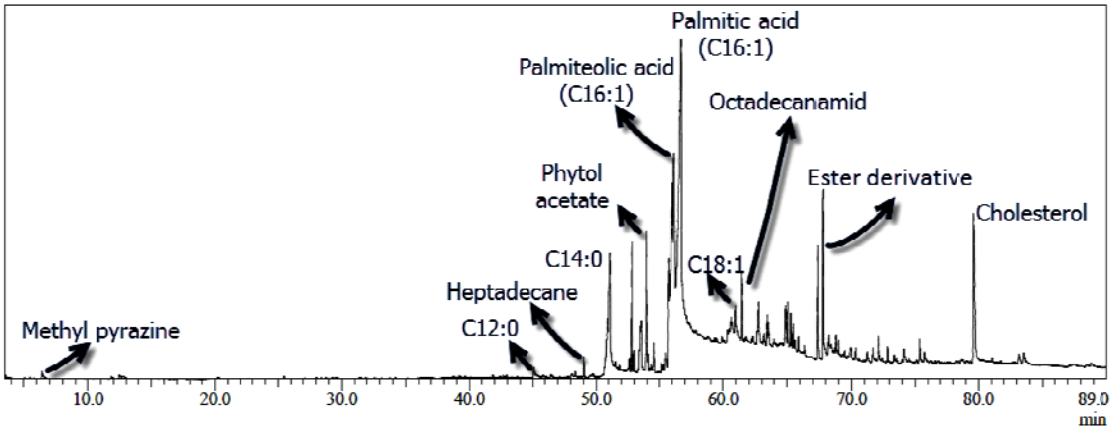

(c)

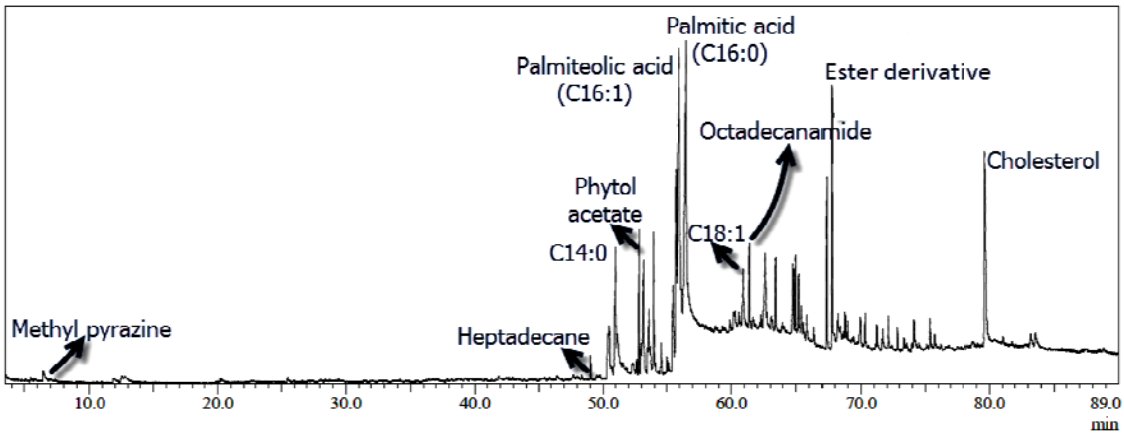

(d)

Figure 3.2. GC/MS of the bio-oil at 210°C for the Sonication time (a) 0s; (b) 30s; (c) 60s; (d) 90s

Table 3.2. Major components of the bio-oil at 210°C for HTL experiment

Peak#	Name	Area %	Peak#	Name	Area %
1	n-Hexadecanoic acid (C16:0)	23.45	8	Piperazinedione derivative	1.97
2	cis-9-Hexadecenoic acid (C16:1)	19.49	9	Pyrazine derivative	1.87
3	Tetradecanoic acid (C14:0)	5.68	10	Phenylalanyl derivative	1.85
4	Oleic acid (C18:1)	4.51	11	2-Hexadecene derivative	1.83
5	Eicosapentaenoic acid (C20:5)	4.09	12	1-(3-Methylbutyryl) pyrrolidine	1.74
6	Cholesterol	4.09	13	Piperazinedione derivative	1.58
7	Phytol acetate	3.15	14	1,3,5-Trisilacyclohexane	1.37

For the UHTL experiment (Figure 3.2.(b-d); Table 3.3 - 3.5), palmitic acid (C16:0) still has the highest peak. However, the total peak area for fatty acids in UHTL experiment is lower than that of HTL. Based on the qualitative analysis and the results presented in Tables 3.2 - 3.5, major components in the bio-oil from HTL and UHTL are very similar, but with different area%. The major difference is in the peak area of fatty acids and esters. The former is higher for HTL and the latter is higher for UHTL. This difference in the HTL-derived and UHTL-derived bio-oil components can be explained by the effect of ultrasonic waves. Applying ultrasonic waves may have accelerated decomposition of lipids into fatty acids. After then, fatty acids were undergone transformation into ester during the hydrothermal liquefaction.

3.3.4. Net energy calculation

In this chapter, it was shown that UHTL could increase the bio-oil yield at a low temperature and pressure. Moreover, the higher heating value of the bio-oil from UHTL was higher than that of HTL. It means that more thermal energy was produced using UHTL compared with HTL as a result of the higher bio-oil yield and heating value. However, using ultrasonic waves results in an increase in the total energy consumption of the process since it requires electrical energy. In other words, UHTL has two countercurrent effects on the

energy consumption of the process. Therefore, the net energy calculation is necessary to evaluate the effect of the sonication on the whole energy consumption. In this regards, the net energy is defined by equation (3.3).

$$
\begin{aligned}
&Net\ Energy\ (kJ) = \\
&Increase\ in\ the\ thermal\ energy\ of\ the\ bio-oil\ using\ UHTL \\
&-Electrical\ energy\ consumed\ by\ sonication \\
&= \eta * \{(bio-oil\ mass * heating\ value)_{UHTL} - (bio-oil\ mass * heating\ value)_{HTL}\} \\
&- Sonication\ Power * Time
\end{aligned}
\tag{3.3}
$$

where η is the conversion efficiency of thermal energy to electrical energy.

Table 3.3. Major components of the bio-oil at 210°C for UHTL experiment (Sonication time = 30S)

Peak#	Name	Area %	Peak#	Name	Area %
1	n-Hexadecanoic acid (C16:0)	28.65	8	Ester derivative	2.44
2	cis-9-Hexadecenoic acid (C16:1)	7.32	9	9-Octadecenamide	2.42
3	Pyrrole derivative	5.39	10	Piperazinedione derivative	2.31
4	Oleic acid (C18:1)	4.74	11	Butyric acid, ethyl ester derivative	1.76
5	Tetradecanoic acid (C14:0)	3.60	12	Isophytol	1.73
6	Cholesterol	3.29	13	Eicosapentaenoic acid, methyl ester	1.59
7	Eicosapentaenoic acid (C20:5)	3.05	14	Phytol acetate	1.52

Table 3.4. Major components of the bio-oil at 210°C for UHTL experiment (Sonication time = 60S)

Peak#	Name	Area %	Peak#	Name	Area %
1	n-Hexadecanoic acid (C16:0)	20.42	8	Piperazinedione derivative	2.78
2	Pyrrole derivative	5.27	9	Phytol	2.65
3	cis-9-Hexadecenoic acid (C16:1)	5.04	10	Oleic acid derivative	2.63
4	Oleic acid (C18:1)	3.77	11	Aziridine derivative	2.5
5	Cholesterol	3.37	12	Ester derivative	2.31
6	Tetradecanoic acid (C14:0)	2.94	13	Propyl ester derivative	2.08
7	9-Octadecenamide	2.91	14	Piperazinedione derivative	1.87

Table 3.5. Major components of the bio-oil at 210°C for UHTL experiment (Sonication time = 90S)

Peak#	Name	Area %	Peak#	Name	Area %
1	n-Hexadecanoic acid (C16:0)	16.45	8	Butane derivative	2.43
2	cis-9-Hexadecenoic acid (C16:1)	14.02	9	Piperazinedione derivative	2.31
3	Cholesterol	6.38	10	Pyrrole derivative	2.03
4	Isophytol	4.57	11	9-Octadecenamide	1.95
5	Ester derivative	3.78	12	3-Eicosyne	1.73
6	Tetradecanoic acid (C14:0)	3.13	13	Piperazinedione derivative	1.73
7	Pyrrolidine derivative	3.02	14	Phytol acetate	1.68

In equation (3.3), the first term is the increase in the thermal energy of the bio-oil (the main product of the process) by applying ultrasonic waves. The thermal energy is calculated for the UHTL- and HTL- derived bio-oils as bio-oil mass (g) multiplied by its heating value (kJ/g). The second term is the electrical energy consumed for sonication which is the sonication power (kW) multiplied by the sonication time (s). Since the quality of the thermal and the electrical energy is different, η has been used to convert thermal energy to the equivalent amount of electrical energy. Calculations were performed for a value of η equals 40%. The net energy is shown in Figure 3.3. In all cases, net energy is positive which means

that the increase in the bio-oil thermal energy produced by UHTL was higher than the electrical energy consumption by the sonicator.

As can be seen in Figure 3.3, at the sonication times of 30s and 60s, the net energy has the highest value at 230°C. However, at the sonication time of 90s, the variation of the net energy with the HTL temperature is different. In this case, the net energy is maximum at 210°C, and decreases with an increase in the temperature. In fact, the net energy has the highest value at the HTL temperature of 210°C and the sonication time of 90s among all experimental conditions. This result can be explained by the increase in the bio-oil yield at 210°C by applying the ultrasonic pre-treatment. According to Figure 3.1, in the conventional HTL, the bio-oil yield had the lowest value at 210°C (11.8%). The ultrasonic pre-treatment resulted in a dramatic increase in the bio-oil yield at 210°C up to 20.8% at the sonication time of 90s, almost twice of that of the conventional HTL. The increase in the bio-oil yield resulted in the high value of the net energy at 210°C and the sonication time of 90s.

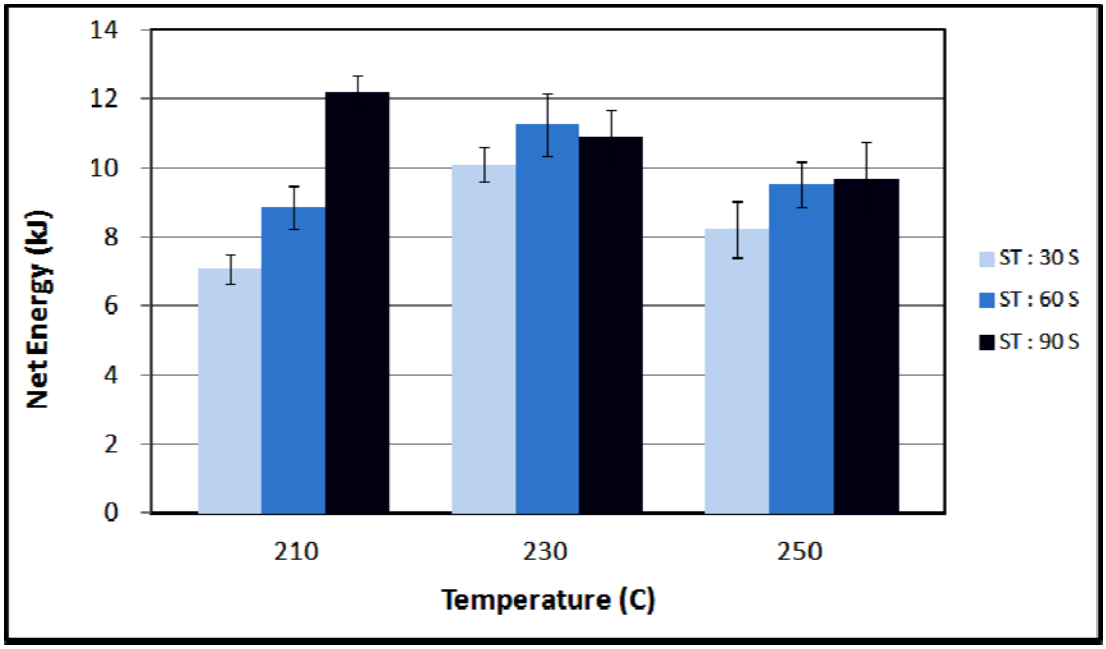

Figure 3.3. Net energy for UHTL experiment (η=40%)

η= Conversion efficiency of the thermal energy to the electrical energy

It should be noted that the definition of net energy (equation 3.3) is different from that of Energy Recovery (equation 3.2). Energy Recovery is a measure to compare the thermal energy of the bio-oil and raw microalgae. It means that what percentage of the microalgae thermal energy is recovered in the bio-oil. On the other hand, the net energy was defined to compare the increase in the thermal energy of the bio-oil from UHTL and the electrical energy consumed by sonicator.

In section 3.3.1., it was shown that increasing the sonication time had a positive effect on the bio-oil yield. However, it requires electrical energy consumption. In order to investigate the effect of a higher sonication time on the bio-oil yield and RNEP, more experiments were conducted at the sonication time of 2.5 min and 5 min. Experiments were carried out at 250°C since the highest bio-oil yield was obtained at this temperature. Figure 3.4 shows the average value of the bio-oil yield and RNEP. Even though higher sonication time resulted in an increase in the bio-oil yield, on the contrary, RNEP was negative at higher sonication times. This result states that higher sonication time does not necessarily have a positive effect on the whole energy consumption of the process.

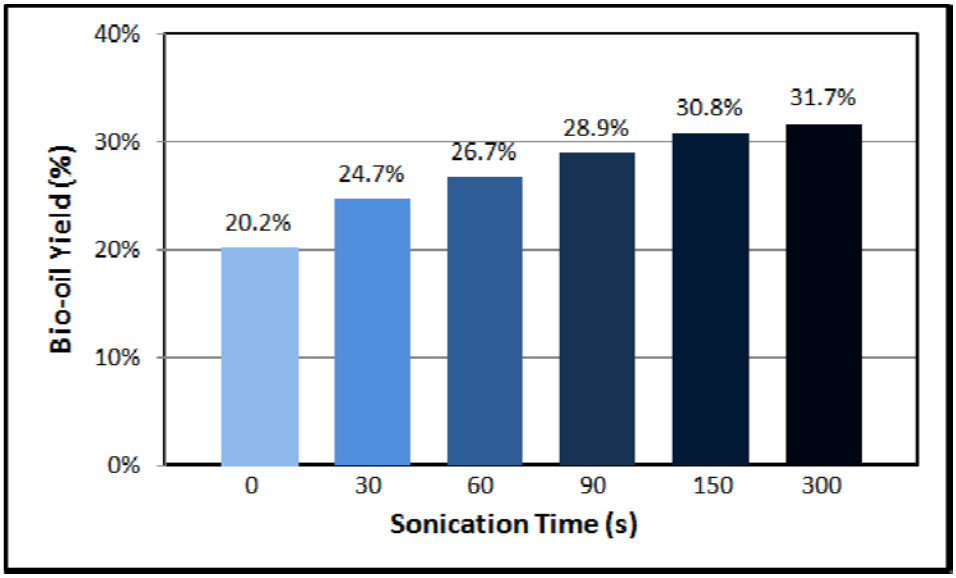

(a)

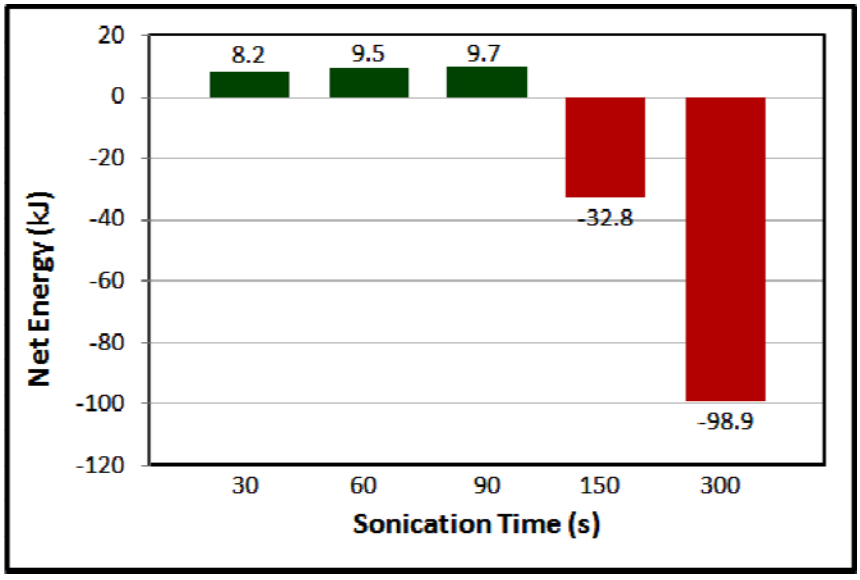

(b)

Figure 3.4. The average bio-oil yield and net energy for UHTL experiment (Temperature: 250°C; η=40%)

Based on the net energy calculations (Figure 3.3), the optimum condition is the HTL temperature of 210°C and the sonication time of 90s. One question then arises "does increase the sanction time will change the optimum condition?" In order to answer the mentioned question, One more test was conducted at the HTL temperature of 210°C and the sonication time of 120s to check whether there is any further increase in the net energy. Figure 3.5 illustrates the bio-oil yield and the net energy for the UHTL experiment (HTL temperature: 210°C; sonication time: 30s - 120s). It can be seen that the net energy for the sonication time of 120s is less than that of the sonication time of 90s. Based on the Figure 3.4 results, it is predictable that further increase in the sonication time will lead to a further decrease in the net energy. Therefore, the optimum experimental condition will not change with an increase in the sonication time.

3.4. Conclusions

We employed the ultrasonic assisted HTL (UHTL) for bio-oil production from microalgae Nannochloropsis sp. at low temperatures. The results were compared with the results of the

conventional HTL. It was shown that UHTL could increase the bio-oil yield while maintaining a positive value for the net energy at short sonication times. It was shown that both the temperature and the sonication time had a positive effect on the bio-oil yield. The highest bio-oil yield was 28.9% at 250°C, 90s sonication time.

Meanwhile, UHTL resulted in a lower oxygen content of the bio-oil as well as a higher heating value. However, the nitrogen content of the bio-oil did not change dramatically by applying UHTL. The component analysis revealed that the major components in the bio-oil from HTL and UHTL were very similar, but with different area%. The major difference is in the peak area of fatty acids and esters. The former is higher for HTL and the latter is higher for UHTL. The net energy was positive at short sonication times, which means that the increase in the bio-oil thermal energy produced by UHTL was higher than the electrical energy consumption of the sonicator. Therefore, the optimum experimental condition did not change with an increase in the sonication time.

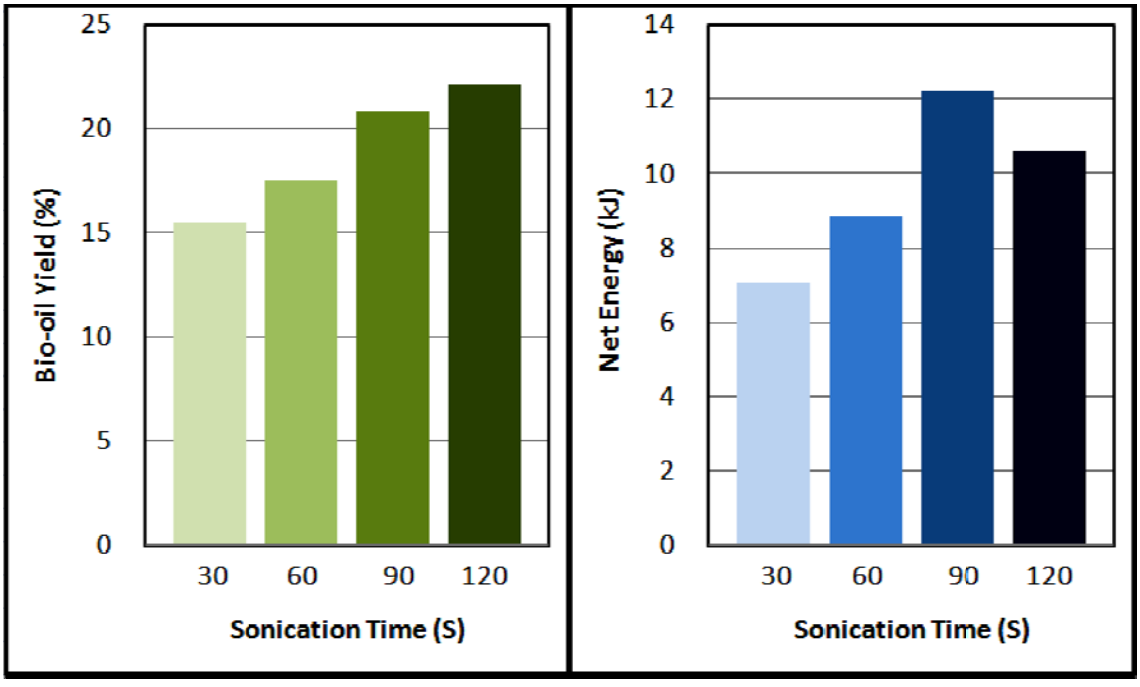

Figure 3.5. The average bio-oil yield and the net energy for UHTL experiment (Temperature: 210°C; η=40%)

3.5. References

[1] Yu G, Zhang YH, Guo B, Funk T, Schideman L. Nutrient Flows and Quality of Bio-crude Oil Produced via Catalytic Hydrothermal Liquefaction of Low-Lipid Microalgae. Bioenerg Res. 2014;7:1317-28.

[2] Yang WC, Li XG, Liu SS, Feng LJ. Direct hydrothermal liquefaction of undried macroalgae Enteromorpha prolifera using acid catalysts. Energ Convers Manage. 2014;87:938-45.

[3] Chen Y, Wu YL, Ding RR, Zhang P, Liu J, Yang MD, et al. Catalytic Hydrothermal Liquefaction of D. tertiolecta for the Production of Bio-Oil over Different Acid/Base Catalysts. Aiche J. 2015;61:1118-28.

[4] Jena U, Das KC, Kastner JR. Comparison of the effects of Na2CO3, Ca-3(PO4)(2), and NiO catalysts on the thermochemical liquefaction of microalga Spirulina platensis. Applied Energy. 2012;98:368-75.

[5] Shakya R, Whelen J, Adhikari S, Mahadevan R, Neupane S. Effect of temperature and Na2CO3 catalyst on hydrothermal liquefaction of algae. Algal Res. 2015;12:80-90.

[6] Chen WT, Zhang YH, Zhang JX, Schideman L, Yu G, Zhang P, et al. Co-liquefaction of swine manure and mixed-culture algal biomass from a wastewater treatment system to produce bio-crude oil. Appl Energ. 2014;128:209-16.

[7] Gai C, Li Y, Peng NN, Fan AN, Liu ZG. Co-liquefaction of microalgae and lignocellulosic biomass in subcritical water. Bioresource Technol. 2015;185:240-5.

[8] Jin BB, Duan PG, Xu YP, Wang F, Fan YC. Co-liquefaction of micro- and macroalgae in subcritical water. Bioresource Technol. 2013;149:103-10.

[9] Pei XK, Yuan XZ, Zeng GM, Huang HJ, Wang JY, Li H, et al. Co-liquefaction of microalgae and synthetic polymer mixture in sub- and supercritical ethanol. Fuel Process Technol. 2012;93:35-44.

[10] D. W. F. Brilman ND, M. Wądrzyk. Hydrothermal co-liquefaction of microalgae, wood, and sugar beet pulp. Biomass Conversion and Biorefinery. 2017;7:1-10.

[11] Biller P, Friedman C, Ross AB. Hydrothermal microwave processing of microalgae as a pre-treatment and extraction technique for bio-fuels and bio-products. Bioresource Technol. 2013;136:188-95.

[12] Zhuang YB, Guo JX, Chen LM, Li DM, Liu JH, Ye NH. Microwave-assisted direct liquefaction of Ulva prolifera for bio-oil production by acid catalysis. Bioresource Technol. 2012;116:133-9.

[13] Liu JH, Zhuang YB, Li Y, Chen LM, Guo JX, Li DM, et al. Optimizing the conditions for the microwave-assisted direct liquefaction of Ulva prolifera for bio-oil production using response surface methodology. Energy. 2013;60:69-76.

[14] Zhang JX, Zhang YH. Hydrothermal Liquefaction of Microalgae in an Ethanol-Water Co-Solvent To Produce Biocrude Oil. Energ Fuel. 2014;28:5178-83.

[15] He YY, Liang X, Jazrawi C, Montoya A, Yuen A, Cole AJ, et al. Continuous hydrothermal liquefaction of macroalgae in the presence of organic co-solvents. Algal Res. 2016;17:185-95.

[16] Jazrawi C, Biller P, He YY, Montoya A, Ross AB, Maschmeyer T, et al. Two-stage hydrothermal liquefaction of a high-protein microalga. Algal Res. 2015;8:15-22.

[17] Yeh TM, Dickinson JG, Franck A, Linic S, Thompson LT, Savage PE. Hydrothermal catalytic production of fuels and chemicals from aquatic biomass. J Chem Technol Biot. 2013;88:13-24.

[18] Ma YA, Cheng YM, Huang JW, Jen JF, Huang YS, Yu CC. Effects of ultrasonic and microwave pretreatments on lipid extraction of microalgae. Bioproc Biosyst Eng. 2014;37:1543-9.

[19] Lee JY, Yoo C, Jun SY, Ahn CY, Oh HM. Comparison of several methods for effective lipid extraction from microalgae. Bioresource Technol. 2010;101:S75-S7.

[20] Grimi N, Dubois A, Marchal L, Jubeau S, Lebovka NI, Vorobiev E. Selective extraction from microalgae Nannochloropsis sp. using different methods of cell disruption. Bioresource Technol. 2014;153:254-9.

[21] Park JY, Lee K, Choi SA, Jeong MJ, Kim B, Lee JS, et al. Sonication-assisted

homogenization system for improved lipid extraction from Chlorella vulgaris. Renew Energ. 2015;79:3-8.

Chapter 4

4. Characteristics and application of hydrochar as a low-cost adsorbent

Abstract

In this chapter, hydrochar prepared from the hydrothermal liquefaction of microalgae is characterized and investigated for copper removal from aqueous solution. Two hydrochars were prepared at 210°C (HD210) and 250°C (HD250). The effect of the initial solution pH, the initial Cu(II) concentration, the contact time and the temperature will be investigated. According to the elemental analysis, the volatile matter in the hydrochars was lower and ash content was higher than those of microalgae. Also, pore characteristic analysis revealed that the surface area of the HD250 was higher than that of the HD210 suggesting a higher potential for the adsorption process. FTIR analysis showed that both hydrochars contained oxygen-containing functional groups on the surface which were effective for the copper removal according to the previous research. The adsorption experiments indicated that the amount of copper adsorbed reached a maximum value at the pH of 5 which was considered as the optimum solution pH. In addition, HD250 had a higher amount of copper adsorption than that of HD210 at all values of the solution pH. The adsorption data at the optimum solution pH was well fitted by the Langmuir's isotherm model and the adsorption process could be well described by the pseudo-2nd order kinetic model. Moreover, thermodynamic analysis revealed that copper adsorption onto the hydrochar was an endothermic process.

4.1. Background

For many years, water pollution by heavy metals has been a major concern. Heavy metals have carcinogenic properties and are not biodegradable, which results in their accumulation in the food chain, causing environmental pollutions as well as health problems in both humans and animals [1, 2].

Copper is an essential trace element in plants, animals, and humans. However, similar to all heavy metals, it is potentially toxic to living organisms. The average intakes of copper by human adults is in the range of 0.6 to 1.6 mg/day [3]. The Food and Nutrition Board in the US has set tolerable upper intake level (UL) for copper at 10 mg/day [4]. Even though, copper is an essential element for human health, an excessive intake of copper results in health problems in human body, such as gastrointestinal problems [5], headaches [6], hair loss [6], hypoglycemia [6], increased heart rate [6], nausea [6], capillary damage [7], central nervous system irritation [7], damage to kidney, and liver [8]. Since copper is widely used in the industry, there are many sources of copper pollution. In fact, copper is one of the most widespread heavy metal contaminants in the environment [5].

Various processes have been used for the removal of heavy metals from wastewater. Some of the conventional methods include the chemical precipitation, the chemical oxidation and reduction, the ion exchange, the reverse osmosis, the electrochemical treatment, the electrodialysis, the electrodeposition, the electrolytic recovery, the evaporative recovery, the filtration, the membrane separation, the neutralization, the flotation, the electroflotation, the biosorption, and the adsorption [1, 6, 9-12]. However, most of these methods are often ineffective and/or expensive when heavy metal concentrations are very low, specifically below 100 mg/L [13, 14]. At low concentrations of heavy metal ions in aqueous waste, the adsorption is recommended for their removal [1]. However, high capital and regeneration costs of commercially available adsorbents often limit industrial application of this process [5]. Therefore, during recent years, substantial researches have been carried out on the production of efficient and low-cost adsorbents from relatively cheap materials.

Various materials have been studied to produce low-cost adsorbents including biomass waste, agricultural by-products and wastes such as hazelnut husk [15], rice husk [16], pinewood [16], wood and bark [17], bamboo [18], potato peel [6], pomegranate peel [10], orange waste [14], soybean stover [19], and peanut shells [19]. The utilization of such

materials in the production of low-cost adsorbents has double benefits to the environment, since these waste materials are converted into high value added adsorbents, and the adsorbents are applied to remove pollutants from aqueous solutions [5]. In other words, the conversion of biomass waste into adsorbent is a ‘‘win–win’’ solution for both protecting the environment and improving waste management [20].

These plant wastes and agricultural by-products have been used in their raw form or after some physical or chemical treatments. Since using waste biomass in the raw form may result in the leaching of organic pollutants to the environment, raw materials are usually carbonized to avoid this problem [16]. Pyrolysis and the hydrothermal treatment are the most commonly used processes to improve the adsorption capacity of the above-mentioned materials [5, 16, 17]. After such a treatment, the resultant materials are usually called biochar and hydrochar, respectively.

The International Biochar Initiative (IBI) (http://www.biochar-international.org/definitions), has defined biochar as

> **"a solid material obtained from thermochemical conversion of biomass in an oxygen-limited environment ".**

while IBI has defined hydrochar as

> **"the solid product of hydrothermal carbonization (HTC) or liquefaction. It is distinct from biochar due to its production process and properties, and typically has higher H/C ratios and lower aromaticity than biochar as well as little or no fused aromatic ring structures "**

Pyrolysis is a thermochemical decomposition of biomass at medium to high temperatures (350–700°C) in the absence of oxygen. Pyrolysis of biomass produces solid (i.e. biochar), liquid, and gaseous products [21]. Gasification is another process for biochar production.

Gasification transforms biomass into a gaseous mixture (i.e. syngas) and a solid product (i.e. biochar) under an oxygen-limited environment and high temperature (above 700°C) [22].

The hydrothermal treatment applies hot compressed water to decompose the feedstock into solid (i.e. hydrochar), liquid and gaseous products. In this process, pressure is high enough to keep water in the liquid phase. Water acts as a solvent, a reactant, and a catalyst. Hydrothermal treatment is particularly suitable for wet biomass since drying of feedstock is not necessary [21]. Depending on the temperature and pressure range, the hydrothermal treatment is divided into three categories: the hydrothermal carbonization (HTC), the hydrothermal liquefaction (HTL), and the hydrothermal gasification (HTG), which is also called supercritical water gasification (SCWG) [23]. HTC uses the mildest temperature and pressure conditions and is aimed to produce char products. HTL is typically carried out at temperatures from 200°C to 370°C, and pressures from 2 to 22 MPa. Since a solvent is used to extract organic compounds from solid and liquid phases, HTL produces two immiscible liquid phases: bio-oil (water-insoluble) which is the main product of the HTL process, and an aqueous phase (water-soluble). Contrary to HTC, where hydrochar is the main product of interest, hydrochar is a by-product of HTL process. If the commercialization of bio-oil production from biomass succeeds, large amounts of hydrochar will be available in the near future, which can be utilized in various applications such as low-cost adsorbent production.

The properties of biochar and hydrochar are compared and reviewed by Kambo, and Dutta [24]. Compared to the commercial activated carbon, biochar and hydrochar have a lower surface area. However, the surface of biochar and hydrochar contains a large amount of oxygen-containing functional groups (e.g. COOH, OH, CO) which can improve their adsorption capacity, especially for the removal of heavy metals through the electrostatic attraction, ion exchange, and surface complexation [20, 24, 25]. In addition, the feedstocks for biochar/hydrochar production are abundant and low-cost. Both biochar and hydrochar have been evaluated in the removal of copper from water and wastewater. Table 4.1 summarizes representative literature data on the application of biochar, hydrochar as well as

a commercial activated carbon in the copper removal from aqueous solution [5, 26-30].

Table 4.1. Representative literature data on the application of biochar, hydrochar, and activated carbon in copper removal from aqueous solution

Feedstock	Method	Surface area (m^2/g)	Optimum initial pH	Amount of copper adsorption (mg/g)[1]	Isotherm	Kinetic model	Ref.
Rice husks	Hydrothermal treatment	-	5	3.49	Linear	PSO[2]	[5]
Orange waste	Hydrothermal treatment	-	5	5.80	Linear	PSO	[5]
Compost	Hydrothermal treatment	-	5	7.72	Freundlich	PSO	[5]
Peanut straw	Slow pyrolysis	-	5	88.97	Langmuir	-	[26]
Soybean straw	Slow pyrolysis	-	5	52.75	Langmuir	-	[26]
Canola straw	Slow pyrolysis	-	5	37.49	Langmuir	-	[26]
Hardwood	Slow pyrolysis	0.43	5	6.79	Langmuir	PSO	[27]
Corn straw	Slow pyrolysis	13.08	5	12.52	Langmuir	PSO	[27]
Pinewood	Slow pyrolysis	29	6.2	2.75	Langmuir	-	[28]
Pinewood	Hydrothermal treatment	21	6.2	4.46	Langmuir	-	[28]
Pig manure	Slow pyrolysis	15.89	5-6	78.36	Langmuir	PSO	[29]
Macroalgae	Slow pyrolysis	N.D.[3]	5.5	19.12	Langmuir	PSO	[30]
Activated carbon	Commercial	-	5	11.44	-	-	[26]

1: The amount of copper adsorption is reported at the optimum pH value selected by the authors in the reference paper or based on the Langmuir isotherm results.

2: Pseudo-second-order model

3: Not detected

The main objective of this research is to evaluate the feasibility of removing Cu(II) from aqueous solutions using hydrochar from low-temperature HTL of microalgae. Microalgae is one of the promising sources for biofuel production, known as the third generation biofuels. Removal of copper from water and wastewater by microalgae hydrochar benefits microalgae cultivation too. If microalgae are cultivated in the wastewater, the presence of heavy metals can inhibit the microalgae growth. It was shown that copper is one of the most toxic heavy metals to microalgae [31]. In other words, microalgae hydrochar can be used to remove copper from wastewater where microalgae are cultivated for biofuel production.

In this chapter, we used hydrochar, as a by-product of HTL of microalage, to remove copper from aqueous solutions. The hydrochar was produced at two levels of temperature (210°C and 250°C). Adsorption experiments were carried out to investigate the effects of the initial solution pH, the initial Cu(II) concentration, the contact time, and the temperature on the copper adsorption onto the hydrochar. Using the data obtained from these experiments, the adsorption isotherm equilibrium, the adsorption kinetics, and the thermodynamic analyses were further studied.

4.2. Experimental section

4.2.1. Materials

Microalgae

Similar to Chapter 2, Nannochloprosis sp. was used in this chapter. The lipid content, the protein content, the proximate and ultimate analysis, and the higher heating value (HHV) of the microalgae are presented in Chapter 2.

4.2.2. Hydrochar preparation

The hydrochar used in this study was prepared by a typical hydrothermal liquefaction process. Briefly, 10 g of dried microalgae was loaded with 150 ml deionized water into a 500-ml autoclave (model MMJ500) purchased from OM Labtech (Japan). Argon gas was used to purge the air outside the reactor. The reactor was then heated to the desired temperatures (210°C and 250°C), and held for 60 minutes as a holding time. Once the holding time was completed, the reactor was cooled down to the room temperature and depressurized before opening. The product was collected and mixed with 150 ml dichloromethane (DCM) (Sigma-Aldrich, 99% purity) to extract bio-oil from both the solid product and the aqueous product. Thereafter, the mixture was filtered to recover the hydrochar as a solid residue (designated as HD210 and HD250 for temperatures 210°C and 250°C, respectively). The obtained hydrochars were then washed several times with deionized water. After then, the hydrochars were dried in an oven at 105°C for 24 h. The dried hydrochar samples were ground to less than 0.250 mm and kept in a desiccator for adsorption experiments. More details about the experimental procedure as well as the bio-oil properties have been explained in Chapter 2. A commercial activated carbon (surface area: 1141.3 m^2/g) was purchased to compare its performance with that of hydrochars.

4.2.3. Characterization of the hydrochar

The proximate analysis was carried out by the thermal gravimetric analysis (TGA) (Shimadzu, TGA-50) using the procedure described in Chapter 2. The ultimate analysis was performed by the elemental analyzer (CHN: JM10, J-Science; S: HSU-20, Yanaco). The surface morphology was studied by SEM on JSM-6610LA (JEOL, Japan), and the functional groups present on the hydrochar surface were analyzed by the Fourier transform infrared spectroscopy (FT-IR) (JEOL, JIR SPX-200). The specific surface area and the pore characteristics of the hydrohars were examined with N_2 adsorption at 77K using the automated surface area analyzer (BEL, BELSORP-miniII). The multipoint Brunauer–Emmett–Teller method was used to calculate the surface area. BJH (Barrette-Joynere-Halenda) method was employed to estimate the volume of the mesopores.

Oxygen-containing functional groups (carboxylic, lactonic, and phenolic) were determined by the Boehm titration method [32].

4.2.4. Copper adsorption experiment

All reagents used in the experiments were of analytical grade. The copper removal experiments were carried out using aqueous copper nitrate ($Cu(NO_3)_2.3(H_2O)$) solutions. Copper nitrate was obtained from Wako Chemicals (Japan).

The batch adsorption experiments were carried out using 100-ml glass vials, in which fixed amount of hydrochar (0.125 g) and 25 mL of copper solution were added (5 g/L hydrochar dosage). The initial solution pH value was adjusted in the range of 2 to 6 by adding small amounts of HCl (0.1 M) or NaOH (0.1 M) solutions to ensure the minimum increase in the solution volume. The solution pH was measured using a pH meter (Horiba scientific, LAQUA F-72). According to the literature, copper was precipitated in the form of hydroxide ($Cu(OH)_2(s)$) when adsorption experiments were carried out at a pH value above 6.2 [5]. Since copper precipitation results in a decrease in the copper concentration by a mechanism other than adsorption, all the experiments were performed at a pH value lower than 6.2. After adjusting the pH value, the vials were then agitated by a shaker (Taitec, Personal-11) equipped with a water bath to control the temperature for a determined time period (0.5 h, 1 h, 2 h, 4 h, 8h, 16 h, and 24 h) at 150 rpm. The temperature was set to 15°C, 25°C, 35°C, and 45°C.

After agitation, the content of the vials was filtered through a 2.7 µm pore size microfiber filter paper (GF/D, Whatman) to separate the adsorbents. The Cu(II) concentration in the aqueous phase was analyzed by ICPS-8100 (Shimadzu, Japan). The effects of the solution pH, the initial Cu(II) concentration, the contact time, and the temperature were studied. A detailed description of the experimental conditions is presented in Table 4.2. Blank experiments were also conducted to check the effect of the filter paper.

Table 4.2. Adsorption experiment conditions

Experiments	pH	Initial Cu(II) concentration (mg/L)	Contact time (h)	Temperature (°C)
Effect of pH	2, 3, 4, 5, 6	100	24	25
Effect of initial Cu(II) concentration	5	25, 50, 100, 200, 300	24	25
Effect of contact time (h)	5	100	0.5, 1, 2, 4, 8, 16, 24	25
Effect of temperature	5	100	24	15, 25, 35, 45

4.2.5. Data evaluation

The amount of copper adsorbed is defined as the mass of copper adsorbed per unit mass of the adsorbent and is calculated using the following equation:

$$q_t = \frac{(C_o - C_t)V}{m} \quad (4.1)$$

where q_t (mg/g) is the amount of copper adsorbed at the contact time of t (h), C_o is the initial copper concentration (mg/L) in the solution, C_t is the copper concentration (mg/L) at the contact time of t (h), V is the solution volume (L), and m is the mass of adsorbent used (g). If the adsorption reaches an equilibrium condition, the amount of copper adsorbed at equilibrium is calculated by equation (4.2).

$$q_{eq} = \frac{(C_o - C_{eq})V}{m} \quad (4.2)$$

where q_{eq} (mg/g) and C_{eq} (mg/L) are the amount of copper adsorbed and the copper concentration at equilibrium, respectively.

Adsorption may reach equilibrium if the contact time is long enough. At a constant

temperature, the model which shows the relationship between q_{eq} and C_{eq} is called the adsorption isotherm. In this study, in order to investigate the Cu(II) adsorption isotherm equilibrium, the Langmuir's isotherm (equation 4.3) and the Freundlich's isotherm (equation 4.4) were used to fit the experimental data. The Langmuir's and Freundlich's isotherms have been widely used to represent the data of the adsorption from solution [2]. The Langmuir's model is represented by the following equation:

$$q_{eq} = \frac{q_{max} K_L C_{eq}}{1 + K_L C_{eq}} \tag{4.3}$$

where q_{max} (mg/g) is the maximum amount of adsorbate particles adsorbed and K_L (L/mg) is a constant dependent on the adsorption energy, and hence on the temperature. In the Langmuir's isotherm model, it is assumed that the available adsorption sites are energetically equivalent and compose a monolayer. Each site can hold at most one adsorbate particle (either ion or molecule), and the adsorbed particles do not interact with each other.

The Freundlich's model is represented by the following equation:

$$q_{eq} = K_F {C_{eq}}^{1/n} \tag{4.4}$$

where K_F ((mg/g)(L/mg)$^{1/n}$) is a proportional constant and n is a dimensionless constant called the Freundlich isotherm constant, which represents the strength of the interaction between the adsorbent and the adsorbate (i.e. the adsorption intensity). In the Freundlich's isotherm model, multilayer adsorption is assumed. Therefore, there is no explicit limit to the amount of adsorbate adsorbed. It often fits the data on rough surfaces better than the Langmuir's model.

The linear forms of Langmuir's and Freundlich's models are as follows:

$$\frac{C_{eq}}{q_{eq}} = \frac{1}{q_{max}K_L} + \frac{C_{eq}}{q_{max}}$$ Langmuir's model linear form (4.5)

$$\ln q_{eq} = \ln K_F + \frac{1}{n}\ln C_{eq}$$ Freundlich's model linear form (4.6)

The values of the parameters were obtained by the linear regression of the two models at a constant temperature and pH value. For this calculation, it was assumed that at 24 h contact time, the adsorption would achieve the equilibrium condition. This assumption is consistent with the literature [5]. By changing the Cu(II) initial concentration in the solution, the amount of copper adsorbed at equilibrium was calculated by the equation (4.2), and the parameters of Langmuir's and Freundlich's models were estimated by the least square method using the linear forms of the isotherm models.

In order to study the kinetics of Cu(II) adsorption, three kinetic models were used: the intra-particle diffusion model (equation 4.7), the pseudo-first order model (equation 4.8), and the pseudo-second order model (equation 4.10).

The adsorption of heavy metals including copper ions on the hydrochar can be described in three distinct phases: (1) diffusion of copper ions through the boundary film to the external surface of the hydrochar (external film diffusion), (2) diffusion of copper ions into the pores of the hydrochar (intra-particle diffusion), and (3) adhesion to the hydrochar surface [30]. The last phase is usually much faster than the other two. Therefore, the overall adsorption rate is determined by either the external film diffusion phase or the intra-particle diffusion phase [30].

When the intra-particular diffusion determines the overall adsorption rate, the

mathematical model described by Weber and Morris [30] is valid as follows:

$$q_t = K_i t^{0.5} + C \quad (4.7)$$

where q_t (mg/g) is the amount of copper adsorbed at the time of t (h), K_d (mg/(g $h^{0.5}$)) is the intra-particle diffusion rate constant, and C (mg/g) is the adsorption constant. If the rate-determining step is the intra-particle diffusion, the plot of q_t against $t^{0.5}$ would result in a straight line. In addition, the line would pass through the origin if the intra-particle diffusion is the only rate-determining step [16].

In the case of a dilute adsorbate concentration and poor mixing, the external film diffusion is the rate-determining step. In this situation, the adsorption rate is determined by the amount of adsorbate and empty active sites on the adsorbent surface. If the depletion of adsorbate due to adsorption is negligible, the adsorption rate is determined by the number of empty active sites on the adsorbent surface, which is described by the pseudo-1st order kinetic model as follows [30]:

$$\frac{dq_t}{dt} = K_1(q_{eq} - q_t) \quad (4.8)$$

where K_1 (1/h) is the pseudo-1st order adsorption rate constant, q_{eq} and q_t (mg/g) are the amount of copper adsorbed at the equilibrium and at the time of t (h), respectively.

Integration of the equation (4.8) results in:

$$\ln(q_{eq} - q_t) = \ln q_{eq} - K_1 t \quad (4.9)$$

If the depletion of adsorbate due to the adsorption cannot be neglected, the following pseudo-2nd order kinetic model describes the adsorption rate [30].

$$\frac{dq_t}{dt} = K_2(q_{eq} - q_t)^2 \quad (4.10)$$

where K_2 (g/(mg h)) is the pseudo-2nd order kinetic rate constant. Integration and linearization of equation (4.10) results in:

$$\frac{t}{q_t} = \frac{t}{q_{eq}} + \frac{1}{K_2 {q_{eq}}^2} \quad (4.11)$$

Equations (4.7), (4.9) and (4.11) were used for the linear regression of the copper removal experimental results at different contact times.

The thermodynamic parameters such as the Gibbs free energy (ΔG^o), the enthalpy change (ΔH^o), and the entropy change (ΔS^o) were estimated by the following equations:

$$K_{eq} = \frac{q_{eq}}{C_{eq}} \quad (4.12)$$

$$\Delta G^o = -RT \ln K_{eq} \quad (4.13)$$

$$\Delta G^o = \Delta H^o - T\Delta S^o \quad (4.14)$$

where q_{eq} (mg/g) is the amount of copper adsorbed at equilibrium, C_{eq} (mg/L) is the equilibrium concentration of copper in the solution, R is the gas constant (8.314 J/gmol.K), T (K) is the absolute temperature, and K_{eq} (L/g) is the adsorption equilibrium constant. Combining equations (4.13) and (4.14) and the linearization will give:

$$\ln K_{eq} = \frac{\Delta S^o}{R} - \frac{\Delta H^o}{RT} \quad (4.15)$$

By plotting lnK_{eq} against 1/T, the values of ΔH° and ΔS° are estimated from the slope and the intercept and the value of ΔG° is calculated from the equation (4.14). The value of ΔG° depicts the spontaneous nature of the adsorption process.

4.3. Results and discussion

4.3.1. Characterization of the hydrochar

The proximate analysis, the ultimate analysis, and the BET surface area of the hydrochars (HD210, HD250) and their source material are shown in Table 4.3. The volatile matter in the hydrochars was lower and the ash content was higher than those of microalgae. It shows the decomposition of biomolecules of microalgae into the organic liquid phase (i.e. bio-oil) during HTL. HTL at a higher temperature led to a greater loss of volatile matter, as well as a decrease in the hydrogen content. The nitrogen content of the hydrochars was lower than their source material. According to the literature, protein of microalgae is decomposed into amino acid and then converted into N-containing compounds in the bio-oil and ammonium which is a water soluble compound [33]. The BET surface area of HD250 was higher than that of HD210 suggesting higher potential for the adsorption process.

The surface property is important for the hydrochar reactivity. The SEM images of microalgae, HD210, and HD250 are shown in Figure 4.1. As can be seen, the hydrochar structure was not homogeneous. In addition, irregular pores with different shapes and sizes were observed.

Table 4.3. Characteristics of microalgae Nannochloropsis sp. and hydrochar

	Nannochloropsis sp.	HD210	HD250
Proximate analysis (wt%)			
Moisture	2.6	3.4	1.8
Volatile matter	81.6	66.0	33.0
Fixed carbon	11.3	19.3	11.5
Ash	4.4	11.2	53.7
Ultimate analysis (wt%)			
C	49.93	54.89	27.33
H	7.91	6.42	3.29
N	6.33	5.98	2.67
O*	28.71	32.19	66.40
S	0.64	0.50	0.25
BET surface area (m^2/g)	Not detected	1.38	12.56
Average pore diameter (nm)	-	4.25	5.47
Mesopore volume (cm^3/g)	-	0.01	0.03

*: Calculated by difference

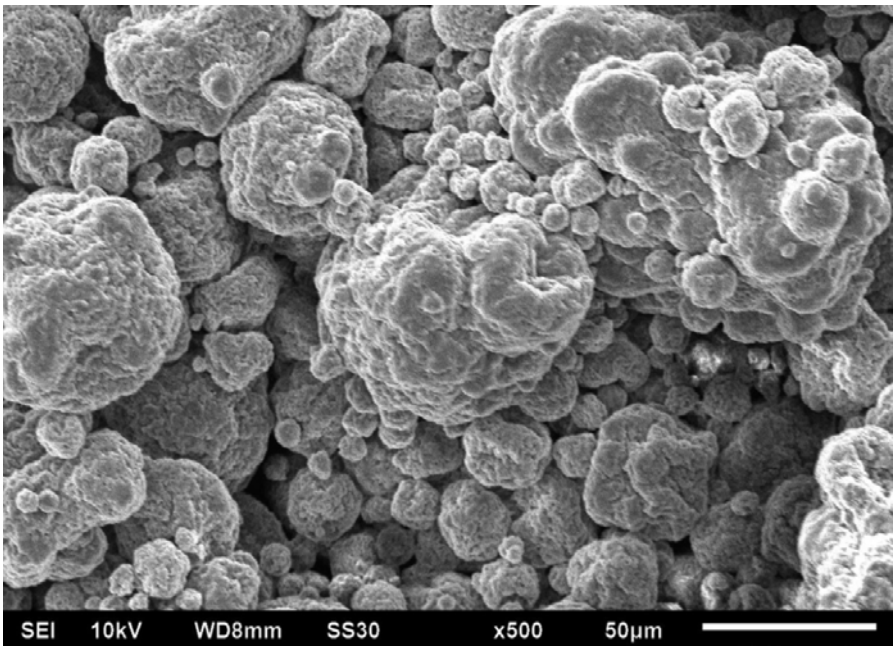

(a)

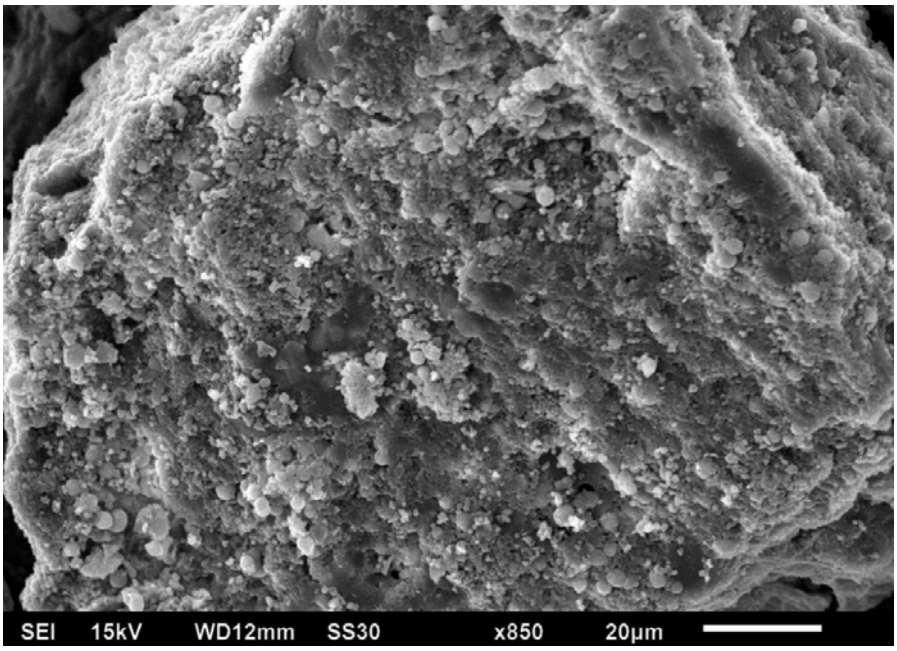

(b)

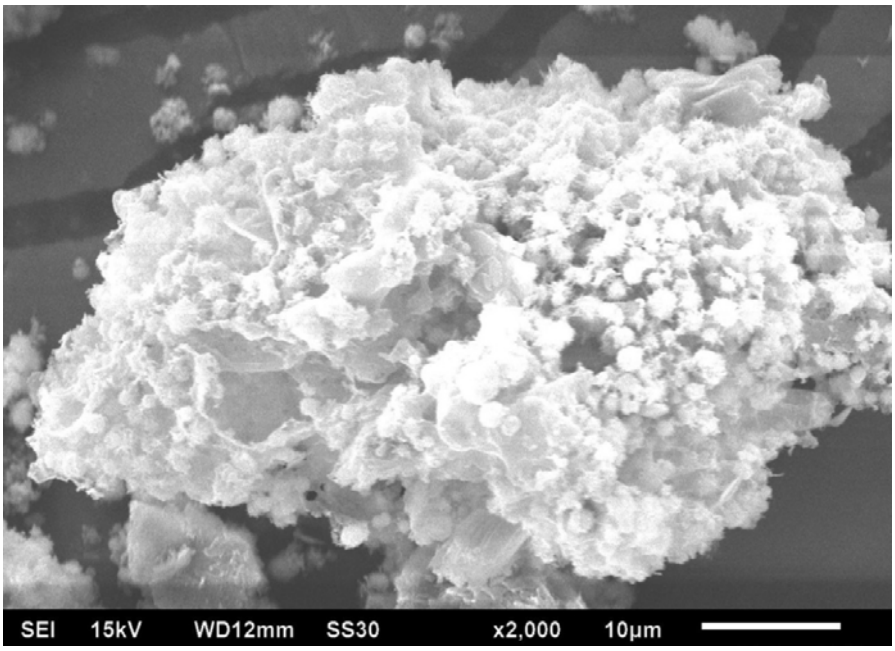

(c)

Figure 4.1. SEM images of (a) microalgae , (b) HD210, (c) HD250

The FTIR spectra of microalgae, HD210, and HD250 are shown in Figure 4.2. In Figure 4.2. a., the characteristic peak around 3418 cm^{-1} is due to the stretching vibration of N-H in amides associated with protein and O-H in water [34], and the peak at 2932 cm^{-1}

corresponds to the stretching vibration of aliphatic groups (C-H) in lipid and protein (i.e., CH_2 or CH_3) [35, 36]. The peak at 2852 cm^{-1} represents the stretching or asymmetric vibration of aldehydes (-CH) [36], and the peak at 1652 cm^{-1} results from the C=O stretching in amides associated with protein [34]. The peak at 1540 cm^{-1} is owing to the stretching vibration of C-N and N-H in protein [36], while the peak at 1456 cm^{-1} is due to the C=C stretching [22]. The peak at 1072 cm^{-1} comes from C-O-C in the carbohydrate of polysaccharides [36]. The FTIR spectrum of HD210 (Figure 4.2.b) is similar to microalgae with a small shift in the wave number of the corresponding peaks of the stretching vibrations. However, the corresponding peaks of the C-N and N-H stretching disappeared in the FTIR spectrum of HD250 (Figure 4.2.c) which shows that decomposition of protein was accelerated by increasing the HTL temperature from 210°C to 250°C. This result is consistent with the nitrogen content of HD250 which was lower than that of microalgae and HD210. The peaks at around 3430 cm^{-1} and 1652 cm^{-1} were retained which means that 250°C was not high enough for complete decomposition of microalgae protein.

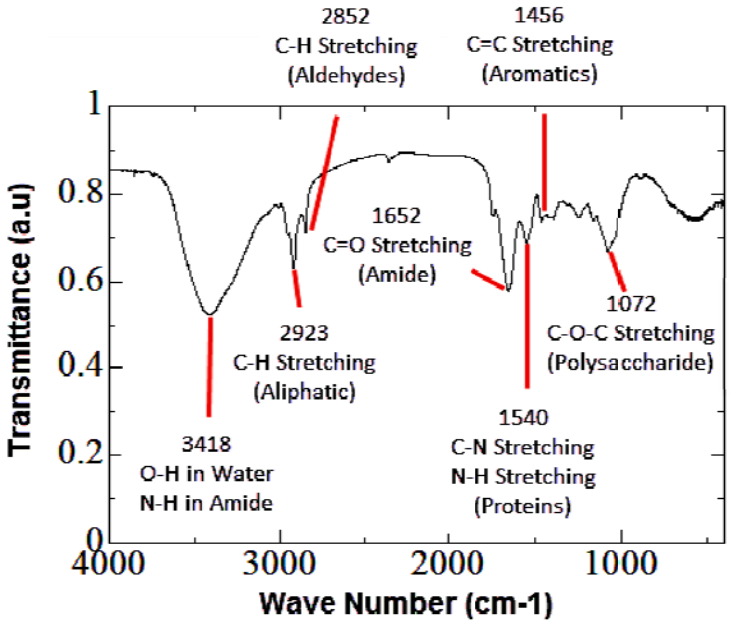

(a)

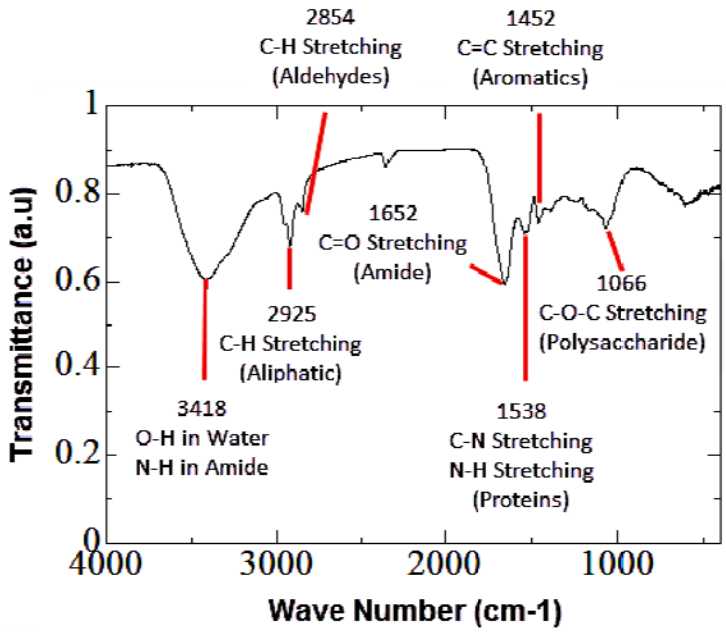

(b)

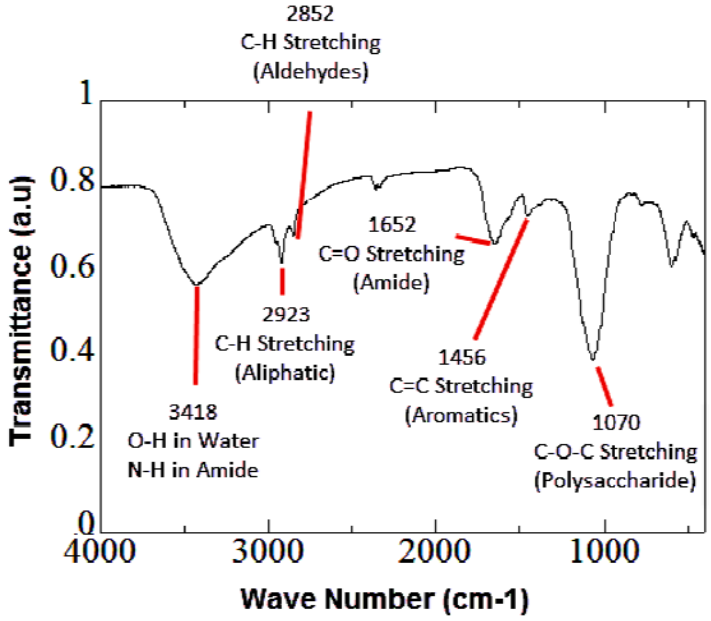

(c)

Figure 4.2. FTIR spectra of (a) microalgae , (b) HD210, (c) HD250

4.3.2. Effects of the solution pH

One of the most important controlling parameters in the heavy metal adsorption process is the solution pH. It affects the surface charge of the adsorbent, speciation of the heavy metal, and degree of ionization in the solution [5]. Figure 4.3 shows the amount of copper removed by the hydrochars vs. the initial solution pH. The amount of copper adsorption was the highest at an initial pH of 5 for both HD210 and HD250. In addition, it decreased from pH 5 to 2 which can be explained in two ways. First, decreasing in the solution pH results in an increase in the H^+ ion concentration. Under the acidic condition, Cu^{2+} ions need to compete with H^+ ions, which are characterized by high mobility, for the active sites on the surface of the hydrochar. Second, the functional groups on the surface of the hydrochar are charged positively by the protonation reaction under acidic conditions which repel copper ions. The decrease in the amount of copper adsorption observed when the initial solution pH was increased from 5 to 6 was likely caused by the formation of soluble hydroxyl complexes $Cu(OH)^-_{aq}$. Formation of the copper hydroxyl results in a decrease in the initial copper ion concentration and consequently a decrease in the amount of copper adsorbed as will be explained in Section 4.3.3.

Based on these results, all subsequent copper adsorption experiments were carried out at the pH value of 5. Comparison between the adsorption capacities of HD210 and HD250 revealed that the amount of copper adsorbed of HD250 was higher at all pH values which was likely due to its higher surface area.

4.3.3. Effects of the initial copper concentration

Figure 4.4 shows the relationship between the amount of copper adsorbed and the initial Cu(II) concentration in the solution. It can be seen that increasing the initial Cu(II) concentration caused an increase in the amount of Cu(II) adsorption. This was due to the increase in the concentration gradient which is the driving force for mass transfer [5].

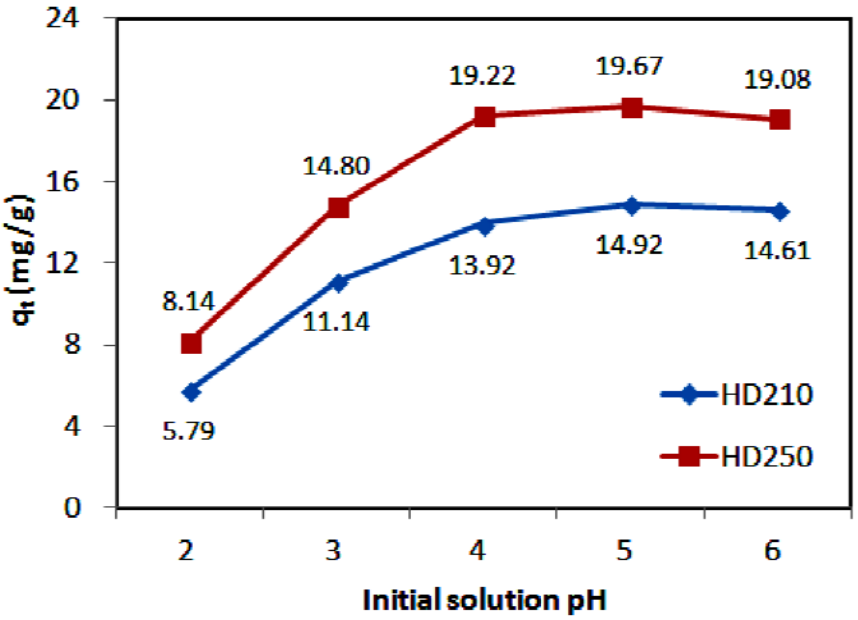

Figure 4.3. Effect of the initial solution pH on the copper adsorption onto HD210 and HD250

(adsorbent dose: 5 g/L; initial copper concentration: 100 mg/L; contact time: 24 h; temperature: 25°C)

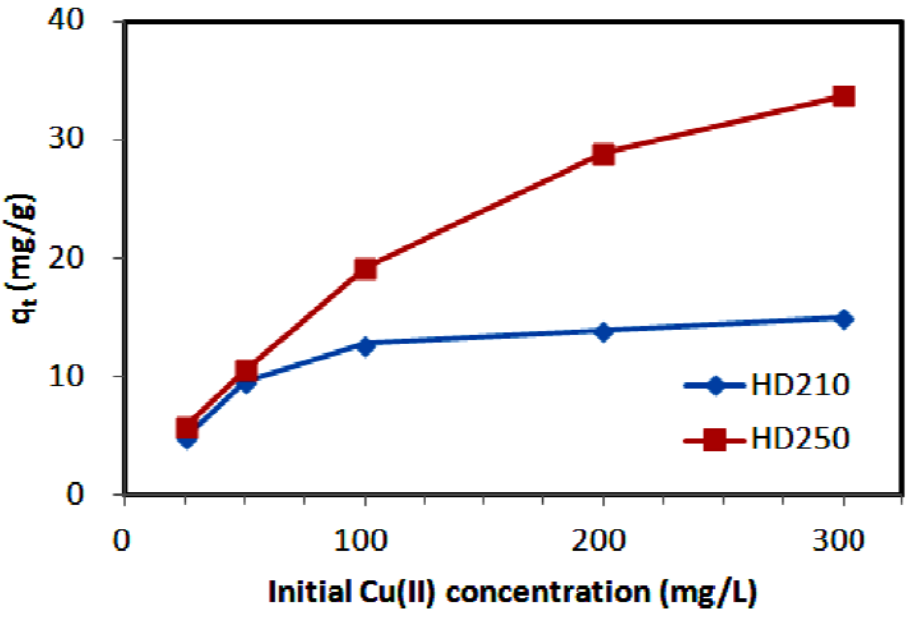

Figure 4.4. Effect of the initial Cu(II) concentration on the copper adsorption onto HD210 and HD250

(adsorbent dose: 5 g/L; pH: 5; contact time: 24 h; temperature: 25°C)

4.3.3.1. Adsorption isotherms

In order to obtain the parameters of the Langmuir's and Freundlich's isotherms, it was assumed that the adsorption would achieve the equilibrium condition at 24 h contact time. The q_{eq} vs. C_{eq} data was curve-fitted with the linear forms of Langmuir's and Freundlich's isotherm models explained in Section 4.2.5. For this purpose, the Langmuir's isotherm was applied by plotting C_{eq}/q_{eq} against C_{eq}, and the values of q_{max} and K_L were determined from the slopes and intercepts of the plots, respectively. Similarly, for fitting the experimental data to the Freundlich's isotherm, the quantity of $\ln(q_{eq})$ was plotted against $\ln(C_{eq})$. The values of n and K_F were calculated from the slopes and the intercepts of the plots, respectively (Figure 4.5). Table 4.4 lists the values of the isotherm model parameters and the coefficient of determination (R^2) obtained by the linear regression.

The results shown in Figure 4.5 and Table 4.4 suggest that the adsorption of copper on the surface of the hydrochar can be explained better by the Langmuir's model than by the Freundlich's model ($R^2 \geq 0.99$ for Langmuir model) with the maximum amount of copper adsorbed of 14.96 and 34.15 mg/g for HD210 and HD250 at 25°C, respectively. The results obtained from the adsorption equilibrium studies in this research is in agreement with most previous studies [26-30] since the Langmuir's model best fitted the experimental isotherm data in previous studies.

Table 4.4. Adsorption isotherm parameters (adsorbent dose 5 g/L; pH 5; contact time 24 h; temperature 25°C)

Adsorbent	Langmuir's model			Freundlich's model		
	q_{max} (mg/g)	K_L (L/mg)	R^2	K_F (mg/g)(L/mg)$^{1/n}$	n	R^2
HD210	14.96	0.28	0.991	6.54	6.14	0.775
HD250	34.15	0.25	0.996	9.60	3.71	0.764

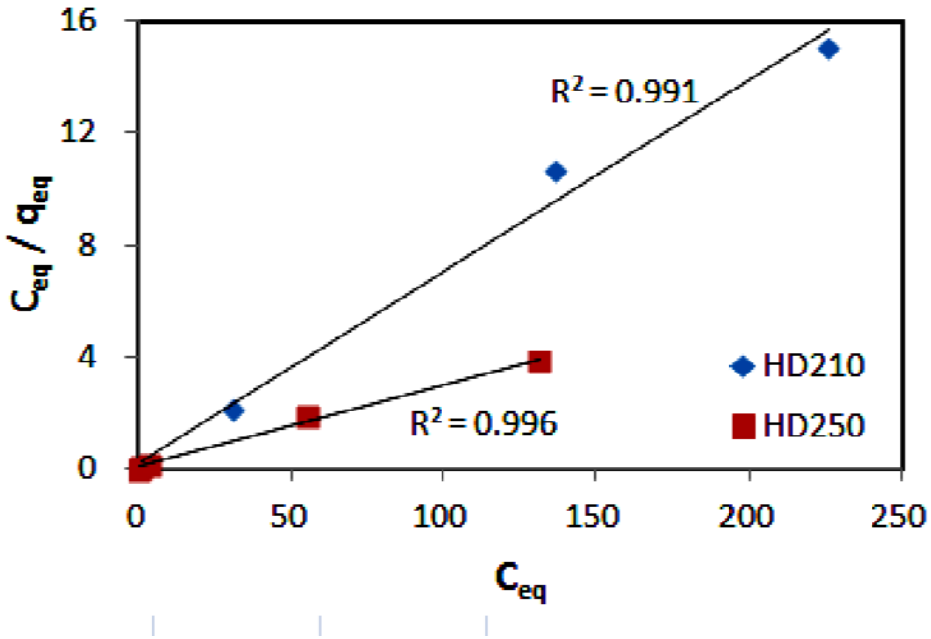

(a): Langmuir's isotherm

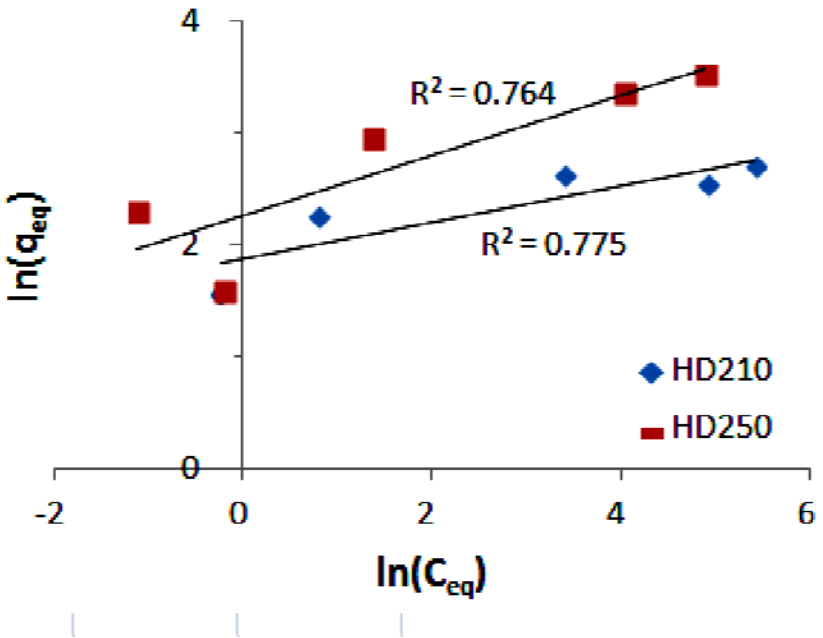

(b): Freundlich's isotherm

Figure 4.5. Langmuir's and Freundlich's isotherm models for copper adsorption onto HD210 and HD250

(adsorbent dose: 5 g/L; pH: 5; contact time: 24 h; temperature: 25°C)

4.3.4. Effects of the contact time

Figure 4.6 shows the variation of the amount of copper adsorbed with the contact time. For both hydrochars, increasing the contact time caused an increase in the amount of Cu(II) adsorption.

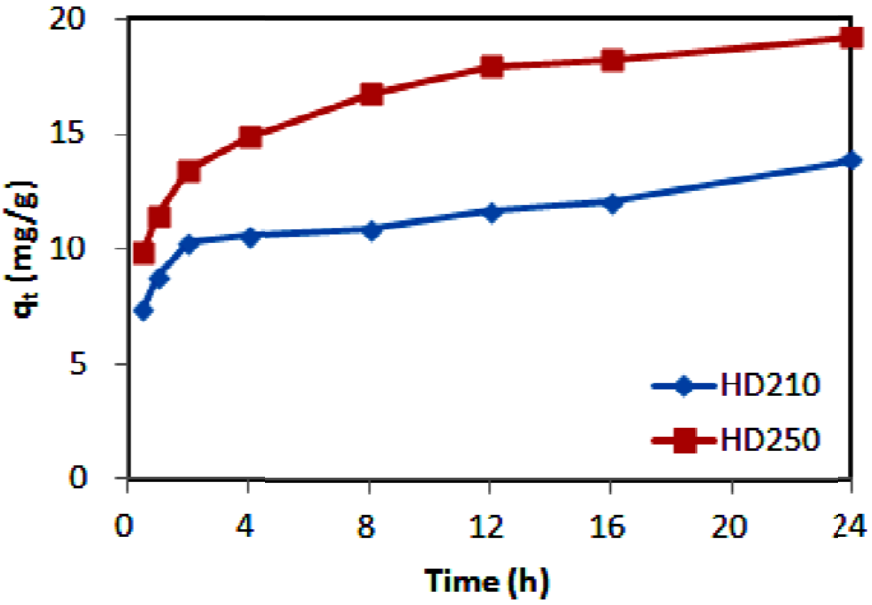

Figure 4.6. Effect of the contact time on the copper adsorption onto HD210 and HD250 (adsorbent dose: 5 g/L; pH: 5; initial copper concentration: 100 mg/L; temperature: 25°C)

4.3.4.1. Adsorption kinetics

Pseudo-1st order (equation 4.9) and pseudo-2nd order (equation 4.11) were applied to study the copper adsorption kinetics onto the hydrochars. For the pseudo-1st order kinetic model, the linear plot of $\ln(q_{eq}-q_t)$ against time t would give the rate constant of K_1 from the slopes and q_{eq} can be calculated from the intercept (Figure 4.7). Table 4.5 lists the corresponding values of K_1, and q_{eq} calculated by the pseudo-1st order kinetic assumption, as well as R^2. According to the results, the coefficient of determination were low (R^2< 0.90) for HD210. In addition, q_{eq} values calculated by the linear regression were lower than that of the experimental data. Therefore, it may conclude that the copper adsorption system did

not follow the pseudo-1st order kinetic model perfectly and higher order rate equations may fit better the experimental data.

By plotting t/q_t against time t, the pseudo-2nd order rate constant K_2 and q_{eq} were determined from the intercept and the slope of the plot (Figure 4.7). Table 4.5 lists the corresponding values of K_2, and q_{eq} calculated by the pseudo-2nd order kinetic assumption, as well as R^2. As can be seen from the results, the coefficient of determination were high (R^2>0.98) for both HD210 and HD250, and the values of q_{eq} were very close to the experimental values. This well fitness of the experimental data suggested that the pseudo-2nd order model could describe the kinetics of the present adsorption system which is consistent with previous studies [5, 27, 29]. Since Cu(II) ion has two positive electric charges, it binds to two vacant adsorption sites on the surface of hydrochar which shows a 2nd order kinetic rate.

Table 4.5. Adsorption kinetics parameters (adsorbent dose 5 g/L; pH 5; initial copper concentration 100 mg/L; temperature 25°C)

Adsorbent	q_{e_exp} (mg/g)	pseudo-1st order model			pseudo-2nd order model		
		K_1 (h^{-1})	q_{e_calc} (mg/g)	R^2	K_2 (g/mg h)	q_{e_calc} (mg/g)	R^2
HD210	13.92	0.069	5.351	0.867	0.0673	13.71	0.988
HD250	19.22	0.147	8.464	0.978	0.0535	19.64	0.998

It should be noted that the quantity of q_{eq}, calculated by the linear regression, is the amount of copper adsorbed at equilibrium calculated by the pseudo-1st order and the pseudo-2nd order kinetic assumption. This quantity is different from q_{eq} obtained by the experiment conducted at the contact time of 24 h. In order to differentiate the experimental equilibrium adsorption amount and the equilibrium adsorption amount obtained by calculation, the latter is shown by q_{e_calc} in Table 4.5.

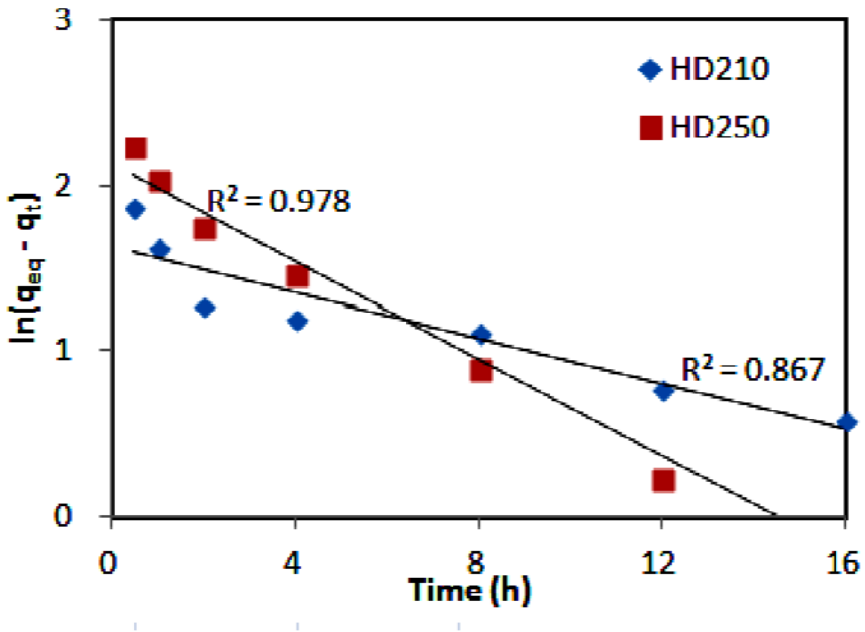

(a): Pseudo-1st order

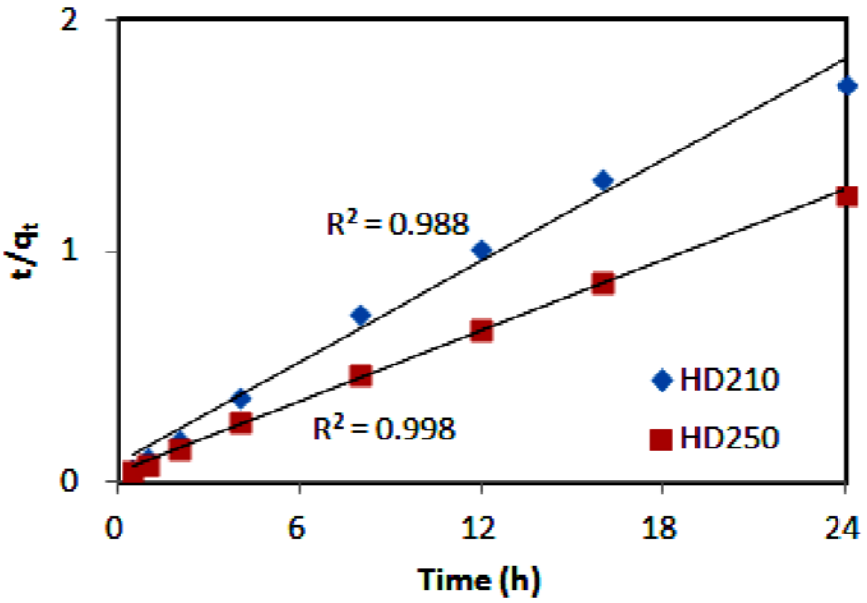

(b): Pseudo-2nd order

Figure 4.7. Kinetic models for the copper adsorption onto HD210 and HD250
(adsorbent dose: 5 g/L; pH: 5; initial copper concentration: 100 mg/L; temperature: 25°C)

Other than above kinetic models, the mathematical model described by Weber and Morris (equation 4.7) was used to describe the adsorption mechanism. The result of the linearity test of q_t against $t^{0.5}$ is shown in Figure 4.8. As can be seen, the plots did not pass through the origin. Also, they could not be fitted to a single linear regression. Since two distinct phases were observed for each plot, the linearity was evaluated separately for each phase, and a single linear regression was applied. The first linearity implied the mass transfer of copper ions across the bulk solution to the external surface of the hydrochar, and the second linearity showed the copper ion diffusion into the adsorbent surface pores (intra-particle diffusion). The larger slopes of the first phase depicted that the external film diffusion was the rate-determining step in this phase since it is faster than the intra-particle diffusion [30]. The lower slopes of the second phase implied that the intra-particle diffusion, which is slower than the external film diffusion, was the rate-determining step.

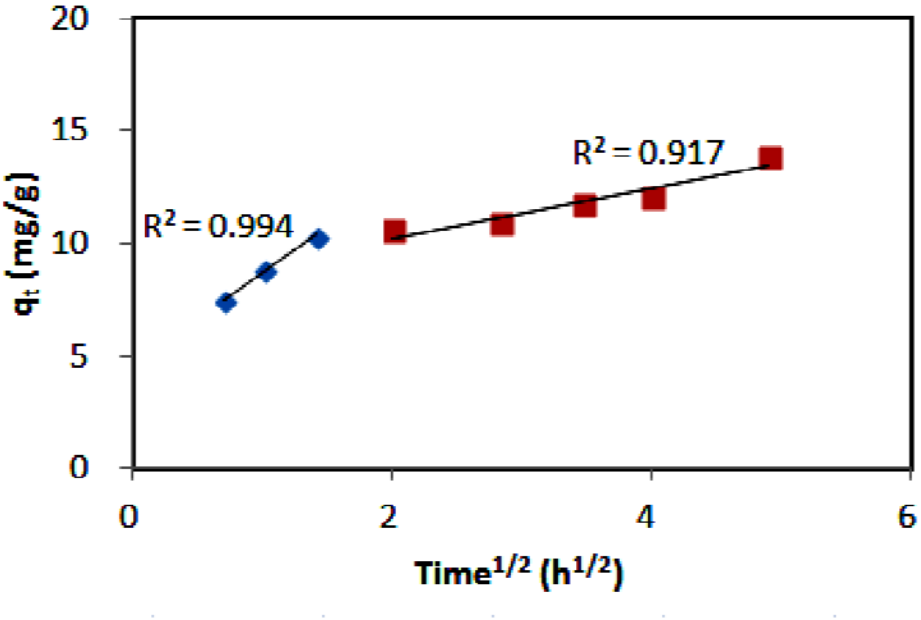

(a): HD210

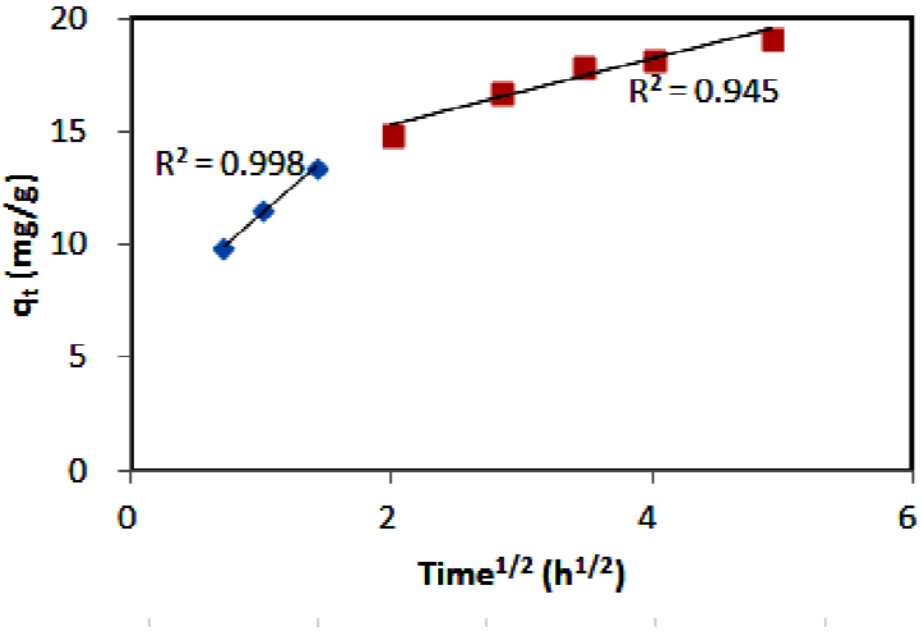

(b): HD210

Figure 4.8. Weber–Morris model for the copper adsorption onto HD210 and HD250
(adsorbent dose: 5 g/L; pH: 5; initial copper concentration: 100 mg/L; temperature: 25°C)

4.3.5. Effects of the temperature

Figure 4.9 shows the change of the amount of copper adsorbed with the temperature. For both hydrochars, increase of the temperature caused an increase in the amount of Cu(II) adsorption.

4.3.5.1. Thermodynamic studies

By plotting $\ln K_{eq}$ against $1/T$, the values of ΔH° and ΔS° were estimated from the slope and the intercept (Figure 4.10), and the value of ΔG° was calculated from the equation (4.14). Table 4.6 represents the thermodynamic parameters of copper adsorption onto HD210 and HD250. For HD250, ΔG° was negative at all levels of the temperature, which shows that adsorption was spontaneous. However, for HD210, only at 45°C, ΔG° had a negative value. The positive value of ΔH° suggested that the adsorption was an endothermic process. This result was confirmed by the effect of the temperature on the copper removal

since by increasing the temperature, the amount of copper adsorption increased for both HD210 and HD250 (Figure 4.9).

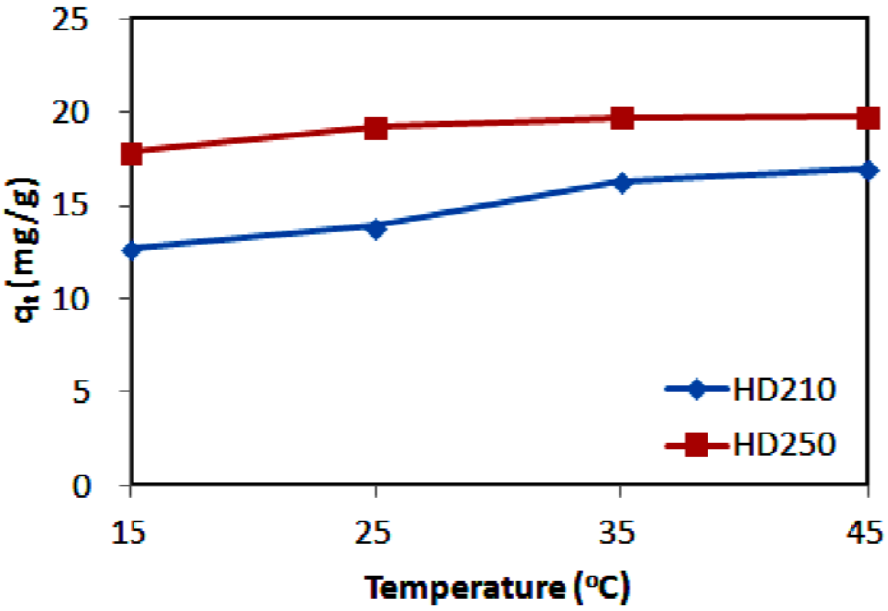

Figure 4.9. Effect of the temperature on the copper adsorption onto HD210 and HD250 (adsorbent dose: 5 g/L; pH: 5; initial copper concentration: 100 mg/L; contact time: 24 h)

Table 4.6. Thermodynamic parameters of the copper adsorption onto HD210 and HD250

Adsorbent	Temperature T(°C)	Thermodynamic parameters		
		$\Delta G°$(kJ/mol)	$\Delta H°$(kJ/mol)	$\Delta S°$(J/mol K)
HD210	15	2.63	32.06	102.15
	25	1.61		
	35	0.58		
	45	-0.44		
HD250	15	-1.63	60.73	216.43
	25	-3.80		
	35	-5.96		
	45	-8.13		

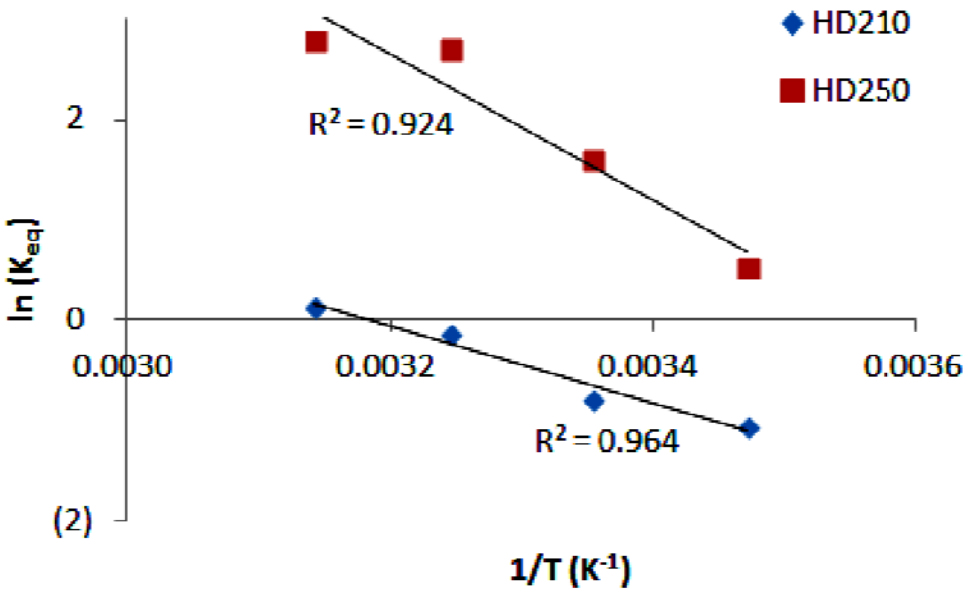

Figure 4.10. Plots of $\ln K_{eq}$ against 1/T for the copper adsorption onto HD210 and HD250 (adsorbent dose: 5 g/L; pH: 5; initial copper concentration: 100 mg/L; contact time: 24 h)

According to Table 4.6, ΔG° is positive for HD210 at a low temperature. It means that adsorption was not spontaneous. The reason for the unexpected value of ΔG° can be explained by considering the assumptions of the thermodynamic model as well as the regression error. Equation 4.13 has been developed with the assumption of a reversible chemical reaction under the equilibrium. This equation has been widely used for the thermodynamic analysis of the adsorption process by defining an adsorption equilibrium constant (equation 4.12). If the adsorption is physical or any irreversible mechanism is effective, there could be a possibility of an error in the thermodynamic analysis results. The other source of the error could be the estimation error in the linear regression. Especially, the value of ΔG° is close to zero and its positive value might be caused by the regression estimation error.

It should be noted that positive values of ΔG° have been reported in other works [27, 37-40]. However, no explanations were provided by the authors except that the adsorption is not easy [38].

4.3.6. Comparison of the copper adsorption performance of the hydrochar with other adsorbents

This section compares the performance of the hydrochars in the copper adsorption with that of a commercial activated carbon (AC). Table 4.7 presents the amount of copper adsorbed for HD210, HD250, and AC. It can be seen that the copper adsorption by AC is higher than that of HD210. However, it is lower than that of HD250, even though AC has the highest surface area. The latter result can be explained by the oxygen-containing functional groups (OFG) on the hydrochar surface which improve the hydrochar adsorption capacity. The quantity of OFG shows the trend of HD250 > HD210 > AC. This result shows that the OFG has an important effect on the copper adsorption by hydrochar. It should be noted that this conclusion cannot be extended to all pollutants since different pollutants have different effective adsorption mechanisms.

Table 4.7. Comparison of the copper adsorption performance of the hydrochars and commercial activated carbon

Adsorbent	Surface area (m^2/g)	Oxygen-containing functional groups (mmol/g)	Amount of copper adsorption (mg/g)[1]
HD210	1.38	1.25	14.92
HD250	12.56	1.61	19.67
AC[2]	1141.3	0.57	17.79

1: Experimental condition (adsorbent dose: 5 g/L; pH: 5; initial copper concentration: 100 mg/L; contact time: 24 h; temperature: 25°C)

2: Commercial activated carbon

Table 4.8 compares the adsorption capacity of HD210 and HD250 with those of the biochars/hydrochars from different biomass materials obtained by Langmuir's isotherm model. It should be noted that different experimental conditions were used by the authors which has an effect on the adsorption experiment results.

Table 4.8. Comparison of the copper adsorption capacities of various biochars/hydrochars

Feedstock	Method	Surface area (m^2/g)	Amount of copper adsorption (mg/g)[1]	Ref.
HD210	HTL	1.38	14.96	This study
HD250	HTL	12.56	34.15	This study
Rice husks	Hydrothermal treatment	-	3.49	[5]
Orange waste	Hydrothermal treatment	-	5.80	[5]
Compost	Hydrothermal treatment	-	7.72	[5]
Peanut straw	Slow pyrolysis	-	88.97	[26]
Soybean straw	Slow pyrolysis	-	52.75	[26]
Canola straw	Slow pyrolysis	-	37.49	[26]
Hardwood	Slow pyrolysis	0.43	6.79	[27]
Corn straw	Slow pyrolysis	13.08	12.52	[27]
Pinewood	Slow pyrolysis	29	2.75	[28]
Pinewood	Hydrothermal treatment	21	4.46	[28]
Pig manure	Slow pyrolysis	15.89	78.36	[29]
Macroalgae	Slow pyrolysis	N.D.[2]	19.12	[30]

1: The amount of copper adsorption is reported at the optimum pH value selected by the authors in the reference paper or based on the Langmuir isotherm results.

2: Not detected

4.4. Conclusions

This study investigated the feasibility of hydrochars from the hydrothermal liquefaction of microalgae as adsorbents for removal of copper from aqueous solution. Based on the obtained results, the irregular hydrochar surface was identified. In addition, oxygen-containing functional groups were identified on the hydrochar surface, which were effective for hydrochar performance as an adsorbent. Copper adsorption onto the hydrochars was strongly influenced by the solution pH, with the maximum amount of copper adsorbed at pH 5. The hydrochar prepared at 250°C had a higher amount of copper

adsorption than that prepared at 210°C. The adsorption isotherm data were fitted well by the Langmuir's model, and the adsorption kinetics was best described by the pseudo-2nd order kinetic model. Finally, the adsorption was found to be an endothermic process.

4.5. References

[1] Demirbas A. Heavy metal adsorption onto agro-based waste materials: A review. J Hazard Mater. 2008;157:220-9.

[2] Kumar U, Bandyopadhyay M. Sorption of cadmium from aqueous solution using pretreated rice husk. Bioresource Technol. 2006;97:104-9.

[3] Tapiero H, Townsend DM, Tew KD. Trace elements in human physiology and pathology. Copper. Biomed Pharmacother. 2003;57:386-98.

[4] Food and Nutrition Board IoM, National Academies. Dietary Reference Intakes for Vitamin A, Vitamin K, Arsenic, Boron, Chromium, Copper, Iodine, Iron, Manganese, Molybdenum, Nickel, Silicon, Vanadium, and Zinc. Washington, D.C.: National Academy Press; 2001.

[5] Pellera FM, Giannis A, Kalderis D, Anastasiadou K, Stegmann R, Wang JY, et al. Adsorption of Cu(II) ions from aqueous solutions on biochars prepared from agricultural by-products. J Environ Manage. 2012;96:35-42.

[6] Aman T, Kazi AA, Sabri MU, Bano Q. Potato peels as solid waste for the removal of heavy metal copper(II) from waste water/industrial effluent. Colloid Surface B. 2008;63:116-21.

[7] Benaissa H, Elouchdi MA. Removal of copper ions from aqueous solutions by dried sunflower leaves. Chem Eng Process. 2007;46:614-22.

[8] Ajmal M, Khan AH, Ahmad S, Ahmad A. Role of sawdust in the removal of copper(II) from industrial wastes. Water Res. 1998;32:3085-91.

[9] Bhatnagar A, Sillanpaa M. Utilization of agro-industrial and municipal waste materials as potential adsorbents for water treatment-A review. Chem Eng J. 2010;157:277-96.

[10] El-Ashtoukhy ESZ, Amin NK, Abdelwahab O. Removal of lead (II) and copper (II) from aqueous solution using pomegranate peel as a new adsorbent. Desalination. 2008;223:162-73.

[11] Zheng W, Li XM, Wang F, Yang Q, Deng P, Zeng GM. Adsorption removal of cadmium and copper from aqueous solution by areca - A food waste. J Hazard Mater. 2008;157:490-5.

[12] Aydin H, Buluta Y, Yerlikaya C. Removal of copper (II) from aqueous solution by adsorption onto low-cost adsorbents. J Environ Manage. 2008;87:37-45.

[13] Hammaini A, Gonzalez F, Ballester A, Blazquez ML, Munoz JA. Simultaneous uptake of metals by activated sludge. Miner Eng. 2003;16:723-9.

[14] Perez-Marin AB, Ballester A, Gonzalez F, Blazquez ML, Munoz JA, Saez J, et al. Study of cadmium, zinc and lead biosorption by orange wastes using the subsequent addition method. Bioresource Technol. 2008;99:8101-6.

[15] Imamoglu M, Tekir O. Removal of copper (II) and lead (II) ions from aqueous solutions by adsorption on activated carbon from a new precursor hazelnut husks. Desalination. 2008;228:108-13.

[16] Liu ZG, Zhang FS. Removal of lead from water using biochars prepared from hydrothermal liquefaction of biomass. J Hazard Mater. 2009;167:933-9.

[17] Mohan D, Pittman CU, Bricka M, Smith F, Yancey B, Mohammad J, et al. Sorption of arsenic, cadmium, and lead by chars produced from fast pyrolysis of wood and bark during bio-oil production. J Colloid Interf Sci. 2007;310:57-73.

[18] Yang Y, Lin X, Wei B, Zhao Y, Wang J. Evaluation of adsorption potential of bamboo biochar for metal-complex dye: equilibrium, kinetics and artificial neural network modeling. Int J Environ Sci Te. 2014;11:1093-100.

[19] Ahmad M, Lee SS, Dou XM, Mohan D, Sung JK, Yang JE, et al. Effects of pyrolysis temperature on soybean stover- and peanut shell-derived biochar properties and TCE adsorption in water. Bioresource Technol. 2012;118:536-44.

[20] Tan XF, Liu YG, Zeng GM, Wang X, Hu XJ, Gu YL, et al. Application of biochar for the

removal of pollutants from aqueous solutions. Chemosphere. 2015;125:70-85.

[21] Saber M, Nakhshiniev B, Yoshikawa K. A review of production and upgrading of algal bio-oil. Renew Sust Energ Rev. 2016;58:918-30.

[22] Qian KZ, Kumar A, Zhang HL, Bellmer D, Huhnke R. Recent advances in utilization of biochar. Renew Sust Energ Rev. 2015;42:1055-64.

[23] Barreiro DL, Prins W, Ronsse F, Brilman W. Hydrothermal liquefaction (HTL) of microalgae for biofuel production: State of the art review and future prospects. Biomass Bioenerg. 2013;53:113-27.

[24] Kambo HS, Dutta A. A comparative review of biochar and hydrochar in terms of production, physico-chemical properties and applications. Renew Sust Energ Rev. 2015;45:359-78.

[25] Mohan D, Sarswat A, Ok YS, Pittman CU. Organic and inorganic contaminants removal from water with biochar, a renewable, low cost and sustainable adsorbent - A critical review. Bioresource Technol. 2014;160:191-202.

[26] Tong XJ, Li JY, Yuan JH, Xu RK. Adsorption of Cu(II) by biochars generated from three crop straws. Chem Eng J. 2011;172:828-34.

[27] Chen XC, Chen GC, Chen LG, Chen YX, Lehmann J, McBride MB, et al. Adsorption of copper and zinc by biochars produced from pyrolysis of hardwood and corn straw in aqueous solution. Bioresource Technol. 2011;102:8877-84.

[28] Liu ZG, Zhang FS, Wu JZ. Characterization and application of chars produced from pinewood pyrolysis and hydrothermal treatment. Fuel. 2010;89:510-4.

[29] Kolodynska D, Wnetrzak R, Leahy JJ, Hayes MHB, Kwapinski W, Hubicki Z. Kinetic and adsorptive characterization of biochar in metal ions removal. Chem Eng J. 2012;197:295-305.

[30] Park SH, Cho HJ, Ryu C, Park YK. Removal of copper(II) in aqueous solution using pyrolytic biochars derived from red macroalga Porphyra tenera. J Ind Eng Chem. 2016;36:314-9.

[31] Debelius B, Forja JM, DelValls A, Lubian LM. Toxicity and bioaccumulation of copper and lead in five marine microalgae. Ecotox Environ Safe. 2009;72:1503-13.

[32] Salame II, Bandosz TJ. Surface chemistry of activated carbons: Combining the results of temperature-programmed desorption, boehm, and potentiometric titrations. J Colloid Interf Sci. 2001;240:252-8.

[33] Guo Y, Yeh T, Song WH, Xu DH, Wang SZ. A review of bio-oil production from hydrothermal liquefaction of algae. Renew Sust Energ Rev. 2015;48:776-90.

[34] Driver T, Bajhaiya AK, Allwood JW, Goodacre R, Pittman JK, Dean AP. Metabolic responses of eukaryotic microalgae to environmental stress limit the ability of FT-IR spectroscopy for species identification. Algal Res. 2015;11:148-55.

[35] Mecozzi M, Pietroletti M, Tornambe A. Molecular and structural characteristics in toxic algae cultures of Ostreopsis ovata and Ostreopsis spp. evidenced by FTIR and FTNIR spectroscopy. Spectrochim Acta A. 2011;78:1572-80.

[36] Chen YC, Chen WH, Lin BJ, Chang JS, Ong HC. Impact of torrefaction on the composition, structure and reactivity of a microalga residue. Appl Energ. 2016;181:110-9.

[37] Hajjaji M, Mountassir Y, Benyaich A. Adsorption of blue copper on a natural and electrochemically treated bentonite. Appl Water Sci. 2016;6:11-23.

[38] Xue YJ, Hou HB, Zhu SJ. Adsorption removal of reactive dyes from aqueous solution by modified basic oxygen furnace slag: Isotherm and kinetic study. Chem Eng J. 2009;147:272-9.

[39] Yargic AS, Sahin RZY, Ozbay N, Onal E. Assessment of toxic copper(II) biosorption from aqueous solution by chemically-treated tomato waste. J Clean Prod. 2015;88:152-9.

[40] Stankovic MN, Krstic NS, Mitrovic JZ, Najdanovic SM, Petrovic MM, Bojic DV, et al. Biosorption of copper(II) ions by methyl-sulfonated Lagenaria vulgaris shell: kinetic, thermodynamic and desorption studies. New J Chem. 2016;40:2126-34.

Chapter 5

5. Conclusions and recommendations

5.1. Conclusions

This research focuses on the low-temperature and low-pressure hydrothermal liquefaction of microalgae. Two techniques were used to increase the bio-oil production yield at low temperatures and pressures, including the heterogeneous catalysts and the ultrasonic pre-treatment. In addition, hydrochar, a by-product of the hydrothermal liquefaction of microalgae, was utilized as a low-cost adsorbent in the adsorption of copper from aqueous solution. The major conclusions of this thesis are as follows.

In Chapter 2, the catalytic hydrothermal liquefaction of microalgae Nannochloprosis sp. was carried out at low temperatures (210°C, 230°C, 250°C). Nanocatalyst (Nano-Ni/SiO_2), an acid catalyst (zeolite), and an alkali catalyst (Na_2CO_3) were applied to investigate their effects on the bio-oil yield and its composition. The major result of this chapter was higher bio-oil yields with the order of nano-Ni/SiO_2 > zeolite > Na_2CO_3 in the hydrothermal liquefaction of Nannochloprosis sp.. The highest bio-oil yield (30.0 wt%) was obtained at 250°C by using nano-Ni/SiO_2.

For the blank experiment, the elemental composition results showed that the oxygen content of the bio-oil decreased by increasing the temperature, and consequently its heating value increased by the increase of the temperature. On the other hand, the nitrogen content of the bio-oil increased with increasing the temperature. For the catalytic experiment, the oxygen and the nitrogen contents of the bio-oil for all types of catalyst were less than that of the blank experiment, and the heating value was higher for the bio-oil produced by the

catalytic HTL. The energy recovery of the bio-oil at 210°C by using Nano-Ni/SiO_2 had the highest value of 30.46% because of the highest bio-oil yield. GC/MS results showed that the major components of the bio-oil by using nano-Ni/SiO_2 were very similar to that of the blank experiment. However, the use of alkali and acid catalysts resulted in the different characterization of the bio-oil. The bio-oil produced by using Na_2CO_3 had more nitrogen-containing components compared to other catalysts. In addition, the catalyst recovery experiment suggested the possibility of nanocatalyst recovery for 2-3 times.

In Chapter 3, ultrasonic assisted HTL (UHTL) was used for bio-oil production from microalgae Nannochloropsis sp. at low temperatures. The results were compared with the results of the conventional HTL. It was shown that UHTL could increase the bio-oil yield while maintaining a positive value for the net energy at low sonication times. It was shown that both the temperature and the sonication time had a positive effect on the bio-oil yield. The highest bio-oil yield was 28.9% at 250°C, 90s sonication time.

Meanwhile, UHTL resulted in a lower oxygen content of the bio-oil as well as a higher heating value. However, the nitrogen content of the bio-oil did not change dramatically by applying UHTL. The component analysis revealed that the major components in the bio-oil from HTL and UHTL were very similar, but with different area%. The major difference is in the peak area of fatty acids and esters. The former is higher for HTL and the latter is higher for UHTL. The net energy was positive at low sonication times, which means that the increase in the bio-oil thermal energy produced by UHTL was higher than the electrical energy consumption of the sonicator.

In Chapter 4, we investigated the feasibility of the hydrochars from hydrothermal liquefaction of microalgae as adsorbents for removal of copper from aqueous solution. Based on the obtained results, the irregular hydrochar surface was identified. In addition, oxygen-containing functional groups were identified on the hydrochar surface, which were

effective for the hydrochar performance as an adsorbent. Copper adsorption onto the hydrochars was strongly influenced by the solution pH, with the maximum adsorption capacity at pH 5. The hydrochar prepared at 250°C had a higher adsorption capacity than that prepared at 210°C. The adsorption isotherm data were fitted well by the Langmuir's model, and the adsorption kinetics was best described by the pseudo-2nd order kinetic model. Finally, the adsorption was found to be an endothermic process.

5.2. Recommendations

Based on the characterization of the bio-oil, described in Chapters 2 and 3, the produced bio-oil cannot be used as transportation fuels directly. Compared to the heavy petroleum fuel oil, the bio-oils have the following undesirable characteristics for fuel applications:

1) high oxygen content and consequently a low heating value

2) high viscosity

3) high corrosiveness (acidity)

4) high nitrogen content

Therefore, upgrading of the bio-oil is necessary to improve its quality to be used as liquid fuels. There is a variety of techniques for bio-oil upgrading including physical and chemical methods. Each upgrading technique has its own advantages and disadvantages. The promising point is that the current infrastructures developed for crude oil (i.e. petroleum refinery) can be used for bio-oil upgrading. Among upgrading techniques, the hydrotreating and the hydro-cracking seem to be promising choices since they have been used in petroleum refineries for many years and the processes are well established.

Figure 5.1 recommends a simple outline for an overall production route from microalgae to liquid fuels by integrating bio-oil production and upgrading processes in a facility called

biorefinery. In the first step, the bio-oil is produced from microalgae by HTL. In order to minimize transportation costs, the bio-oil production should be carried out in smaller plants located close to the microalgae cultivation farms. The bio-oil is then transported to a central biorefinery. In the biorefinery, the bio-oil is first treated by the hydrotreating to improve its quality and then is fed to the distillation unit to separate light and heavy oils. The heavy oil is further processed through the cracking which can be performed by the hydro-cracking or the fluid catalytic cracking. Afterward, the cracked oil is joined with the light oil fraction. Finally, a distillation of the light oil is performed to separate liquid fuels. The hydrogen gas, required for the hydrotreating and the hydro-cracking, is supplied by steam reforming of the bio-oil.

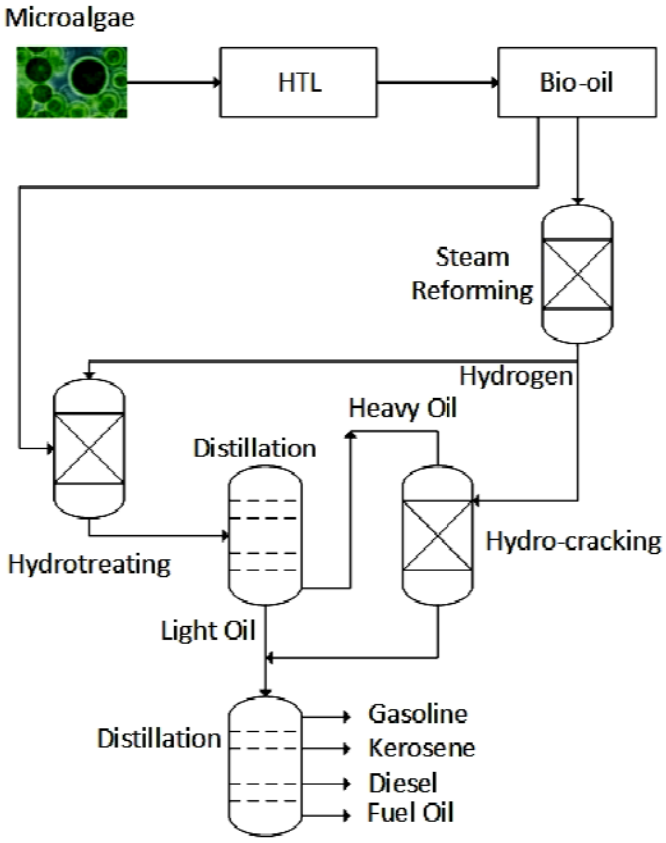

Figure 5.1. Simple outline for algal biorefinery

Based on the recommended biorefinery scheme, the future research roadmap can be a

research on the upgrading of algal bio-oil by the hydrotreating and the hydro-cracking techniques. Even though these processes are well established, more efforts are needed to resolve the problems of the cocking and the catalyst deactivation. Upgrading of bio-oil has drawn attention from researchers around the world, but a little works have been published on the upgrading of algal bio-oil which opens a new route for future research work. In addition, there is not any comprehensive research on the economic evaluation of upgrading techniques for algal bio-oil. Hence, the economic evaluation and the scale-up could be one of the interesting topics for future researches.

Appendix A

Appendix A: Investigation on the possibility of the cation exchange of copper with other cations

One of the mechanisms in the adsorption of heavy metals is the cation exchange. If exchangeable cations like Na^+ exist on the hydrochar surface (i.e. as a complex with the oxygen-containing functional groups), copper may exchange with the cations on the hydrochar surface. In order to investigate the possibility of the cation exchange in the copper adsorption, instead of using Cation Exchange Capacity (CEC) measurement methods which are developed for soil, another approach was used in this study. The quantity of the exchangeable cations (Na^+, K^+, Ca^{2+}, Mg^{2+}, Al^{3+}) in the hydrochar samples was measured in the real experimental setting. For this purpose, 125 mg of HD210 and HD250 were placed in the 25 ml deionized water, separately. pH was adjusted to be 5. After shaking for 24 h and filtration of hydrochar, the concentration of the exchangeable cations in the filtrate was measured by the ICP analyzer. This quantity shows any leaching of the mentioned cations from hydrochars into the water.

In the next step, the same amount of HD210 and HD250 were placed in 25 ml deionized water, containing Cu^{2+} with the concentration of 100 mg/L. The same procedure was followed and the concentration of the exchangeable cations was measured. The ICP result shows the effect of Cu^{2+} on the leaching of the exchangeable cations into the water, and the possibility of cation exchange between Cu^{2+} and other cations.

Table A.1 presents the results of the ICP analysis for the above-mentioned samples. The ICP analysis was also conducted for the deionized water to investigate the existence of any

cations. In Table A.1, TCE is defined as the total concentration of exchangeable cations (Na^+, Mg^{2+}, Al^{3+}, K^+, Ca^{2+}) in the filtrate having the possibility of exchanging with Cu^{2+}. TCE is calculated by the equation A.1. Since copper cation has two positive electric charges, the concentrations of Na^+ and K^+ are divided by two. Al^{3+} was not detected in the filtrate, and therefore it was excluded from the equation A.1.

$$TCE\ \left(\frac{mg}{L}\right) = [Na^+]/2 + [Mg^{2+}] + [K^+]/2 + [Ca^{2+}] \quad \text{(A.1)}$$

where [X] is the concentration of the element X (mg/L)

Table A.1. Concentration of the exchangeable cations in the solution

Hydrochar	Initial Cu^{2+} concentration (mg/L)	Concentration in the filtrate (mg/L)						
		Cu^{2+}	Na^+	Mg^{2+}	Al^{3+}	K^+	Ca^{2+}	TCE[1]
HD210	0	0	13.88	24.73	ND[2]	0.77	1.57	33.63
HD210	100	33.90	27.35	25.78	ND	10.91	19.15	64.06
HD250	0	0	14.78	10.27	ND	5.84	1.13	21.71
HD250	100	3.71	11.34	12.37	ND	4.75	9.91	30.33
Blank[3]	-	0	0	0	0	0	0	-

1: Total concentration of the exchangeable cations (Na^+, Mg^{2+}, Al^{3+}, K^+, Ca^{2+}) in the filtrate (excluding Cu^{2+})

2: Not detected

3: Only deionized water (no mixing with hydrochar was performed)

As can be seen in Table A.1, TCE of HD250 is less than that of HD210. HD250 was prepared at a higher temperature and perhaps has a higher stability compared to HD210. Also, TCE is higher when Cu^{2+} was added to the samples for both HD210 and HD250. It means that the concentration of the exchangeable cations in the solution increased because of the presence of Cu^{2+}. This result shows that Cu^{2+} has the ability to exchange with other cations on the surface of hydrochar which resulted in an increase in TCE. However, it does not prove that

the cation exchange is the only active mechanism in the copper adsorption. Especially, the reduction in the copper concentration (from the initial concentration of 100 mg/L to the final concentration in the filtrate) is higher than the quantity of TCE.